Technical University of Crete

School of Mineral Resources Engineering
MSc in Petroleum Engineering

Thesis title:

# *Thermal modelling of petroleum source rocks in Prinos-Kavala basin*

By Ourania Maria Kokaraki
Supervisor: Professor Nikos Pasadakis

Chania
January 2019

*The MSc Program in Petroleum Engineering of the Technical University of Crete was attended and completed by Miss Ourania Maria Kokaraki due to the Hellenic Petroleum Group Scholarship award.*

# ABSTRACT

Prinos-Kavala basin is the only geological area in Greece where oil and gas are being produced for more than twenty years. The geology and stratigraphy of this particular offshore area are well-known, because many geological and geophysical surveys and studies have been conducted due to the high interest for hydrocarbon exploration. Nowadays, a powerful tool for oil and gas companies in order to evaluate prospects and reducing investment risk in hydrocarbon exploration is basin modelling. Basin modelling is a forward simulation of geological history, hydrocarbon generation, expulsion, migration, and accumulation in a sedimentary basin applying a wide variety of data, such as well data, seismic sections, outcrops, etc.

The objective of this thesis is to perform 1D basin modelling in three selected well locations within the Prinos-Kavala basin. The investigation centred upon the reconstruction of temperature and maturity histories of the examined well locations in order to address questions like if, when, where, and how much, and what type of hydrocarbons have been generated and expelled by the assigned source rocks in each well. Moreover, during this project, a sensitivity analysis was conducted in order to test the influence of some input data and boundary conditions as well as to assess the resultant effect on the simulated temperature and maturity histories.

A lack of data imposed certain limitations on the produced 1D models resulting to a not completely representative modelling of the study area. However, a reasonable first estimation of past conditions and thermal and maturity histories was achieved. It was found that the assigned source rock formations of Pre-Prinos 3 and Pre-Prinos 1 have generated hydrocarbons in all well locations. Well K-1 seems to have the most mature source rocks with the highest present-day transformation ratio (55.60%) and is the only well in which the source rock has reached peak oil expulsion, which started at 0.44Ma.

Sensitivity analysis results indicated that timing and duration of the erosional event between the Evaporitic and Post-Evaporitic sequences, the original thickness of eroded sediments, the paleo water depth boundary condition and the source rock characteristics (TOC and HI) do not affect the temperature and maturity histories. On the contrary, the heat flow boundary conditions plays an important role to the temperature and maturity modelling.

# ACKNOWLEDGEMENTS

First and most of all, I would like to express my gratitude to my supervisor Professor Nikos Pasadakis for his scientific advice and directions throughout the entire project. His guidance and comments during this thesis contributed to its successful completion. Additionally, I want to thank Dr. Paschalia Kiomourtzi from Energean Oil & Gas for providing me with data, and recommendations on questions that arose during this work. Finally, I would like to thank Ms. Eleni Chamilaki from the Laboratory of PVT and Core Analysis in the Technical University of Crete for carrying out the geochemical procedure of Rock-Eval pyrolysis.

# TABLE OF CONTENTS

ABSTRACT ..... 2
ACKNOWLEDGEMENTS ..... 3
LIST OF FIGURES ..... 6
LIST OF TABLES ..... 9
1 INTRODUCTION ..... 10
1.1 Aim of the thesis ..... 10
1.2 Study area ..... 11
1.2.1 Geographical location ..... 11
1.2.2 Exploration and production history ..... 12
1.3 Description of the flow of the thesis ..... 14
2 GEOLOGICAL BACKGROUND PRINOS-KAVALA BASIN ..... 16
2.1 Basins of the north Aegean Sea ..... 16
2.2 Prinos-Kavala Basin ..... 18
2.2.1 Geotectonic evolution ..... 19
2.2.2 Stratigraphy ..... 21
2.2.3 Petroleum system ..... 24
3 BASIN MODELLING BACKGROUND ..... 29
3.1 Introduction to basin modelling ..... 29
3.2 Burial history modelling ..... 31
3.3 Thermal history modelling ..... 33
3.4 Modelling maturation, generation and expulsion ..... 38
3.4.1 Maturation modelling ..... 38
3.4.2 Generation modelling ..... 39
3.4.3 Expulsion modelling ..... 40
4 DATA AND METHODOLOGY ..... 42
4.1 Main input parameters ..... 42
4.1.1 Depositional events ..... 42
4.1.2 Erosions ..... 44
4.1.3 Age assignment ..... 44
4.1.4 Lithology ..... 46
4.1.5 Petroleum system elements (PSE) ..... 47
4.1.6 Source rock properties ..... 47
4.2 Boundary conditions ..... 52
4.2.1 Paleo water depth ..... 52

4.2.2 Sediment water interface temperature ..... 55
4.2.3 Heat flow ..... 57
4.3 Simulation ..... 61
4.4 Calibration ..... 62
4.4.1 Temperature ..... 62
4.4.2 Vitrinite reflectance ..... 66
4.5 Assumptions in the input data ..... 68
5 RESULTS ..... 70
5.1 Burial history ..... 70
5.2 Temperature history ..... 71
5.3 Present-day vitrinite reflectance values ..... 73
5.4 Transformation ratio ..... 75
5.5 Petroleum generation and expulsion history ..... 78
5.6 Sensitivity analysis ..... 82
6 CONCLUSIONS ..... 91
7 BIBLIOGRAPHY ..... 93
8 APPENDIX ..... 99

# LIST OF FIGURES

Figure 1: Geographical overview map of the Prinos-Kavala basin (revised from Kiomourtzi et al., 2007, 2008). ..... 11
Figure 2: Map showing the location of the three wells within the basin (Google maps). ..... 12
Figure 3: Map of the license blocks and oil and gas fields in the Prinos-Kavala basin (https://www.energean.com). ..... 13
Figure 4: Tertiary basins in the north Aegean Sea (Koukouvelas and Aydin, 2002). ..... 17
Figure 5: SW-NE cross section of the Prinos basin showing the roll-over syngenetic faulting that formed the dome-like anticlines (Proedrou and Sidiropoulos, 1992). ..... 19
Figure 6: Paleo geographical model of the Prinos-Kavala basin (Kiomourtzi, 2016). ..... 21
Figure 7: Chronostratigraphic column of the Prinos basin (Proedrou and Papaconstantinou, 2004). 22
Figure 8: SW-NE seismic section of the Prinos-Kavala basin presenting the active petroleum system. Source rocks are highlighted in red, green and light blue, reservoir rovks in grey and seal rocks in orange. Red dotted arrows indicate the migration pathways. (Figure from Kiomourtzi (2016)) ..... 25
Figure 9: Major geological processes in basin modelling (Hantschel and Kauerauf, 2009). ..... 30
Figure 10: Depth versus porosity plot for a series of lithologies based on the Sclater and Cristie (1980) exponential model using empirically determined initial porosities and compaction factors. ..... 32
Figure 11: Kozeny-Carman relationship of porosity with permeability (Ungerer et al., 1990). ..... 32
Figure 12: An example of a burial history curve for a horizon with and without compaction correction (Dembicki, 2017). ..... 33
Figure 13: Two main sub-problems of heat flow analysis, (a) the calculation of the heat in-flux into the sediments and (b) the subsequent calculation of temperature into the sediments (Hantschel and Kauerauf, 2009). ..... 36
Figure 14: The simple (3 component) model for kerogen generation of oil, gas, and a carbon residue (Dembicki, 2017). ..... 39
Figure 15: Main input data for burial and thermal histories reconstruction in PetroMod for the PN-2 well. ..... 51
Figure 16: Main input data for burial and thermal histories reconstruction in PetroMod for the E-1 well. ..... 51
Figure 17: Main input data for burial and thermal histories reconstruction in PetroMod for the K-1 well. ..... 52
Figure 18: 3D map of wells within the Prinos-Kavala basin created by Kiomourtzi (2016) in Petrel software. ..... 53
Figure 19: Bathymetric map of Kavala bay constructed by Kiomourtzi (2016) in Surfer software. ..... 53
Figure 20: Diagram showing depositional environments and bathymetric changes used in paleoenvironmental interpretations (modified after Allen, 1965, 1970). Figure form Okosun and Osterloff (2014). ..... 54
Figure 21: Paleo water depth profile through time for well PN-2. ..... 54
Figure 22: Paleo water depth profile through time for well E-1. ..... 55
Figure 23: Paleo water depth profile through time for well K-1. ..... 55
Figure 24: Global mean surface temperature through geological time. The black line shows changes in latitude with time for Prinos-Kavala basin. ..... 56
Figure 25: Estimated sediment water interface temperature (SWIT) trend defined for the PN-2 well location. ..... 56
Figure 26: Estimated sediment water interface temperature (SWIT) trend defined for the E-1 well location. ..... 56

Figure 27: Estimated sediment water interface temperature (SWIT) trend defined for the K-1 well location. ..... 56
Figure 28: Summary of the typical heat flows associated with sedimentary basins of various types (Allen and Allen, 2005). ..... 58
Figure 29: Modelled heat flow curve over time for PN-2. ..... 59
Figure 30: Modelled heat flow curve over time for E-1. ..... 59
Figure 31: Modelled heat flow curve over time for K-1. ..... 60
Figure 32: Original (left graph) and modified (right graph) temperature measurements from well E-1. ..... 64
Figure 33: Bottom-hole temperature calibration plot for modelled well location PN-2. ..... 64
Figure 34: Bottom-hole temperature calibration plot for modelled well location E-1. ..... 65
Figure 35: Original (left graph) and modified (right graph) temperature measurements from well K-2. ..... 65
Figure 36: Bottom-hole temperature calibration plot for modelled well location K-1. ..... 66
Figure 37: Vitrinite reflectance calibration plot for well PN-2. ..... 67
Figure 38: Vitrinite reflectance calibration plot for well E-1. ..... 67
Figure 39: Vitrinite reflectance calibration plot for well K-1. ..... 68
Figure 40: Reconstructed burial history for the PN-2 well. ..... 70
Figure 41: Reconstructed burial history for the E-1 well. ..... 71
Figure 42: Reconstructed burial history for the K-1 well. ..... 71
Figure 43: Burial history of the PN-2 well with temperature overlay. ..... 72
Figure 44: Burial history of the E-1 well with temperature overlay. ..... 72
Figure 45: Burial history of the K-1 well with temperature overlay. ..... 72
Figure 46: Modelled present-day maturity (vitrinite reflectance) of the assigned source rock layers in the PN-2 well. ..... 74
Figure 47: Modelled present-day maturity (vitrinite reflectance) of the assigned source rock layer in the E-1 well. ..... 74
Figure 48: Modelled present-day maturity (vitrinite reflectance) of the assigned source rock layers in the K-1 well. ..... 75
Figure 49: Burial history plot of the PN-2 well with a transformation ratio overlay. ..... 77
Figure 50: Burial history plot of the E-1 well with a transformation ratio overlay. ..... 77
Figure 51: Burial history plot of the K-1 well with a transformation ratio overlay. ..... 78
Figure 52: Transformation ratio time plots in the three modelled wells (PN-2, E-1 and K-1). ..... 78
Figure 53: Potential generation oil and gas masses by Pepper & Corvi (1995) for the assigned source rocks in the PN-2 well. ..... 80
Figure 54: Potential generation oil and gas masses by Pepper & Corvi (1995) for the assigned source rock in the E-1 well. ..... 80
Figure 55: Potential generation oil and gas masses by Pepper & Corvi (1995) for the assigned source rock in the K-1 well. ..... 81
Figure 56: Burial plots of the modelled wells with an expulsion onset overlay. ..... 81
Figure 57: Temperature and maturity (vitrinite reflectance) histories plots in PN-2 for: the optimized model (1) and multiple scenarios regarding the timing and duration of the erosional event in Pliocene-Pleistocene boundary and the original thickness of eroded sediments (2-6). ..... 86
Figure 58: Temperature and maturity (vitrinite reflectance) histories plots in PN-2 for: the optimized model (1) and multiple scenarios about PWD (2-3). ..... 87
Figure 59: Comparison graphs of temperature and vitrinite reflectance histories between the optimized model (model 1) and the high (model 2) and low (model 3) heat flow scenarios in the three modelled wells (PN-2: top, E-1: middle and K-1: bottom). ..... 88

Figure 60: Comparison graphs of simulated TR and vitrinite reflectance between the optimized model (model 1) and the high (model 2) and low (model 3) heat flow scenarios in the three modelled wells (PN-2: top, E-1: middle and K-1: bottom). ..... 89
Figure 61: Temperature and maturity (vitrinite reflectance) histories plots in all three wells (PN-2: top, E-1: middle and K-1: bottom) for the optimized model (model 1) and increased TOC and HI scenario (model 4). ..... 90

# LIST OF TABLES

Table 1: Assigned ages for the model of well PN-2 (ages for the depositional events correspond to the tops of the layers). ..... 45
Table 2: Assigned ages for the model of well E-1 (ages for the depositional events correspond to the tops of the layers). ..... 45
Table 3: Assigned ages for the model of well K-1 (ages for the depositional events correspond to the tops of the layers). ..... 46
Table 4: Rock-Eval pyrolysis results from selected samples of well PN-2. ..... 48
Table 5: Rock-Eval pyrolysis results of well PN-2 by Kiomourtzi (2016). Results are shown for the samples used for Rock-Eval pyrolysis conducted during the present study. ..... 48
Table 6: Heat flow input data for wells PN-2, E-1, and K-1 from left to right, respectively. ..... 60
Table 7: Heat flows of the optimized model (1) and the high (2) and low (3) heat flow scenarios in well PN-2. ..... 84
Table 8: Heat flows of the optimized model (1) and the high (2) and low (3) heat flow scenarios in well E-1. ..... 84
Table 9: Heat flows of the optimized model (1) and the high (2) and low (3) heat flow scenarios in well K-1. ..... 84

# 1 INTRODUCTION

## 1.1 AIM OF THE THESIS

Basin and petroleum systems modelling is a forward simulation of the geological history, hydrocarbon generation and migration processes within a sedimentary basin through time in order to calculate the volume of hydrocarbons available for entrapment and to predict the volumes and locations of accumulations as well as their properties. The term petroleum system is now commonly used within the petroleum industry and describes a pod of mature source rock and all of the migration paths, reservoirs rocks, caprocks, and traps that can be charged by that source rock to produce oil and gas accumulations (Allen and Allen, 2005).

Nowadays, oil and gas companies perform basin modelling on a routine basis, as it is a key element in the processes of evaluating prospects and reducing investment risk in hydrocarbon exploration. Based on Welte and Yalçin (1988), the reasons for which this method has gained widespread recognition are the following. First of all, it provides petroleum geologists/geoscientists/modellers with the capability of predicting the likelihood of hydrocarbons existence in the total coverage of the basin beyond the drilled locations and even in deeper parts where only seismic methods can access these depths. Secondly, a 3D view of the evolution of the basin through geological time is produced. Thirdly, it follows physical and chemical laws. And eventually, the integration and the iterative modelling of different types of data (geological, geochemical and geophysical) are a means of control each other.

In the context of basin modelling, special attention needs to be given to the thermal history of the basin, which is directly related to the maturation of source rocks. Therefore, optimal source rock maturity and hydrocarbon generation estimates require accurate thermal boundary conditions.

Prinos-Kavala basin is the only geological area in Greece where oil and gas are being produced for more than twenty years. The geology and stratigraphy of this particular offshore area are very well-known because many geological and geophysical surveys and studies have been conducted due to the high interest for hydrocarbon exploration. This study focuses on the thermal modelling of petroleum source rocks in three specific well locations within Prinos-Kavala basin in order to reconstruct the thermal history of the source rocks and evaluate the level of maturity of the organic matter contained in the examined source rocks. The software PetroMod by Schlumberger was used to construct 1D models for the three selected locations within Prinos-Kavala basin.

## 1.2 STUDY AREA

### 1.2.1 Geographical location

The Prinos-Kavala basin (Figure 1) is an offshore basin located in Kavala bay in the northern Aegean Sea. It is bounded to the north by the city of Kavala on the mainland of north Greece and to the southeast by the island of Thassos. Whereas, it is open to the Aegean Sea to the southwest. Its bathymetry reaches smaller than 50m throughout the whole extent of the basin, shallower than the bathymetry of the trench (between Chalkidiki and north Sporades) of the north Aegean Sea, which reaches about 1500m (Kiomourtzi, 2016).

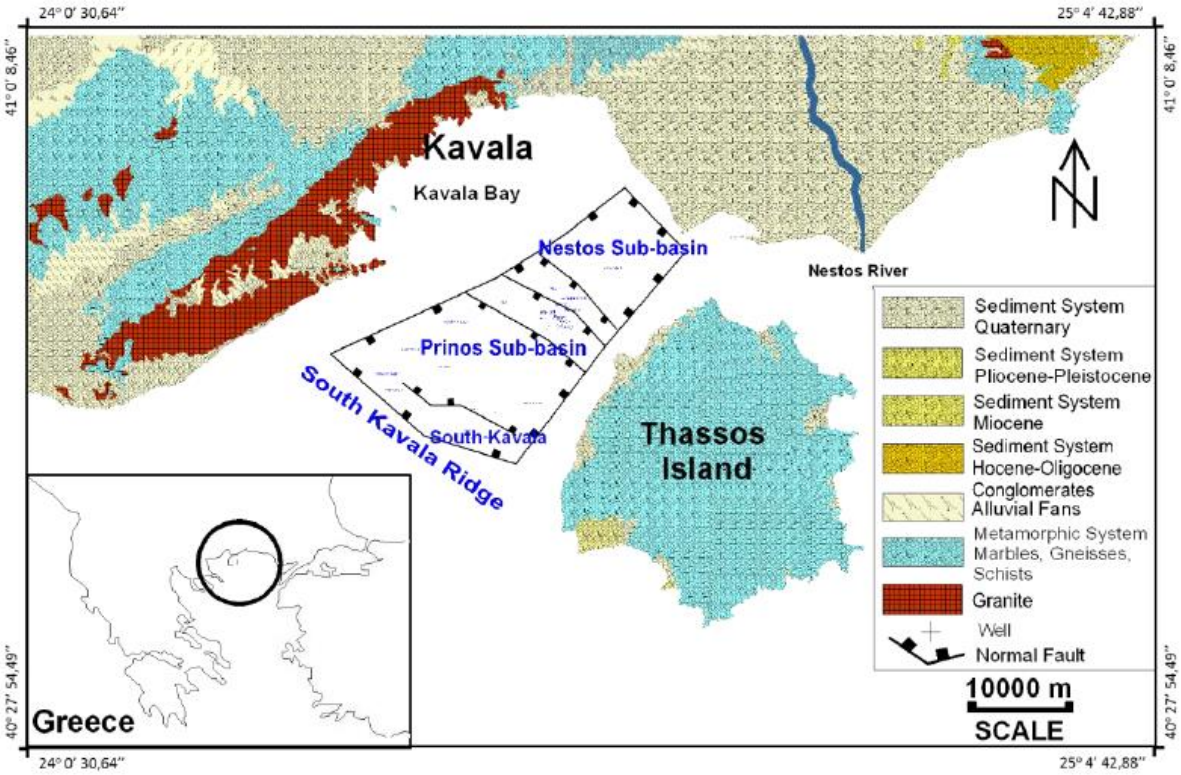


*Figure 1: Geographical overview map of the Prinos-Kavala basin (revised from Kiomourtzi et al., 2007, 2008).*

The Prinos-Kavala basin is a small scale elongated shallow marine basin, which is developed in NE-SW direction, its area is about 275km$^2$, and its length and width are 25km and 11km, respectively (Kiomourtzi, 2016). The basin is located between 40°41' and 40°54' parallels and 24°15' and 24°38' meridians east of Greenwich (Kiomourtzi, 2016).

Three locations were selected within the basin for the thermal history reconstruction. The first one is at the location of the PN-2 exploration well at the NE area of the basin, the second one is at the

position of well E-1 at the north side of the basin, and the last location is in well K-1, south of the basin (Figure 2).

*Figure 2: Map showing the location of the three wells within the basin (Google maps).*

### 1.2.2 Exploration and production history

Although the Prinos-Kavala basin is a young basin in terms of geological time scale, it presents special interest due to the fact that it is the only geological area in Greece that hosts proven hydrocarbon reserves that can be recoverable (Lalechos and Savoyat, 1977; Proedrou, 1979). Petroleum exploration in the Prinos-Kavala basin has a long history dating back to the seventies (Proedrou and Papaconstantinou, 2004) with several wells drilled in the area since then. The interest for hydrocarbons in the basin was steadily growing as the findings reassured the existence of hydrocarbons in several parts of the basin. The successful exploration activities led to the acquisition of new geophysical data on the basis of which several interpretations and studies of the structure, stratigraphy and lithology of the basin were carried out.

Hydrocarbon exploration in the offshore Prinos-Kavala basin has started in the beginning of the seventies. The first seismic campaign was conducted in the sea of Thrace in 1970, and in 1973, the first oil discovery occurred in Prinos basin. Although the biggest part of the basin is located offshore between the island of Thassos and the opposite mainland to the west, its north-eastern part is onshore in the plain of Nestos delta. The total area is about 800km$^2$. The above information was derived from Proedrou and Papaconstantinou (2004).

The continuous and extensive exploration activity in the specific area showed that the basin of such a young age fulfils all the requirements for the generation, migration and accumulation of enormous quantities of hydrocarbons (Proedrou and Papaconstantinou, 2004).

The acquired geophysical, geological and geochemical data can be analysed and turned into basin models to better understand the petroleum systems and predict the maturity level of source rocks (Hantschel and Kauerauf, 2009). Consequently, this indicates how important the reconstruction of the temperature distribution and history is, since it is directly associated with the maturation of source rocks and subsequently, the generation of hydrocarbons.

The information for the oil and gas fields in the area presented below are from the website of Energean Oil & Gas PLC (https://www.energean.com). The Prinos-Kavala basin consists of four fields as shown in Figure 3.

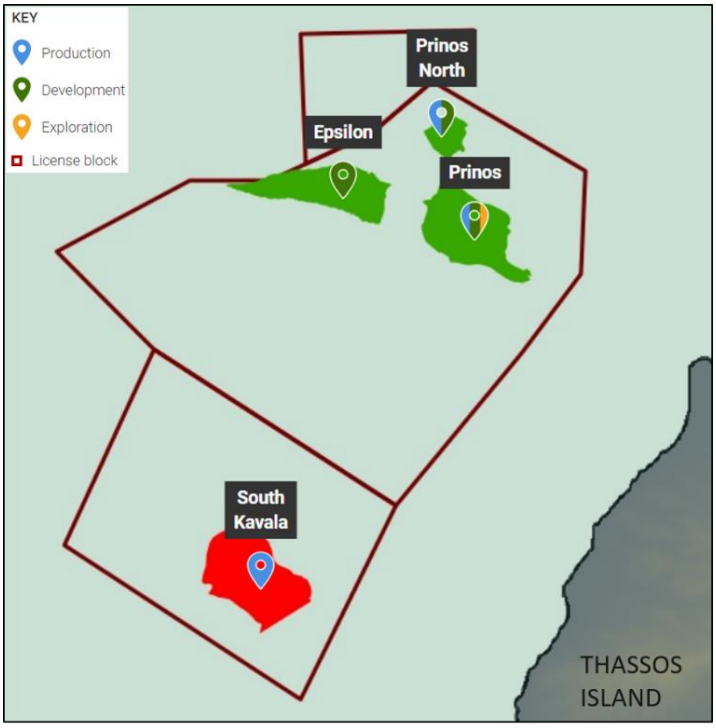


*Figure 3: Map of the license blocks and oil and gas fields in the Prinos-Kavala basin (https://www.energean.com).*

The first field is the Prinos Oil Field, which is the main structure in the basin and was discovered just a few years (1974) after the initial development of the basin (1970s). The field lies 8km north-west of the island of Thassos and 18km of the mainland of Northern Greece. It covers an area of 6km$^2$ and its bathymetry reaches 31m. During the summer of 2015, Energean Oil & Gas conducted a 340km$^2$

broadband 3D seismic survey over the field and the surrounding licenses. Prinos 2P (proven and probable) reserves have been audited at 17.8MMbbls of oil and 2.9Bcf, whereas 2C contingent resources (best estimate of contingent resources) have been recorded to 15.6MMbbls of oil and 4.9Bcf of gas. Production started in 1981, and now there are fourteen production wells in the field. The averaged oil production presents an increasing trend since 2015, which reached 3823bbls at 2017. The produced under-saturated sour crude oil has an API gravity that ranges between 27 and 30 degrees.

The second field is the Prinos North Oil Field at the north-east side of the basin. It was initially discovered as a potential exploration opportunity in 1976. The field was developed as a satellite field to Prinos field in 1996, then it was brought into production and produced until 2004 where it was interrupted due to water breakthrough and was redeveloped in 2008 by Energean Oil & Gas. Currently, there is only one production well. 2P (proven and probable) reserves have been independently audited at 3.3MMbbls of oil and 0.2Bcf. 2C contingent resources (best estimate of contingent resources) have been recorded to 2.4MMbbls of oil and 0.4Bcf of gas.

The Epsilon Oil Field lies at the north-west of Prinos field, and was discovered in 2000. Currently, it is at the stage of development. Exploration activity in the Epsilon Field started in the 1990s, and in 1997 a 3D seismic survey, which covered the whole area, mapped the anticlinic Epsilon structure. The field has 19MMboe 2P reserves.

The last field in the area is the South Kavala Gas Field, which was discovered in 1972, during the same exploration campaign that discovered the main Prinos Oil Field. During the period 1979-1980, it was developed as a remote satellite well. Since then, two production wells are active. Energean Oil & Gas holds 100% working interest in the South Kavala licence. Gas from the field is produced periodically and used for Energean's facilities needs in Kavala. The remaining gas reserves are about 2.6Bcf. The already depleted field is planned to be converted into an Underground Gas Storage (UGS).

## 1.3 DESCRIPTION OF THE FLOW OF THE THESIS

This MSc thesis outlines the procedure for the thermal history reconstruction, the analysis of the simulation outcome, the correlation with the maturity level of the petroleum source rocks and sensitivity analysis of the model.

Chapter 2 provides a geological understanding of the evolution of the Prinos-Kavala basin. Specifically, it gives information about the geology of the broader area, the stratigraphy and the tectonic structures of the Prinos-Kavala basin. In addition, it presents the petroleum system elements of the basin.

The third chapter describes briefly the theoretical background of the Basin and Petroleum System Modelling (BPSM) as well as the basic principles for the development of the models.

Chapter 4 summarizes the data available for building as well as calibrating the models and presents analytically the methodology that was followed.

The 5$^{th}$ chapter is referred to the simulation results. Moreover, it describes the findings from the sensitivity analysis that was carried out.

Chapter 6 presents the conclusions of this study.

# 2 GEOLOGICAL BACKGROUND PRINOS-KAVALA BASIN

This chapter will present the structural elements and evolution of the Prinos-Kavala basin as well as the stratigraphy of the area where the fields/prospects of interest are located. Emphasis has been given on the main area of study. The following subsections are based on Kiomourtzi (2016), in which a detailed and extensive overview of the regional geology and petroleum geology of the examined area is presented.

## 2.1 BASINS OF THE NORTH AEGEAN SEA

The region of the north Aegean Sea represents the back-arc basin of the subduction zone in the south Aegean, and since Miocene is one of the areas with the quickest rate of pull-apart tectonic activity in the world (Pe-Piper and Piper, 2001). This tectonic activity started from the Rhodope massif and migrated to the south (Brun and Faccenna, 2008), due to the progressive accumulation of continental and oceanic segments in the subduction zone, and the displacement of the trench to the south as a result of the detachment zones (Jolivet et al., 2013; Reilinger et al., 2010).

Other results of the large scale geodynamic processes that controlled the evolution of the north Aegean Sea region in the Miocene – Quaternary period are the exhumation of the metamorphic rocks of the Rhodope and Serbomacedonian zones (McKenzie, 1978; Dewey and Sengor, 1979; Dinter and Royden, 1993), the formation of basins, the extension of Anatolia's fault to the west during Pliocene, and the creation of north Aegean's trench.

The source of the sediments that filled all the Tertiary basins in the south and east edges of the Rhodope zone was the Rhodope massif. These basins are comprised of the younger Neogene basins of Orphanos, Prinos-Kavala and East Thassos, but also contain the older Paleogene basins such as the north part of Thrace basin in Greece as well as in Turkey (Maravelis and Zeilidis, 2013). Figure 4 shows all Tertiary basins that exist in the north Aegean Sea.

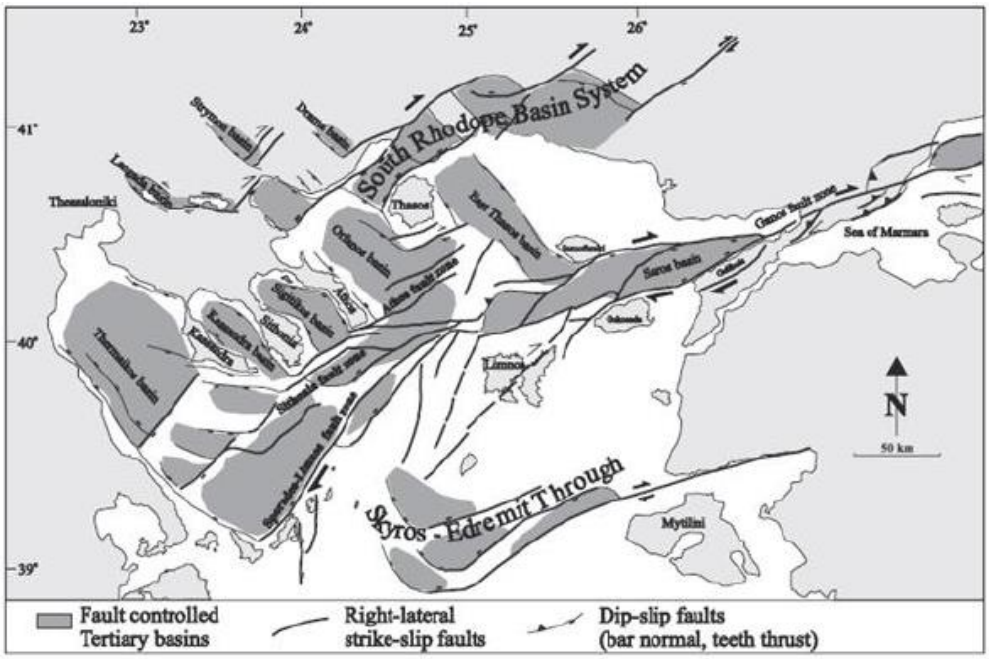


*Figure 4: Tertiary basins in the north Aegean Sea (Koukouvelas and Aydin, 2002).*

The formation of these basins is correlated with the exhumation of Miocene age granites (Brun and Sokoutis, 2007). This correlation has also been shown from geochemical analyses, which present the genetic connection between the magmatic intrusions and the tectonic evolution of the basins (Maltezou and Brooks, 1989).

One very important tectonic element that characterizes the broader area of the north Aegean Sea is faults, which act as limits to the Tertiary basins. Offshore seismic data reveal the normal character of these faults, and the presence of strike-slip faults. According to Koukouvelas and Aydin (2002), the faults in the area are divided into two groups. The first one contains normal or reverse faults with NE-SW and ENE-WSW direction, mainly with right-lateral horizontal displacement, and the second group includes normal faults with NW-SE direction and left-lateral horizontal displacement.

The big syngenetic (active during sedimentation) faults in the north Aegean Sea in combination with the magmatic intrusions increased the regional heat flow and as a consequence, geothermal fluids reached shallow depths and important geothermal fields were created (Kilias and Mountrakis, 1998; Papazachos and Scordilis, 1998).

The organic matter rich sediments that filled the north Aegean Sea basins (Rigakis et al., 2001), the high geothermal gradient of the area, due to the plutonic and volcanic intrusions, in combination with the isolation of the basins from the open sea during the Messinian are factors that play an important role to the interest of scientists and oil and gas companies for checking the suitability of the specific conditions for hydrocarbon generation and preservation.

## 2.2 PRINOS-KAVALA BASIN

The Prinos-Kavala basin is the only region in Greece currently producing commercial quantities of oil and gas, and therefore it is the most economically-significant basin in the country. The basin remains the focus of a considerable effort to find more hydrocarbons reserves and the key component for ongoing exploration is the up-to-date information on the geology of the basin.

The extensive exploration for hydrocarbons in the offshore area of the Prinos-Kavala basin and the information provided from well drilling data helped scientists to obtain a better understanding of the geotectonic evolution of the region. Several authors have presented this information and a complete model for the geology and the depositional model of Prinos-Kavala basin is available (Pollak, 1979; Proedrou, 1979; 1988; Proedrou and Sidiropoulos, 1992; Georgakopoulos, 1998; 2000; Proedrou, 2001; Proedrou and Papaconstantinou, 2004; Mertzanides et al, 2010; Kiomourtzi, 2007; 2008; 2009; 2016).

The taphrogenetic Prinos-Kavala basin is located at the southern edge of the Rhodope massif and was created in the north Aegean region during the Paleocene due to post-alpidic tectonics (Haubold, 2007). The area remained above the sea level during the Tethys cycle and only during the middle Miocene started subsiding as a result of the extensional post-alpidic tectonics which led to the breaking of the Aegean plate and the subsidence of the Rhodope massif (Proedrou, 1979). Marginal, long-extended and of large scale gravity faults of various angles and very often in echelon form surround the basin in NE-SW and NW-SE direction from the delta of the Nestos river in the north to the South Kavala ridge in the south (Proedrou and Papaconstantinou, 2004). Major internal faults striking NW-SE cross the basin and initiate the trapping mechanism. Roll-over trapping mechanisms are formed syngenetically in front of these faults as it shown in Figure 5 (Proedrou and Papaconstantinou, 2004).

The Prinos-Kavala basin is sub-divided into two smaller basins by a ridge located in the Ammodhis area (Proedrou, 1979). The southern sub-basin is deeper and is called Prinos basin, whereas the northern basin is shallower and is called Nestos basin.

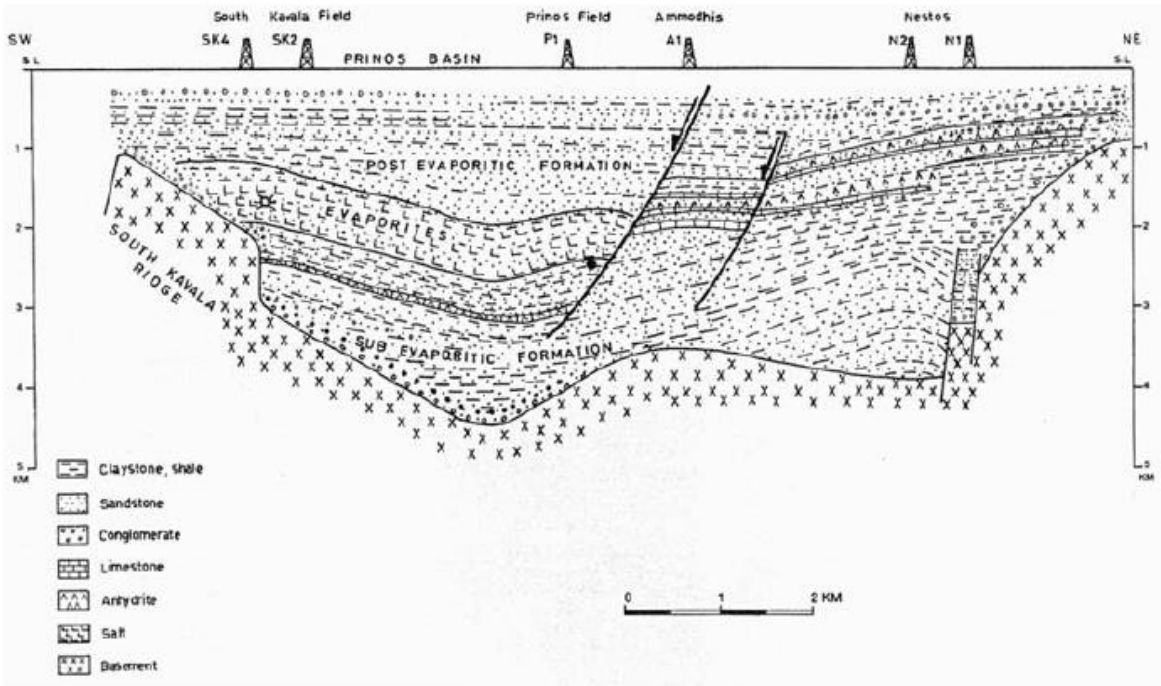


*Figure 5: SW-NE cross section of the Prinos basin showing the roll-over syngenetic faulting that formed the dome-like anticlines (Proedrou and Sidiropoulos, 1992).*

### 2.2.1 Geotectonic evolution

According to Kiomourtzi (2016), major stages of the geodynamic history of the area, which describe the paleo-evolutionary model of the basin, may be summarized in the following chronological order:

First, the formation of the basin started at the Lower-Middle Miocene where the activity of NE-SW normal faults created a restricted elongated basin. The first sediments in the basin are terrestrial, lagoonal shallow marine facies and consist of claystones, siltstones, marls, limestones, dolomites and coarse layers even breccia (Proedrou and Papaconstantinou 2004). The fine-grained sediments of this stage were rich in organic matter and constitute source rocks of hydrocarbons. Among the sediments of this stage, fine intercalations of salt and anhydrite are observed, revealing a hyper-saline environment of a restricted and protected basin.

At the second stage during the Middle Miocene, the basin gets bigger by extending to the NE due to the activity of NE-SW normal faults. The basin fills with deltaic deposits that seem to prograde to the SW indicating that the sediments supply is the paleo-Nestos river. The depositional environment becomes more deltaic and the deposits are still rich in organic matter.

During the third stage at the Middle Miocene, the basin extends to the SW controlled by NE-SW faults. It continues sinking and its size getting bigger especially in the central and southern part. The depositional environment is still reducing and hyper-saline. The clastic deposits of this stage are rich

in organic matter and the sedimentation rate keeps increasing. However, the presence of coals and red colour conglomerates in the north and south areas of the basin show a transition to terrestrial depositional environments in the periphery of the basin.

At the next evolutionary stage during the Middle-Upper Miocene, the basin keeps deepening and extending to the SW reaching its boundaries as they are today. This is the phase at which the turbidites of the Prinos Unit (is also referred as Prinos Equivalent) were deposited, they have well-developed channel and lobe facies to the central and NE parts of the basin prograding to fine-grained distal fan deposits to the SW, this shows a main NE direction of the source rock. The depositional environment is still reducing and hyper-saline with salt occurrences, and the sedimentation rate keeps increasing.

The fifth stage during the Messinian is characterized by further deepening of the basin. At this stage, quite important is the fact that the basin almost dries due to the Messinian Salinity Crisis that occurred in the Mediterranean Sea. The fall of the sea level caused the deposition of evaporites, which interchange with clastic sediments. Also, anticlinic trap structures were formed due to the re-activation of NE-SW faults and sliding surfaces, assisted by the plastic evaporitic layers which transferred sediments towards the central and deeper part of the basin.

The last stage begins at the Miocene-Pliocene boundary, in which the deposition of the evaporitic layers stops due to the flooding of the Mediterranean Sea that took place at this time period. Thus, there is again connection with the open sea and the basin turns from a restricted lagoon to a shallow marine basin. Deltaic clinoforms prograde to the SW indicating the connection with the Aegean Sea and the source of sediments, that is, the paleo-Nestos river.

Nowadays, the Prinos-Kavala basin is still a shallow marine basin (<50m sea bed), while its bathymetry changes rapidly southern of the South Kavala ridge (<250m sea bed), revealing active tectonic movements outside the basin boundary.

All the evolutionary stages of the Prinos-Kavala basin are displayed in Figure 6 as they were produced by Kiomourtzi (2016).

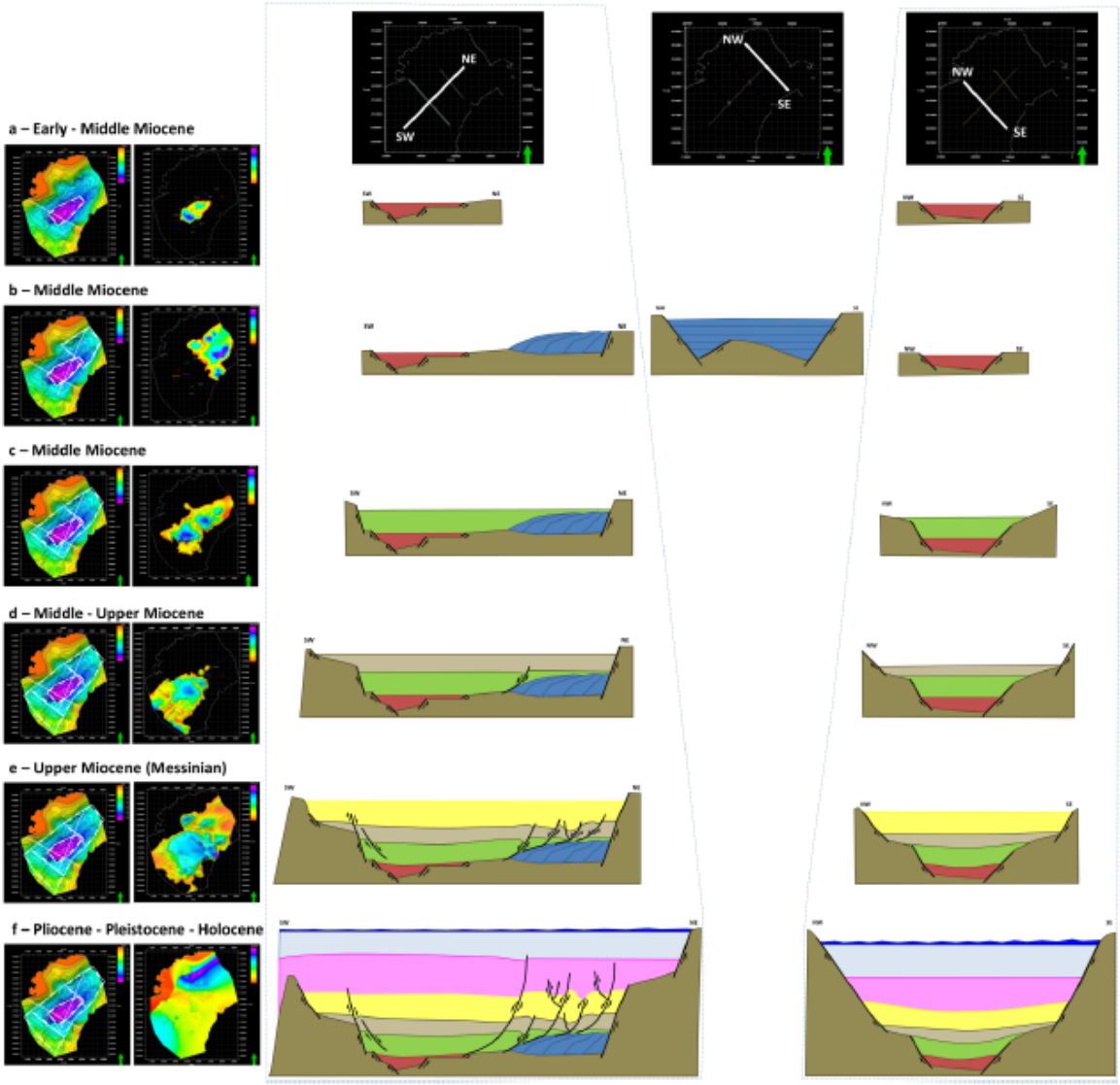


*Figure 6: Paleo geographical model of the Prinos-Kavala basin (Kiomourtzi, 2016).*

### 2.2.2 Stratigraphy

According to the findings that were derived from the study conducted by Kiomourtzi (2016), which are in accordance with several older studies (Pollak, 1979; Proedrou, 1979; Proedrou and Sidiropoulos, 1992), this section describes the sedimentary succession that has been deposited and preserved in the region of the Prinos-Kavala basin. Based on the above-mentioned authors, the stratigraphic model of the basin (Figure 7) is divided into three series above the basement: the Pre-Evaporitic Series, the Evaporitic Series and the Post-Evaporitic Series.

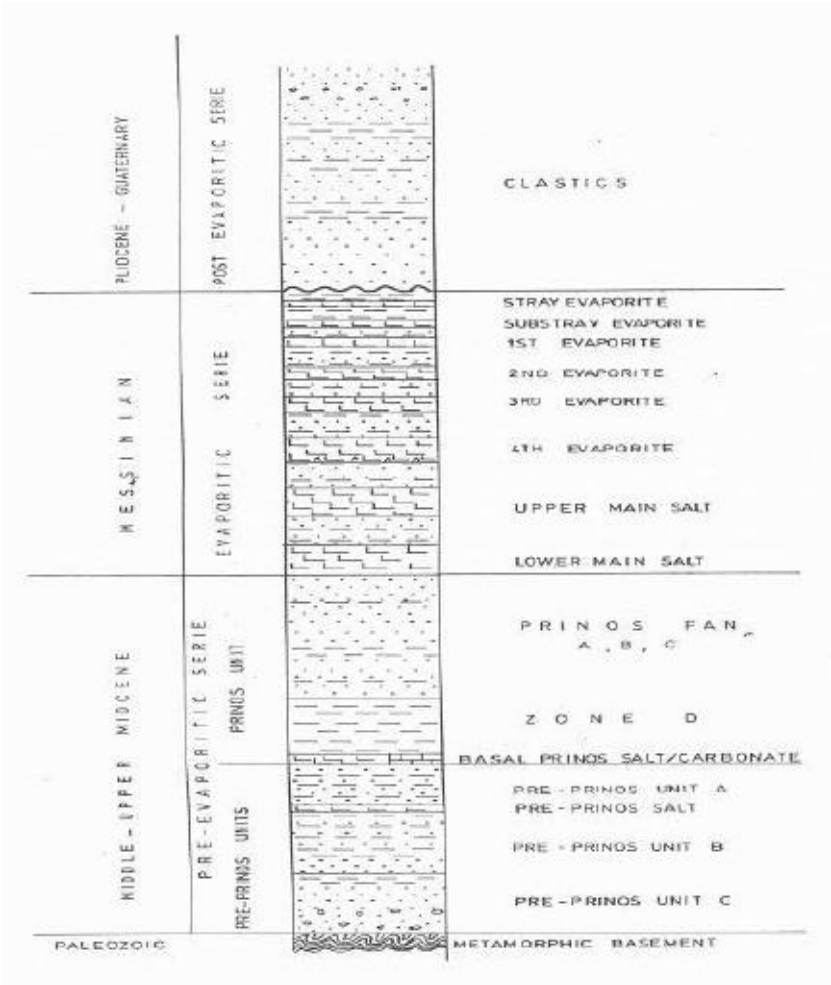


*Figure 7: Chronostratigraphic column of the Prinos basin (Proedrou and Papaconstantinou, 2004).*

The basement is of Palaeozoic age and consists of metamorphic rocks, mainly, gneiss, quartzite and dolomite marble (Proedrou and Papaconstantinou, 2004). The following presentations of the sequences from oldest to youngest are mainly based on the descriptions of Kiomourtzi (2016).

The **Pre-Evaporitic Series** starts with the break-up of the basin with the basal sediments and terminates just before the deposition of the Evaporitic Series (Proedrou and Papaconstantinou, 2004). It consists of lagoonal, shelf to terrestrial deposits of Miocene (Tortonian-Langhian) age. The upper part of the sequence is characterized by sub-sea deltaic sediments laterally prograding to turbiditic facies and distal fan deposits to the SW. The lower part contains reducing lagoonal deposits as well as shallow and even terrestrial sedimentation, indicating repeated changes of the sea level. This sequence encompasses the source rocks in a reduced environment, the reservoir rocks of the petroleum system of the basin, the main trap mechanism and the migration paths.

The Pre-Evaporitic Series comprises the Pre-Prinos 4, Pre-Prinos 3, Pre-Prinos 1 and Prinos Unit formations. The analysis of Kiomourtzi (2016) showed that the Pre-Prinos 4 formation is absent in the biggest part of the basin as it only exists on the deepest central part of the basin. Additionally, none of the wells, which were used in the study of Kiomourtzi (2016), drilled this formation.

The overlying formation of Pre-Prinos 3 is observed in the NE part of the basin and at this stage the sediments might have been deposited as pro-delta in front of the paleo-Nestos river (Kiomourzi, 2016). The formation consists of sandstones with intercalations of claystones, marl, siltstones and limestones in the deepest part, while gravels intercalations are observed in the shallower depths (Kiomourzi, 2016). Another characteristic of the Pre-Prinos 3 formation is the calcareous and anhydrite matrix as well as the presence of coals.

The next formation of the Pre-Evaporitic Series is the Pre-Prinos 1 unit, which has been deposited during the third evolutionary stage of the basin. At that time, the basin extends to the SW along its main axis. The formation may be separated into two parts. The lower part consists of marls and thin intercalations of sandstones, gravels, claystones, siltstones and limestones, without the presence of anhydrite matrix. Whereas, the upper part contains sandstones alternating with claystones and siltstones in anhydrite matrix. At the top of the unit, there is a thin salt layer.

The youngest formation of the Pre-Evaporitic series is the Prinos Unit, which extends mainly towards the SW of the basin. The formation consists of turbidites in the upper part, which have well-developed the coarse facies of channels and lobes mainly in the centre and east of the basin. To the west, the deposits are fine-grained distal fan deposits. The deeper strata of the unit consist of siltstones and often dolomites, which alternate with thin layers of sandstones and siltstones, whereas thin layers of anhydrite and gypsum are observed as well.

The overlying **Evaporitic Series** is related to the Messinian Salinity Crisis of the Mediterranean Sea and is present throughout the whole basin. It includes two facies, the first one is observed in the northern part of the basin and consists of alternating anhydrite and limestone layers interbedded with sandstones, claystones and marls. The second series is observed in the southern part and consists of seven to eight evaporitic cycles with increasing thickness towards the base of the section, alternating with clastic deposits. The top boundary of the series is an erosional unconformity of Miocene-Pliocene age. The Evaporitic Series acts as the seal rock of the petroleum system in the basin.

The **Post-Evaporitic Series** was deposited during Pliocene, Pleistocene and Holocene in a shallow open marine environment and is observed in the whole basin. This series acts as the overburden rock in the petroleum system, applying lithostatic pressure and leading to the quick burial of the deeper deposits

below the oil and gas window. The sediments that were deposited during Pliocene consist of alternations of sandstones, claystones and siltstones. The following sub-unit (delta bottom) of the Post-Evaporitic series was deposited during Pliocene-Holocene and is described by clinoforms prograding to the SW consisting of sandstones, claystones and siltstones alternating with each other. Finally, the unit of Pleistocene (sea bottom – top of delta), which continues depositing until now, contains mainly sands with smaller intercalations of claystones, siltstones and gravels.

### 2.2.3 Petroleum system

A petroleum system is defined by Magoon and Dow (1994) as: "*A petroleum system is a geologic system that encompasses the hydrocarbon source rocks and all related oil and gas, and which includes all of the geologic elements and processes that are essential if a hydrocarbon accumulation is to exist*."

The basic elements for a petroleum system are: source rock, reservoir rock, seal rock and overburden rock. Quite important are also the processes of trap formation and the generation, migration and accumulation of hydrocarbons (Magoon and Beaumont, 1999). The petroleum system elements are facies, which contained, transported or sealed the generated petroleum from one source rock (Hantschel and Kauerauf, 2009). As it is observed the names of these facies and processes show their function. These elements and processes must occur in the correct timing so as the organic matter in a source rock to be transformed into petroleum and then, to be preserved.

Figure 8 displays a SW-NE cross section of the Prinos-Kavala basin highlighting the elements of the petroleum system. Given the exploration and production of hydrocarbons in the area, the petroleum system in the Prinos-Kavala basin is known and active.

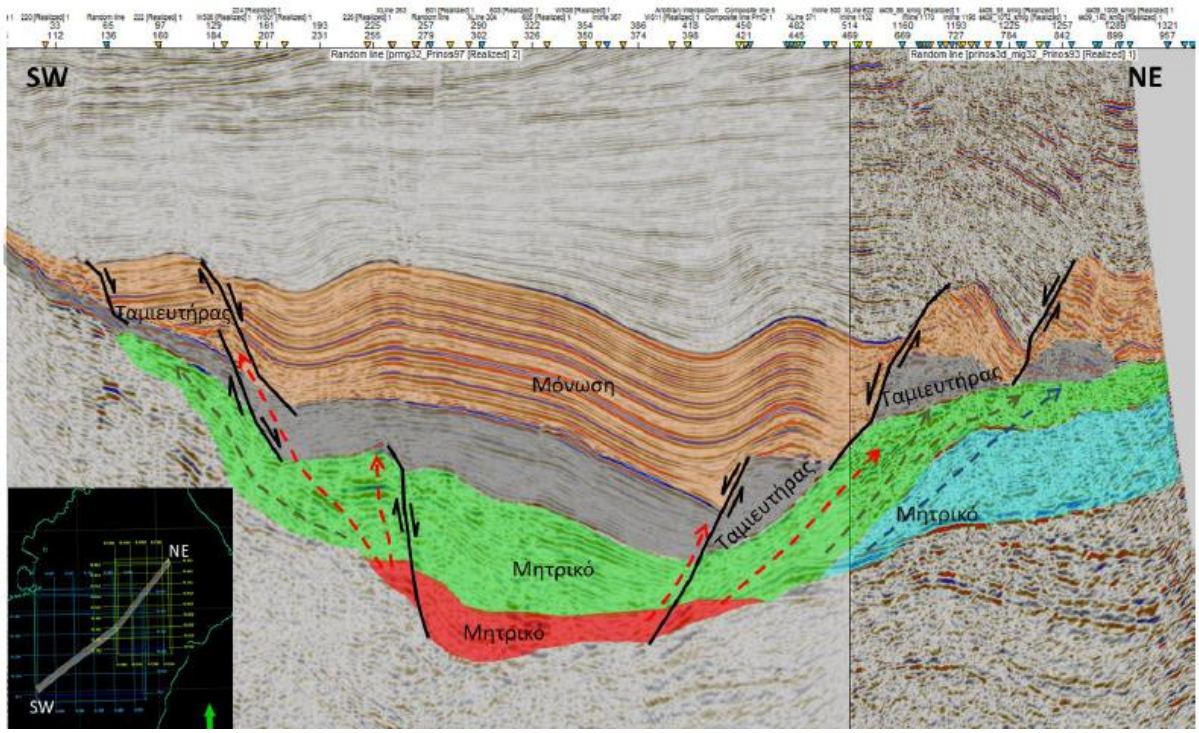


*Figure 8: SW-NE seismic section of the Prinos-Kavala basin presenting the active petroleum system. Source rocks are highlighted in red, green and light blue, reservoir rovks in grey and seal rocks in orange. Red dotted arrows indicate the migration pathways. (Figure from Kiomourtzi (2016))*

**Source rocks**

Several formations that have been recognized as potential source rocks in the Prinos-Kavala basin, mainly belong to the Pre-Evaporitic Series. The interpretation of seismic reflection data and the stratigraphy analysis of Kiomourtzi (2016) showed that the source rocks of the formations of Pre-Prinos 4, Pre-Prinos 3, Pre-Prinos 1, Prinos Unit (or Prinos Equivalent) and the even deeper formations of the Evaporitic Series have entered the oil window and can produce hydrocarbons. From the same results, it was drawn that the source rocks of Pre-Prinos 4 have already entered the gas window, which is reported at 4000m depth by Proedrou and Sidiropoulos (1992). Thus, these formations can also produce gas, for example, the gas field in South Kavala.

The designated source rocks deposited during the Lower-Middle Miocene in a dry, hyper-saline and strongly reducing environment. These conditions helped the organic matter to get preserved in carbonate and argillaceous sediments, hindering biodegradation (Kiomourtzi, 2016). The origin of the organic matter is mainly algal, plankton and bacteria, with some terrestrial input (Kiomourtzi, 2016). Regarding the depositional environment during that period, it was shelf (lagoonal-continental), whereas in North Prinos and Ammodhis to the NE, and in Peramos area to the west, the presence of lignite reveals a shallow marine, deltaic depositional environment in the periphery of the basin (Kiomourtzi, 2016). The lignite layers to the west could potentially be considered as secondary source

rocks (Kiomourtzi, 2016). Finally, the studies of Georgakopoulos (1998) and Kiomourtzi (2016) regarding the TOC index inferred that the sediments are rich in organic matter throughout the entire basin.

In general, the kerogen in the area is characterized as thermally immature except for some sporadic indications of early mature to mature kerogen in the fields of North Prinos, Prinos, Kallirachi and in the area of well P-4. Specifically, high level of maturity is observed in South Kavala field and in the area of well P-4, whereas low level of maturity is observed in North Prinos field.

The oil window is set in the depth range of 2600-2800m by Kiomourtzi (2016). However, it has been set at shallower depths by older studies, for example, just below 2600m (Georgakopoulos, 1998) or at 2500m (Proedrou and Sidiropoulos, 1992).

**Reservoir rocks**

The reservoir rocks in the Prinos-Kavala basin consist of the turbiditic deposits of the top section of the Pre-Evaporitic Series, which filled the basin under dry, hyper-saline and strongly reducing conditions in a coastal to shelf depositional environment (Kiomourtzi, 2016). According to palynology and nannofossils studies (Kavala Oil records), their age is determined from the Middle to Upper Miocene (Tortonian-Langhian). The work of Kiomourtzi (2016) showed that due to the proximity of the main feeder channel of the basin, and the high energy sedimentation, the reservoir rocks at the NE part of the basin are of good quality, wide lateral extension and large thickness, whereas the reservoir rocks at the SW part of the basin are of poor quality, limited lateral extension and small thickness. Moreover, Kiomourtzi (2016) found that secondary reservoir rocks of limited lateral extension are suggested to have been developed along the southern boundaries of the basin, as well as at the periphery of the deepest stratigraphic units of the NE parts of the basin.

**Seal rocks**

The sealing rocks in the petroleum system of the Prinos-Kavala basin belong to the Evaporitic Series, which is related to the Messinian Salinity Crisis in the Mediterranean Sea (Proedrou, 1988). The Evaporitic Series extends to the entire basin and constitutes the sealing capacity and the plasticity so as the hydrocarbons to be kept in the underlying formations. The sediments of this sequence filled the basin under hyper-saline, reducing conditions in a lagoonal depositional environment, with rare events of fresh water and terrestrial deposits (Proedrou, 1979; Ioakim et al., 2005). Within the Evaporitic Series, evaporites of varying thickness and facies alternate with clastic layers indicating active tectonic activity and changes in the sea level (Proedrou, 1979; 2001; Roussos, 1994; Proedrou and Sidiropoulos, 1992; Proedrou and Papaconstantinou, 2004; Kiomourtzi, 2016). To the NE, the

Evaporitic Series changes to calcareous facies (Proedrou and Papaconstantinou, 2004) in which marl and limestone layers provide now the sealing capacity, which at this part has limited efficiency (Kiomourtzi, 2016). Finally, Kiomourtzi (2016) suggests that an additional sealing rock is the claystone layers that separate structures with different fluids (hydrocarbons of different quality, water and oil, etc.)

**Overburden**

The function of the overburden rock, based on Magoon and Dow (1994), is to thermally mature the source rock. This was achieved in the Prinos-Kaval basin by the rapid sedimentation and the constant basin subsidence, which caused the quick burial of the source rocks and their entrance to the oil and gas windows (Kiomourtzi, 2016). Moreover, the organic matter and the produced hydrocarbons were preserved due to the reducing environment through all evolutionary stages of the basin, until the accumulation process (Kiomourtzi, 2016).

**Migration-Trapping**

In the Prinos-Kavala basin, faults play a key role in controlling hydrocarbon migration pathways. The generated hydrocarbons migrated from the deeper source rock formations in the centre of the basin to the periphery of the basin, in every direction, mainly through the faults (Kiomourtzi, 2016). These intra-basin faults were activated on different stages during the evolution of the basin, providing migration paths from the sources to the traps along different directions each time (Kiomourtzi, 2016). Consequently, one migration path pattern fed the sweet oil accumulations to the NE and the west parts of the basin, another migration path pattern fed the sour and more immature oil of Prinos and Epsilon fields, and another migration path pattern fed the sweet gas South Kavala field (Kiomourtzi, 2016). In all cases, the migrated hydrocarbons were trapped in dome-like anticlines that were created by roll-over syngenetic faults (Proedrou and Sidiropoulos, 1992).

**Timing of petroleum system elements and processes**

For a petroleum system to exist, it is quite important, the petroleum system elements and processes to occur in the correct temporal sequence for a hydrocarbon accumulation to be possible (Dembicki, 2017). For instance, to capture the maximum amount of hydrocarbons, trap formation should occur before expulsion/migration (Dembicki, 2017).

According to Magoon and Dow (1994), the critical moment is defined as a point in time that best depicts the most generation-migration-accumulation of hydrocarbons in a petroleum system, which is selected by the investigator. The critical moment is usually the onset of expulsion/migration and is often estimated from basin model results (Dembicki, 2017).

In the case of the Prinos-Kavala basin, Kiomourtzi (2016) suggests the following regarding the “critical moment” element of the petroleum system. The source rocks are of Lower to Middle Miocene age, while the reservoir rocks were deposited during the Middle to Upper Miocene, and the sealing rocks are of Messinian age. The activation of intra-basin faults created the trap structures during the Messinian and continued to the Pliocene, while the hydrocarbon generation must have started at the Messinian-Pliocene boundary, when the source rocks (Pre-Prinos 4) gradually entered the oil window. During the Pliocene and Pleistocene, the overlying source rocks followed entering gradually the oil window. The migration paths provided by open fault systems allowed the generated hydrocarbons to move from the deeper central parts and accumulated them into the trap structures, which were already formed, mainly during the Messinian and the Pliocene. This process continues until now resulting in younger source rocks entering the oil window and thus, producing new hydrocarbons.

# 3 BASIN MODELLING BACKGROUND

This chapter discusses the principal concepts and processes involved in basin evolution and simulation. The main emphasis is given on the type of data needed to run the simulation as well as the considerations involved in defining and adjusting the conceptual model. They are presented according to the order of the steps that the modeller needs to follow in order to construct the model.

## 3.1 INTRODUCTION TO BASIN MODELLING

Modelling the history of a sedimentary basin requires primarily to understand all the geological processes and events that have occurred in the basin. However, this needs a wide variety of data, for instance, geological, geophysical and geochemical, in order to develop a comprehensive and quantitative expression of the basin history and evolution. In particular, this is performed by integrated basin analysis, which, through numerical modelling, shows the changes in the controls and the products created during the geological evolution of the basin. One of the products that has great economic interest is the petroleum accumulations, which are produced by the direct response of the basin deposits to geological events and processes.

Welte and Yalcin (1988) mention that the space-time continuum of generation, migration, and accumulation of hydrocarbons involves many complex, dynamic and multivariable processes, which occur during the long basin history and are part of integrated basin analysis. These processes are caused by progressive changes in physical conditions occurring during the basin history.

According to Welte et al. (1997), basin modelling is defined as the temporal reconstruction of basin history and refers to the procedure of establishing the sequential record of changes in controls and products, which have occurred during the geological history of a basin. In other words, basin modelling is the numerical procedure of dynamic simulation of geological processes over geological time spans in a basin. Basin models are simulated only forward because the processes occurring in a sedimentary basin are mainly irreversible, and thus can't be used in inverse modelling (Cross and Harbaugh, 1990). This means that the simulation starts from the oldest layers and continues to the younger ones until the present time. Several geological processes are calculated and updated at each time step of the simulation. As the diagram (Figure 9) of Hantschel and Kauerauf (2009) shows, the most important processes of them are the following: deposition, compaction, heat flow analysis, petroleum generation, expulsion, phase dissolution and accumulation.

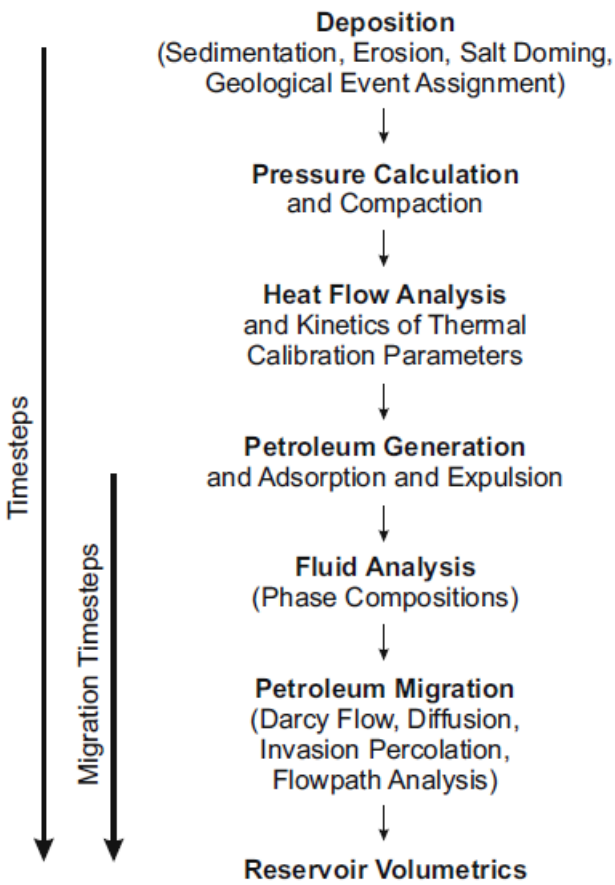


*Figure 9: Major geological processes in basin modelling (Hantschel and Kauerauf, 2009).*

The different type input data during basin modelling, which may come from wells, outcrops, seismic surveys or remote sensing surveys, are used in order to build a present-day conditions model, i.e. the final result of all processes having acted through geological time on the basin.

Based on Dembicki (2017), the main goals of basin modelling are to: 1) determine if, when, where, how much, and what type of hydrocarbons have been generated and expelled by a source rock; 2) to compare the timing of generation and expulsion with the timing of the trap development; 3) to trace potential migration pathways from source rocks to traps; and 4) to estimate the amount of hydrocarbons that are filling a trap. The achievement of these goals depends on the type of the basin model used and the availability and amount of data. Specifically, 1D models, which are based on a single point on the Earth's surface (e.g. a well), try to answer the question if and when hydrocarbon generation and expulsion may have occurred. 2D models use a cross section of the stratigraphy of the area and additionally to the previous predictions, possible vertical migration pathways may be predicted. A 3D model using a cube or other basin volumes tries to address, except for the previous

questions, if potential migration pathways in all three dimensions can be predicted and to estimate the volumes of migrated and trapped hydrocarbons.

For all types of basin models, the first and most basic step is the design of a conceptual model of the geological history of the area. The conceptual model provides the temporal framework, which is needed to structure the input data (Wygrala, 1988), that is, for the reconstruction of the burial and thermal histories. The conceptual model is also defined as a condensed description of the geological history of the basin (Welte and Yalcin, 1987). Therefore, it is directly related to the interpretation of geological, geophysical, and geochemical observational data placed in a temporal framework indicating how important role stratigraphic analysis plays.

This study focuses on 1D models. Thus, the migration timesteps of fluid analysis, petroleum migration and reservoir volumetrics are not relevant for this study.

## 3.2 BURIAL HISTORY MODELLING

One of the initial processes during basin modelling is the construction of a burial history of the area. The geological processes of deposition, and pressure calculation and compaction (Figure 9) are included in this stage. Based on Dembicki (2017), burial history simulates the sedimentation events represented in a stratigraphic column and consists of a depth-time plot that shows all the geological events. In particular, the curves on the plot portray tops/bottoms of formations and surfaces of unconformities, representing periods of deposition, erosion or even hiatus (non-deposition).

However, it should be taken into account that the formations thicknesses are not the same now and when the sediments were deposited. The weight of the overburden rocks causes some of the pore fluid to come out collapsing the pore space and reducing the thickness of the formations. This is known as compaction due to porosity reduction or mechanical compaction Dembicki (2017). Therefore, the sediments thicknesses must be corrected for compaction. Several researchers have developed empirical relationships for predicting changes in porosity due to compaction. All these relationships are based on the fact that different lithologies will have different initial porosities and different compaction rates with increasing burial depth. One of these relationships is presented on Figure 10, which shows how the porosity of different lithologies changes with increasing depth.

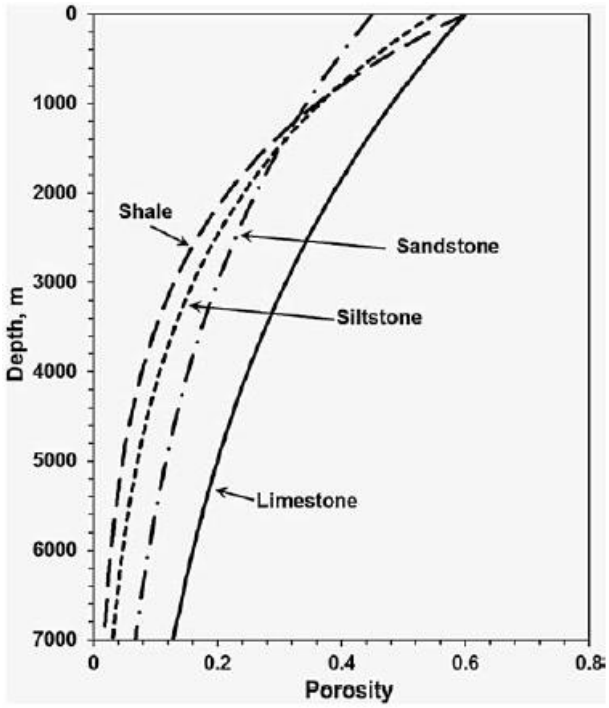


*Figure 10: Depth versus porosity plot for a series of lithologies based on the Sclater and Cristie (1980) exponential model using empirically determined initial porosities and compaction factors.*

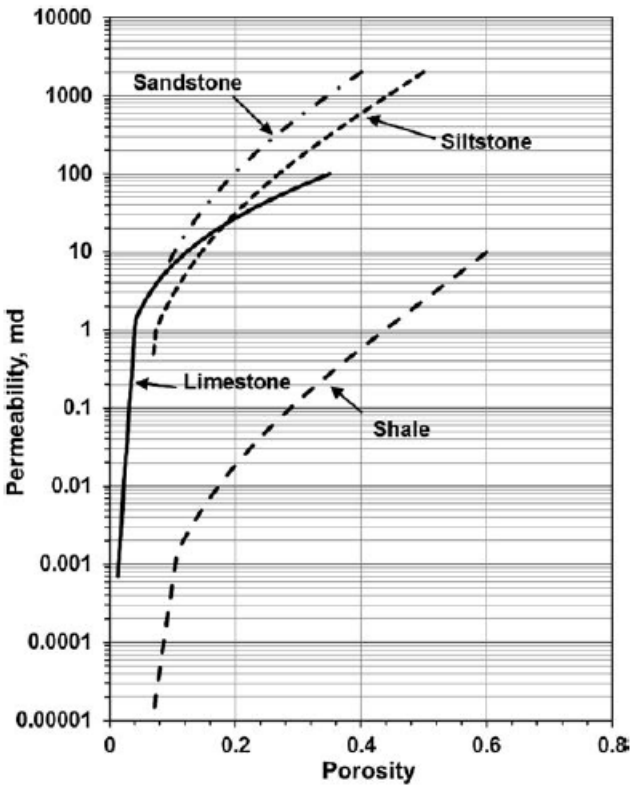


*Figure 11: Kozeny-Carman relationship of porosity with permeability (Ungerer et al., 1990).*

Nevertheless, another important factor that should be taken into consideration is permeability. Because for fluids to leave the rock due to the overburden weight, the sediment must have adequate permeability. The Kozeny-Carman equation (Ungerer et al., 1990) is the most common porosity-permeability relationship that is used in compaction models for the sediment and Darcy's Law is applied for the fluid flow rate prediction. Figure 11 indicates an example of porosity-permeability relationship that is used during compaction correction.

The correction for compaction is quite significant because it has a major impact on the modelling of maturation and hydrocarbon generation. Specifically, a not corrected curve is placed in shallower depth compared to a corrected curve in which the compaction of the overburden rocks has been taken into account. Shallower depth means that the sediments would have experienced lower temperatures resulting in lower level of maturity and less hydrocarbon generation, which is not the actual one if compaction has not been taken into account. Figure 12 presents the difference in a burial history curve for a horizon with and without compaction correction.

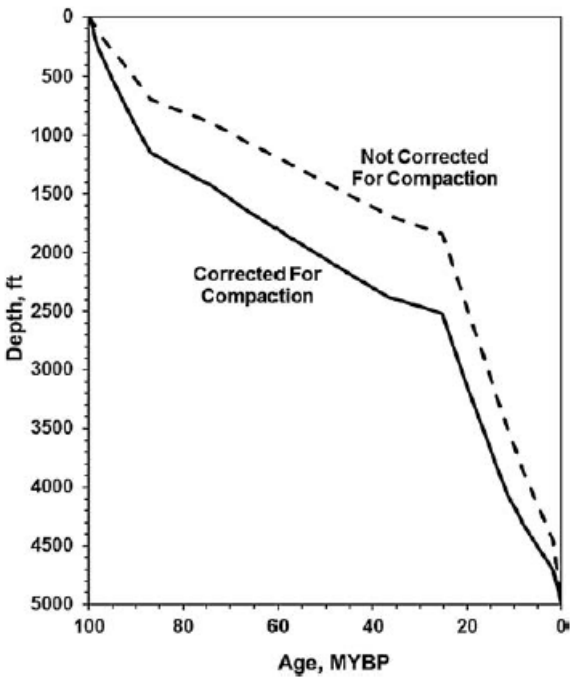


*Figure 12: An example of a burial history curve for a horizon with and without compaction correction (Dembicki, 2017).*

## 3.3 THERMAL HISTORY MODELLING

Thermal history modelling follows burial history modelling and is used in order to estimate the temperature history of stratigraphic layers in a sedimentary basin. Organic matter maturation and hydrocarbon generation are kinetic processes, which are controlled by time and temperature. Burial history modelling puts the stratigraphic sequence into a time-depth context. However, the stratigraphic sequence needs to be set in a time-temperature context so as the prediction of

maturation and generation to be feasible. This is achieved by thermal history modelling, which converts the depth component of the burial history to temperature. Dembicki (2017) mentions that thermal history modelling is a simulation of the heat flow and temperatures experienced by sediments in a stratigraphic column during their burial history, and is controlled by the heat flow, surface temperature, thermal properties of the rocks, intrusions of igneous bodies and circulating fluids.

Temperature is a very important parameter in basin modelling and special attention has been given to it by simulation programs. There are two methods for the approximation of the thermal history of a basin, i.e. the estimation of the paleo heat flow and paleo temperatures. The first method calculates the paleo temperature at a given depth from a given geothermal gradient and surface temperature, whereas the second method uses the heat flow at the base of the formation, thermal conductivity of rocks and surface temperature. The second method is mentioned as conductivity method.

The first methodology designs geothermal gradients for the present time and past geological times. One limitation of this methodology is associated with the linear geothermal gradients. In particular, geothermal gradients assume that the thermal properties of the rocks are constant with depth. But, this is not the case, because the thermal properties of the rocks change with depth. This is observed when the subsurface temperatures estimated from the geothermal gradients do not match with actual temperature measurements from wells. For this reason, it is more appropriate to approach the thermal history of a basin by applying the heat flow – conductivity method.

The heat flow – conductivity technique, due to the fact that is based on fundamental physical principles, it can produce complex and more realistic thermal histories in comparison to those created by the geothermal gradient method (Waples, 1984).

This technique requires as input data heat flow values for each geological event and each grid point of the model. Recent heat flow values can be taken by regional heat flow maps based on well data or surface measurements, and past heat flow values can be obtained by using analogies of the basin to be modelled with known plate tectonic situations (Welte et al., 1997). Therefore, the characterization of the basin in terms of plates tectonic framework is highly important as well as the usage of crustal evolutional models for the estimation of heat flow history.

## Heat flow analysis

Heat flow is the movement of heat from a body/region of higher temperature to a body/region of lower temperature. For a stratigraphic sequence, heat flow refers to the movement of the heat from within the Earth to the surface. Heat can be transferred by conduction, convection, and radioactive decay in sediments (Beardsmore and Cull, 2001; Hantschel and Kauerauf, 2009). Among the three

processes, heat conduction plays the primary role in the shallow lithosphere (Hantschel and Kauerauf, 2009), this is why affects more the analysis of heat flow. On the other hand, heat radiation is negligible in sediments, however, it should be taken into account in the deep parts of the lithosphere (Hantschel and Kauerauf, 2009).

As Hantschel and Kauerauf (2009) present, the conductive heat flow law states that a temperature difference between two locations causes a heat flow, q, and its magnitude depends on the thermal conductivity of the material and the distance between these locations. The heat flow law is described by the equation:

$$q = -\lambda \cdot \nabla T$$

where, $\nabla T$ is the temperature gradient, and $\lambda$ is the thermal conductivity vector which has two independent components, $\lambda_h$, the conductivity along a geological layer and $\lambda_u$, the conductivity across a geological layer (Hantschel and Kauerauf, 2009).

At any location, the main direction of the heat flow vector is along the steepest decrease of temperature from a specific location (Hantschel and Kauerauf, 2009). In the lithosphere, it is the difference between the surface or the sediment water interface (in case of offshore location) temperature, and the temperature in the boundary of asthenosphere and lithosphere (Hantschel and Kauerauf, 2009). As it can be observed from the equation of the conductive heat flow law, the heat in-flux into the sediments is controlled by the average thermal conductivity and the thickness of the mantle and crustal layer (Hantschel and Kauerauf, 2009). The lower boundary condition of the heat flow analysis in the sediments is described by this heat flow into the sediments, whereas the upper boundary condition is the sediment water interface temperature (SWIT) (Hantschel and Kauerauf, 2009).

In the context of thermal modelling, heat flow analysis is considered as two problems, the first one is the calculation of the heat in-flux into the sediments and then, the calculation of the temperature into the sediments (Hantschel and Kauerauf, 2009). Figure 13 portrays these two aspects of heat flow analysis.

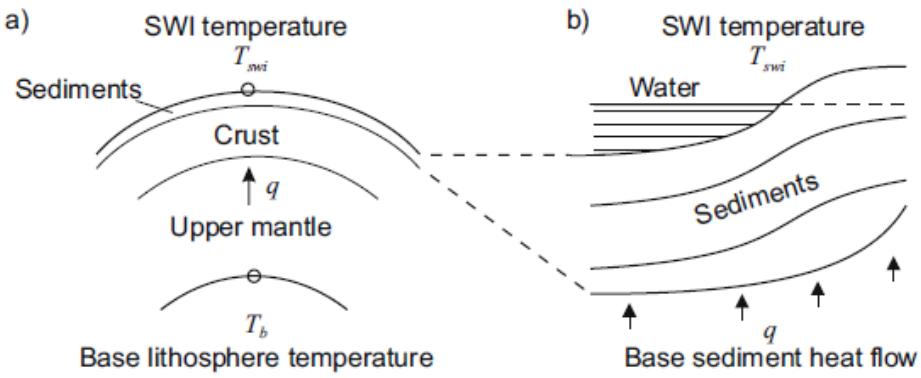


*Figure 13: Two main sub-problems of heat flow analysis, (a) the calculation of the heat in-flux into the sediments and (b) the subsequent calculation of temperature into the sediments (Hantschel and Kauerauf, 2009).*

1D models assume that all heat flow vectors are directed vertically. The simplest case of 1D models are those under steady state conditions. In this case, the conductive heat flow is constant with depth, and the local geothermal gradient is inversely proportional to the local thermal conductivity (Dembicki, 2017). But, in basins there are only brief periods of steady conditions, these are when heat flow equilibrium is achieved again after changes during the sedimentation. Changes of a thermal boundary condition, geometry, properties or temperatures induce transient heat flow conditions and thus, the conductive heat flow is not constant any more with depth (Hantschel and Kauerauf, 2009). Some cases of these changes are the following: rapid deposition, erosion, magmatic intrusions, salt domes and radiogenic sediments.

Regarding the boundary conditions of heat flow analysis, it should be noted that they may change through time. Surface temperature or sediment water interface temperature may be affected by changes in the water depth, and basal heat flow is affected mainly by geological events as it was mentioned previously.

In basin modelling, crustal models are used to estimate the basal heat flow in sediments. McKenzie (1978) proposed the uniform stretching model. This model, which is quite well-known and is frequently used in basin modelling, is based on the fact that heat flow changes with time. It consists of two phases, the first one is a stretching phase with constant thinning of the crust and the upper mantle, and the second phase is described by a cooling event with restoration of the original thickness of the lithosphere (Hantschel and Kauerauf, 2009). A stretching factor, β, which is the ratio of the initial thickness to the final one, describes the total thinning of the layers (Hantschel and Kauerauf, 2009). Therefore, the greater the amount of stretching, the greater the amount of crustal thinning and higher heat flow (Dembicki, 2017).

## Surface temperatures

Surface temperatures or sediment water interface temperatures (SWIT) constitute the upper boundary condition of heat flow analysis.

In onshore areas, the surface temperature can be estimated from the mean annual surface temperature (Gretener, 1981). However, it should be noted that while calculating the mean annual surface, factors like solar heating at the surface, climatic conditions, and the thermal properties of the surface rocks need to be considered (Dembicki, 2017). Otherwise, the temperature value will not be accurate.

In the case of offshore areas, the sediment water interface temperature varies with depth and latitude (Pickard, 1963). Beardsmore and Cull (2001), suggested an equation, which uses the latitude and the depth to estimate the sediment water interface temperature with an error bar of 2°C.

Welte et al. (1997) summarize the requirements for an approximation of the surface temperature of the SWIT. These are: 1) the paleo latitude position of the basin through geological time using paleo geographic maps, 2) the mean annual paleo air temperatures from maps of global paleo temperature distribution for a given geological time slice, 3) contemporary surface temperatures, and 4) contemporary sediment/water interface temperatures. Regarding the mean annual paleo air temperatures, they can be derived from the Wygrala (1989) chart in which mean surface paleo temperatures are plotted against latitude and geological time between the Carboniferous and the recent past.

## Thermal conductivity

Thermal conductivity is a measure of the ability of a material to transfer thermal energy via conduction. When a material or a substance is characterized as a good conductor, this means a high heat flow, or there is a small temperature difference for a given heat flow. On the contrary, large temperature differences (i.e. high geothermal gradients) indicate low thermal conductivities. The material in this case is a good insulator.

Thermal conductivity is a dynamic quantity, therefore, it must be defined in terms of the matrix and fluid components of the sediments. The matrix thermal conductivity of a specific lithology do not change with depth, whereas the bulk thermal conductivity changes, as the porosity and the fluid content will be different with depth. As most bulk property (e.g. density, heat capacity) values, the bulk thermal conductivity derives from the appropriate mixing of the matrix and fluid components of the sediment. Here, whether the mixture of lithologies describing the sediment is defined as homogeneous or layered plays a quite significant role because it affects the mixing rules between the

matrix and fluid. Sedimentary rocks are anisotropic with higher horizontal thermal conductivity than vertical. The thermal conductivity is a symmetrical tensor with six independent components, but often is considered with only two, the conductivity along a geological layer and the conductivity across a geological layer (Hantschel and Kauerauf, 2009).

During basin modelling, the values of thermal conductivities are assigned by the software based on the lithologies that have been imported in the model. However, these values are estimates and not accurate, therefore, they can be calibrated with measured temperature data in order to optimize the heat flow data (Waples, 1994).

## 3.4 MODELLING MATURATION, GENERATION AND EXPULSION

The next step in basin modelling is the simulation of the maturation, hydrocarbon generation and expulsion from the source rocks. Maturation modelling predicts the level of maturation of a stratigraphic layer and also builds its maturation history. Usually, it is expressed as estimated vitrinite reflectance in % Ro equivalence. Modelling of hydrocarbon generation aims to predict how much, what type and when oil and gas generated in the source rock. At the end, expulsion modelling predicts how much and when the generated hydrocarbons expulse from the source rock to a carrier bed. Two main inputs are needed for expulsion modelling, these are the output from the generation modelling and the predicted porosity and permeability.

### 3.4.1 Maturation modelling

Maturation, or thermal maturation, is the process of chemical changes in sedimentary organic matter under the influence of increasing temperature over geologic time due to burial (Dembicki, 2017). Therefore, the technical term maturation is used in petroleum geochemistry to address thermally induced changes in the organic matter during catagenesis (Welte et al., 1997).

In coal petrography, coalification is the corresponding term of maturation, which follows peat diagenesis and shows increases in the coal rank (Welte et al., 1997). White (1915) noticed that the limits of oil occurrence can be related to the rank of associated coal beds. Coal rank was the first maturity indicator applied in petroleum geochemistry (Welte et al., 1997).

Vitrinite is a type of kerogen particle, or maceral, formed from humic gels that are thought to be derived from the lignin-cellulose cell walls of higher plants (Teichmuller, 1989; Dembicki, 2017), and except for coals, it is also very common in source rocks. Vitrinite reflectance is a measure of the percentage of incident light reflected from the surface of vitrinite particles in a sedimentary rock and is referred to as %Ro (https://wiki.aapg.org/Vitrinite_reflectance). The increase of vitrinite reflectance

with increasing time and temperature is used for determining a coal's rank (Teichmuller, 1982a), but also is used as an indicator for assessing the maturation level of kerogen.

The fact that vitrinite particles are abundant in sediments led to the application of vitrinite reflectance as 1) a maturity parameter estimating the stage of oil generation mainly from macerals other than vitrinite, and 2) a calibration tool for numerical simulations of temperatures histories in sedimentary basins (Lopatin, 1971; Waples, 1980).

Nowadays, the most widely accepted thermal maturation indicator is the reflectance of the vitrinite maceral in coal, coaly particles, or dispersed organic matter (Hantschel and Kauerauf, 2009).

Since 1970, the early days of basin modelling, several methods have been suggested for predicting thermal maturation. But, as Dembicki (2017) mentions only at early 1990s, a number of kinetic models were suggested for predicting vitrinite reflectance. These models include Burnham and Sweeny (1989), Larter (1989), Sweeny and Burnham (1990), and Suzuki et al. (1993). The EASY%Ro model of Sweeny and Burnham (1990) is the most widely used. Dembicki (2017) mentions that this model is a robust model for estimating vitrinite reflectance in various basin settings and can handle difficult circumstances like igneous intrusions and circulating hydrothermal fluids.

### 3.4.2 Generation modelling

Hydrocarbon generation is the process of change of the kerogen contained in a sediment to oil, gas, and a carbon-rich residue due to the influence of time and temperature (Dembicki, 2017). Figure 14 shows the simple (3 component) model of generation of oil, gas, and a carbon-rich residue. As it is observed in Figure 14, the generated oil can further decompose to form more gas and carbon-rich residue. This simple model is also the basis for the concept of oil window. Although the simple model gives a good estimate of hydrocarbon generation, more accurate approximation is achieved by considering models with a series of parallel reactions.

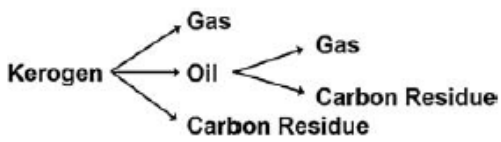


*Figure 14: The simple (3 component) model for kerogen generation of oil, gas, and a carbon residue (Dembicki, 2017).*

Main input for hydrocarbon generation modelling is the burial and thermal histories in order to simulate the oil and gas reactions in source rocks. After Tissot (1969), the reactions that produce oil and gas have been observed in nature to approximately follow first-order Arrhenius kinetics.

The first-order Arrhenius kinetics assume that the reaction is irreversible. Basically, the change in the concentration of the reactant $(X)$ over time $(dX/dt)$ is governed by the reaction rate, $k$, as $dX/dt = -kX$ . The reaction rate is equal to (Ungerer, 1990):

$$k = Aexp(-E/RT)$$

where A is the frequency factor, that is, a statistical estimate of how often the reaction can take place, E is the activation energy, i.e. the amount of energy required to overcome the free energy barrier in order for the reaction to happen, R is the universal gas constant, and T is the temperature. The comparison of the influence of time and temperature, indicates that the exponential relationship of temperature is highly significant making temperature the primary factor controlling the reaction, in contrast to the linear relationship of time.

Dembicki (2017) points out that a better understanding of hydrocarbon generation from different kerogen types is obtained by comparing the kinetic parameters for each kerogen type. These parameters are estimated experimentally. According to Tissot et al. (1987), the main activation energies for the series of parallel reactions for a specific kerogen type are determined by methods which artificially mature kerogen by a series of laboratory heating experiments. Regarding the main kerogen types, several works have been conducted over the years determining the kinetic parameters for hydrocarbon generation. Most of them are available in basin modelling software.

Also, it should be mentioned that although oil accumulations are formed only from oil-prone kerogens, gas accumulations can be derived from gas-prone and oil-prone kerogens. Additionally, as it is mentioned in Dembicki (2013), oil-prone source rocks after the completion of the generation of oil, can produce more gas than the gas-prone source rocks.

Finally, apart from the burial and thermal histories, hydrocarbon generation modelling requires source rock input parameters, as well. These are, the total organic carbon (TOC), which provides a measure of the total organic matter, the hydrogen index (HI), which gives the amount of hydrocarbon that can be generated with respect to the TOC, and the type of the kerogen(s) so as the correct kinetic parameters to be applied.

### 3.4.3 Expulsion modelling

Expulsion is the process during which hydrocarbons move out from a source rock into the pore spaces, forming a continuous oil-wet migration pathway along which hydrocarbons can leave the source rock (Dembicki, 2017). Overpressure of the pore fluids (water and petroleum) due to compaction, tectonic stress, thermal expansion of water, and hydrocarbon generation helps expulsion process (Dembicki, 2017).

Based on Dembicki (2017), the most important factors that affect hydrocarbon expulsion are: the amount and type of organic matter in the source rock, the sediment type, and the sedimentation rate. In particular, the minimum saturation is reached sooner when the amount of organic matter is large. Some kerogen types give more hydrocarbons than others, and different kerogen types produce hydrocarbons at different points in their time-temperature history, affecting the timing that the minimum saturation is reached. One important factor is lithology, which controls the porosity and permeability evolution of the sediment, and subsequently the pore needed to be filled by hydrocarbons. Finally, the sedimentation rate can influence the thermal history, overpressure, and rate of hydrocarbon generation.

In 1D basin modelling, the main expulsion model is the porosity saturation model (Dembicki, 2017). Based on hydrocarbon generation and porosity reduction/compaction model results, the expulsion model uses an estimate of the hydrocarbon saturation of the pore spaces in a source rock (Ungerer et al., 1988b).

# 4 DATA AND METHODOLOGY

During current thesis project, 1D basin modelling is performed by using three exploration wells (Figure 2) from the Prinos-Kavala basin. In this study, it should be noted that the modelling is focused on maturation, generation and expulsion processes, which play an important role. The steps beyond expulsion process (Figure 9) will not be considered in this study as they are not part of the aim of the project.

This section will describe the entire procedure followed for building the structural model and running the simulation using Schlumberger's PetroMod (version 2017.1) petroleum systems modelling software. "PetroMod petroleum systems modelling software combines seismic, well, and geological information to model the evolution of a sedimentary basin. The software predicts if, and how, a reservoir has been charged with hydrocarbons, including the source and timing of hydrocarbon generation, migration routes, quantities, and hydrocarbon type in the subsurface or at the surface conditions" (https://www.software.slb.com/products/petromod).

The data requirements for 1D basin modelling include depth surfaces of the imported formations, lithological properties, a time-line of tectonic events, source rock characteristics, boundary conditions, and calibration data.

The majority of the main input parameters for building the models have been given by Dr. Paschalia Kiomourtzi from Energean Oil & Gas. The provided data constitute data as well as results from the work that she conducted for her doctoral thesis. In particular, her work was about the study of the North Aegean Sea basins, focusing on Prinos-Kavala basin. Therefore, a complete research of the basin was conducted by Kiomourtzi (2016), who applied a variety of different methodologies (e.g. sedimentological research, well logs correlation, seismic interpretation, organic geochemical research, etc.) and integrated their individual results, in order to define in detail the geological evolution of Prinos-Kavala basin as well as the conditions that led to its active petroleum system. Consequently, Kiomourtzi (2016) provides a comprehensive present-day model of the study area representing the final result of all processes acting on the basin throughout geological time.

## 4.1 MAIN INPUT PARAMETERS

### 4.1.1 Depositional events

The first step for building the model is to create a depth-based structural model of the area under investigation. In particular, this stage involves defining stratigraphic surfaces in the form of formation tops and layer thicknesses. PetroMod (version 2017.1) gives the possibility to the modeller to enter

either the top depth or the thickness of the layer, and the software calculates the other. All types of events (depositional, erosional, hiatus) were imported in chronological order, with the youngest event at the top of the table and the oldest at the bottom. In this study, events were entered using the top depths.

The depth information for the vertical wells PN-2, E-1, and K-1 were obtained from the composite lithostratigraphic columns of the wells, which were constructed by Kiomourtzi (2016) using the results from the lithological analysis and wells correlation. Stratigraphic intervals that had great thickness were subdivided into smaller, in order to achieve more representative results and the required level of detail.

**PN-2**

Well PN-2 has a total vertical depth (TVDSS) of 2722m, and based on its lithological description, it was divided into 12 depositional events. These events possibly reach up to the depth of the formation of Pre-Prinos 1. In particular, three layers describe the Post-Evaporitic series, 5 layers the Evaporitic series, and 4 the Pre-Evaporitic Series. However, due to available information from wells in the nearby area and interpreted seismic data, one more depositional event was imported beyond 2722m depth. This layer, which is on top of the basement, possibly reflects the unit of Pre-Prinos 3. A detailed overview of all layers of the PN-2 well can be seen in Figure 15.

**E-1**

Well E-1 has a total vertical depth (TVDSS) of 2954m and was split into 21 depositional events up to the end of the well. 2 of them belong to the Post-Evaporitic series, 17 to the Evaporitic series and 2 to the Pre-Evaporitic series. As in PN-2, the model of well E-1 was extended deeper than 2954m depth by adding two more layers using information from adjacent wells and interpreted seismic sections. The first layer seems to be part of the Prinos Unit, and the second one possibly belongs to the formation of Pre-Prinos 1 and is in contact with the basement. All layers of the E-1 model can be seen in Figure 16.

**K-1**

The third well K-1 has a total drilled depth (TVDSS) of 2530m and its model was split into 23 depositional events. 3 layers constitute the Post-Evaporitic series, 17 the Evaporitic series and 2 the Pre-Evaporitic series. Advising adjacent wells and interpreted seismic sections of the area, one more layer was imported below the deeper formation, which is part of the formation of Pre-Prinos 1. Exact depths imported in the model can be seen in Figure 17.

### 4.1.2 Erosions

Erosions are another type of events that can be imported in PetroMod. In the study area, erosions are seen throughout each well. The duration and amount of erosions are uncertain. Due to the lack of available erosional thickness data, the amount of eroded material is estimated for each erosional period.

Specifically, the main erosional event observed in the area represents the boundary between the Post-Evaporitic series and Evaporitic series. This erosion corresponds to the end of the Messinian Salinity Crisis in the Mediterranean Sea, and the onset of the subsequent flooding and reconnection to the open sea. The second erosion was imported as the oldest event in all three models reflecting the contact with the underlying basement. Both erosions can be seen in Figure 15, Figure 16, and Figure 17 for wells PN-2, E-1, and K-1, respectively.

Regarding the erosion between the Post-Evaporitic and Evaporitic sequences, there is no available data for the thickness of the eroded Evaporitic sediments. However, taking into account the relative short duration of the erosion, other coeval erosional events in the broader area, and literature review for the period of the strong erosion of Mediterranean continental margins (Roveri et al., 2016; Bache et al., 2009; Karakitsios et al., 2017; personal communication with Dr.Paschalia Kiomourtzi), the eroded thickness was assumed at 30m in all three models for the purposes of modelling. Later, in the section of sensitivity analysis, trial runs with significant but also smaller amounts of erosion were tested to determine the effect of erosion on the models, with little change.

### 4.1.3 Age assignment

Once all layers were defined in the main input tables of the models, depositional ages were assigned to them by specifying a depositional period to each layer between the upper and lower boundaries. The age of each horizon is based on data from Kiomourtzi (2016) and has been imported in PetroMod's main input table.

According to the chronostratigraphic column of the Prinos basin (Figure 7) created by Proedrou and Papaconstantinou (2004), the ages of the boundaries between the Post-Evaporitic and Evaporitic sequences, and the Evaporitic and Pre-Evaporitic sequences are 5.33Ma and 7.246Ma, respectively. Based on that, each of the main stratigraphic sequences has been further subdivided into smaller layers.

Ages in the sub-layers of the Evaporitic series in all three models were assigned with uniform thickness and age ratios. Assuming that during the deposition of the Evaporitic sequence, the depositional environment remained the same, which was lagoonal under hyper-saline, reducing conditions with

rare events of fresh water and terrestrial deposits (Proedrou, 1979; Ioakim et al., 2005), the ages were calculated proportional to the thicknesses of the layers.

Regarding the other two series, the age assignment of the sub-layers was done on the basis of the results from palynology and nanno-fossils analyses conducted by Kiomourtzi (2016), and also taking into account the general geotectonic evolution of the basin. The estimated ages of all sub-layers in the three models can be seen in the following tables.

| ***SERIES*** | ***FORMATION*** | ***AGE (Ma)*** |
|---|---|---|
| *Post-Evaporitic* | *Post-Evaporitic Series L1* | *0.00* |
| | *Post-Evaporitic Series L2* | *3.00* |
| | *Post-Evaporitic Series L3* | *4.00* |
| *Evaporitic* | *Erosion 1* | *5.33* |
| | *Calcaceous Claystone* | *6.00* |
| | *Stray Evaporite* | *6.39* |
| | *SlstAnhLmstClstSst* | *6.42* |
| | *Lower Main Salt* | *7.12* |
| | *Cap rock* | *7.16* |
| *Pre-Evaporitic* | *Prinos Turbidites* | *7.25* |
| | *Prinos Unit* | *8.00* |
| | *Pre-Prinos 1 L1* | *10.00* |
| | *Pre-Prinos 1 L2* | *11.00* |
| | *Pre-Prinos 3* | *12.00* |
| | *Erosion 2* | *15.00* |

*Table 1: Assigned ages for the model of well PN-2 (ages for the depositional events correspond to the tops of the layers).*

| ***SERIES*** | ***FORMATION*** | ***AGE (Ma)*** |
|---|---|---|
| *Post-Evaporitic* | *Post-Evaporitic Series L1* | *0.00* |
| | *Post-Evaporitic Series L2* | *3.60* |
| *Evaporitic* | *Erosion 1* | *5.33* |
| | *Calcareous Claystone* | *6.00* |
| | *Stray Evaporite* | *6.04* |
| | *CalcSlstSstLmst 1* | *6.09* |
| | *Sub-stray Evaporite* | *6.16* |
| | *CalcSlstSstLmst 2* | *6.16* |
| | *Evaporite 1* | *6.30* |
| | *SstClstCalcSlstLmst 1* | *6.35* |
| | *Evaporite 2* | *6.43* |
| | *SstClstCalcSlstLmst 2* | *6.50* |
| | *Evaporite 3* | *6.60* |
| | *SstClstCalcSlstLmst 3* | *6.65* |
| | *Evaporite 4* | *6.81* |
| | *SstClstCalcSlstLmst 4* | *6.88* |
| | *Upper Main Salt* | *7.01* |
| | *SstClstCalcSlstLmst 5* | *7.08* |
| | *Lower Main Salt* | *7.19* |
| | *Cap rock* | *7.23* |
| *Pre-Evaporitic* | *Prinos Turbidites* | *7.25* |
| | *Prinos Unit L1* | *8.00* |
| | *Prinos Unit L2* | *8.50* |
| | *Pre-Prinos 1* | *10.00* |
| | *Erosion 2* | *12.00* |

*Table 2: Assigned ages for the model of well E-1 (ages for the depositional events correspond to the tops of the layers).*

| SERIES | FORMATION | AGE (Ma) |
|---|---|---|
| Post-Evaporitic | Post-Evaporitic Series L1 | 0.00 |
| | Post-Evaporitic Series L2 | 3.00 |
| | Post-Evaporitic Series L3 | 4.00 |
| Evaporitic | Erosion 1 | 5.33 |
| | Calcareous Claystone | 6.00 |
| | Stray Evaporite | 6.09 |
| | CalcClstLmst | 6.11 |
| | Sub-stray Evaporite | 6.14 |
| | SlstSstLmst | 6.15 |
| | Evaporite 1 | 6.22 |
| | CalcClstSstLmst1 | 6.24 |
| | Evaporite 2 | 6.37 |
| | CalcClstSstLmst2 | 6.42 |
| | Evaporite 3 | 6.51 |
| | CalcClstSstLmst3 | 6.56 |
| | Evaporite 4 | 6.70 |
| | CalcSlstSstAnh | 6.74 |
| | Upper Main Salt | 6.87 |
| | CalcClstSstAnh | 6.98 |
| | Lower Main Salt | 7.05 |
| | Cap rock | 7.22 |
| Pre-Evaporitic | Prinos Unit | 7.25 |
| | Pre-Prinos1 L1 | 10.00 |
| | Pre-Prinos1 L2 | 11.00 |
| | Erosion 2 | 12.00 |

*Table 3: Assigned ages for the model of well K-1 (ages for the depositional events correspond to the tops of the layers).*

### 4.1.4 Lithology

The lithologies imported in PetroMod for all three models are in accordance with the lithology description of Kiomourtzi (2016) and Mertzanides et al. (2010).

As most of the layers in all three wells have variations, the Lithology Editor of PetroMod was used in order to mix lithologies, to better match the specific lithologies in each well location. The percentage of each lithology that makes the interval was determined trying to better represent the lithological description of the interval. The lithologies of the individual layers were derived by mixing standard and premixed lithologies that come with PetroMod, and new lithologies that were created by mixing the already provided lithologies in ratio that should add up to 100%.

For each lithology, PetroMod automatically assigns default physical and thermal rock properties. These are: thermal conductivity, radiogenic heat, heat capacity, mechanical compaction, chemical compaction, permeability, seal properties and fracturing. Then, PetroMod uses this data to calculate, for instance, heat flow trends, temperatures and thermal conductivities of the models.

All lithologies created for the three models can be found in Appendix.

### 4.1.5 Petroleum system elements (PSE)

Petroleum system elements, including source rocks, reservoir rocks, seal rocks and overburden, were defined in the models according to the research of Kiomourtzi (2016). Source rock intervals in all three locations (PN-2, E-1, and K-1) are included within the formations of Pre-Prinos 1 and Pre-Prinos 3. Turbidites of Prinos Unit as well as the rest of the formation have been defined as reservoirs rocks. The entire Evaporitic series is considered as the seal rock of the petroleum system, and the Post-Evaporitic series has been defined as the overburden of the system.

### 4.1.6 Source rock properties

The identification of source rocks is a fundamental factor for generation modelling. This means that information like source rock richness (total organic carbon) and potential yield (hydrogen index) need to be defined. Source rock properties in PetroMod include TOC, HI kerogen types and petroleum kinetics. Apart from TOC (source rock richness) and HI (potential yield) that have to be imported for the layers of source rocks to simulate the reactions that govern the degradation of organic material to produce hydrocarbons, kinetic parameters need also to be defined for the thermal conversion of the kerogen to oil and gas (Al-Hajeri et al., 2009). In general, TOC and HI maps are usually used to define a non-uniform distribution of values within a layer (Hantschel and Kauerauf, 2009). However, in this model the source rocks were given uniform values laterally and vertically of the layers for simplicity.

Total Organic Carbon (TOC) and Hydrogen Index (HI) for the three modelled wells were obtained from the study of Kiomourtzi (2016). Kiomourtzi (2016) has performed source rock analysis on core samples retrieved from six different wellbores drilled in different structures within the basin. Three of these wells are the modelled ones (PN-2, E-1, and K-1). The results from the geochemical procedures of Rock-Eval pyrolysis and TOC index were used to define the input data of TOC and HI in the three models.

The results from Kiomourtzi's (2016) organic geochemical research showed that the organic matter varies a lot among the fields within the Prinos-Kavala basin. It is mainly characterized as marine, but with intense terrestrial input in the NE part of the basin (North Prinos field). Two types of source rocks were suggested, these are carbonate and argillaceous. It was also determined that the depositional environment was strongly reducing and hyper-saline throughout the whole basin. Nevertheless, smaller sub-environments were suggested as estuarine to lagoonal especially in the fields of Prinos, Epsilon, and Kallirahi. Regarding the thermal maturity of the potential source rocks, the findings showed that it is rather immature, with some variations among the fields to be observed. For instance,

the thermal maturity level of the organic matter in the North Prinos field is described as more immature.

## PN-2

Kiomourtzi (2016) performed organic geochemical research at the Laboratory of PVT and Core Analysis in School of Mineral Resources Engineering at the Technical University of Crete and all samples are stored in the specific lab. In the context of the present study, Rock-Eval pyrolysis was performed again on selected samples of PN-2, using the newer version of Rock-Eval analyser of the Laboratory of PVT and Core Analysis. The purpose for this was to confirm the Rock-Eval pyrolysis results by Kiomourtzi (2016), which had been done with an older Rock-Eval analyser. Rock-Eval pyrolysis was conducted by Ms. Eleni Chamilaki from the PVT and Core Analysis Laboratory.

The samples from well PN-2, which were used for Rock-Eval pyrolysis and TOC index from Kiomourtzi (2016), are divided into three groups based on their depth of retrieval. The findings from Kiomourtzi (2016) showed that the shallower group of samples contains contaminated hydrocarbons. For this reason, samples for performing again Rock-Eval pyrolysis were selected only from the other two groups. Table 4 and Table 5 present the results from Rock-Eval pyrolysis conducted for the same samples during the current thesis and by Kiomourtzi (2016), respectively.

**Rock-Eval Pyrolysis (September 2018)**

| SAMPLE ID | DEPTH (m) | Tmax | S1 | S2 | S3 | TOC | PI | PC | HI | OI |
|---|---|---|---|---|---|---|---|---|---|---|
| pn3e | 2655.33 | 428 | 0.20 | 4.06 | 1.16 | 1.56 | 0.05 | 0.40 | 260 | 74 |
| pn4e | 2655.49 | 427 | 0.18 | 3.60 | 1.60 | 1.37 | 0.05 | 0.37 | 263 | 117 |
| pn31e | 2655.56 | 427 | 0.19 | 3.29 | 1.16 | 1.33 | 0.05 | 0.34 | 247 | 87 |
| pn30e | 2656.22 | 427 | 0.22 | 5.80 | 1.30 | 2.01 | 0.04 | 0.55 | 289 | 65 |
| pn10e1 | | 426 | 0.14 | 1.63 | 1.33 | 0.99 | 0.08 | 0.20 | 165 | 134 |
| pn10e2 | 2706.95 | 425 | 0.15 | 1.63 | 1.37 | 0.99 | 0.08 | 0.20 | 165 | 138 |
| pn10e3 | | 427 | 0.13 | 1.61 | 1.37 | 1.10 | 0.07 | 0.20 | 146 | 125 |
| pn29e | 2709.05 | 429 | 0.14 | 2.89 | 0.80 | 1.18 | 0.04 | 0.28 | 245 | 68 |
| pn23e | 2709.81 | 426 | 0.17 | 2.25 | 1.17 | 0.91 | 0.07 | 0.25 | 247 | 129 |

*Table 4: Rock-Eval pyrolysis results from selected samples of well PN-2.*

**Rock-Eval Pyrolysis (Kiomourtzi, 2016)**

| SAMPLE ID | DEPTH (m) | Tmax | S1 | S2 | S3 | TOC | PI | PC | HI | OI |
|---|---|---|---|---|---|---|---|---|---|---|
| PN2 3 | 2655.33 | 430 | 1.01 | 6.61 | 0.95 | 1.79 | 0.13 | 0.63 | 369 | 53 |
| PN2 4 | 2655.49 | 432 | 0.98 | 6.11 | 1.19 | 1.66 | 0.14 | 0.59 | 367 | 72 |
| 31 | 2655.56 | 428 | 1.13 | 4.62 | 0.68 | 1.42 | 0.20 | 0.48 | 325 | 48 |
| 30 | 2656.22 | 430 | 1.50 | 7.68 | 0.68 | 1.96 | 0.16 | 0.76 | 392 | 35 |
| PN2 10 | 2706.95 | 433 | 0.41 | 2.77 | 0.93 | 1.04 | 0.13 | 0.26 | 266 | 89 |
| 29 | 2709.05 | 435 | 0.86 | 4.01 | 0.44 | 1.05 | 0.18 | 0.40 | 382 | 42 |
| PN2 23 | 2709.81 | 431 | 0.81 | 4.07 | 0.85 | 1.31 | 0.17 | 0.41 | 310 | 65 |

*Table 5: Rock-Eval pyrolysis results of well PN-2 by Kiomourtzi (2016). Results are shown for the samples used for Rock-Eval pyrolysis conducted during the present study.*

As it can be seen from the two data sets, S1 and S2 are reduced in the results of the current Rock-Eval pyrolysis. This reduction could possibly be explained as oil that had migrated from other layers and now was removed. On the other hand, the new values of S2 reflect kerogen or heavy oil that wasn't extracted, but continued to the stage of pyrolysis. S3 corresponds to oxygen that exists in kerogen, the observed increase in the new values is possibly caused by the fact that the samples were in standard conditions and were oxidized. Tmax values were slightly reduced, and they are out of range for the oil window (immature: Tmax<435, mature: Tmax=435-470, postnature: Tmax>470) (Magoon and Dow, 1994). Finally, another observation is the reduction in the values of HI, but this is expected as S1 is also reduced.

After the comparison of the two sets of data, it was decided to use TOC and HI values from the new results. The input TOC and HI are average of measurements of the rock samples at the modelled location of well PN-2. Thus, TOC was entered 1.34% and HI 244mgHC/gTOC.

The comparative interpretation by Kiomourtzi (2016) of the Rock-Eval pyrolysis and TOC index results between the fields within the basin showed that the samples from PN-2 contain kerogen type III.

**E-1**

As far as well E-1 is concerned, the organic geochemical research of Kiomourtzi (2016) showed that the examined samples of this well have been contaminated by migrated hydrocarbons. Therefore, TOC and HI values from these samples couldn't be used for modelling because they wouldn't be representative. For this reason, TOC and HI values for the model of E-1 were obtained from bibliography data (Kavala oil records) included in the work of Kiomourtzi (2016), in order to better represent the source rock intervals in this well.

In particular, it was found that the well which is closer to PN-2 and could possibly be used to better approximate the source rock intervals in PN-2 is P-4. Averaging TOC and HI measurements of source rock intervals at the respective depths with those of PN-2, TOC was set equal to 1.51%, and HI to 119 mgHC/gTOC.

From Kiomourtzi's (2016) analysis, it was determined that the source rock intervals in the location of well E-1 would have type II kerogen.

**K-1**

In the case of well K-1, the examined samples were retrieved from reservoir rock intervals, and for that reason, it is estimated that the results from Rock-Eval pyrolysis and TOC index are not related to

organic matter of source rocks. Hence, TOC and HI values for this model were obtained again from bibliography data (Kavala oil record) available in Kiomourtzi (2016).

From the provided wells, the closer to K-1 is SK-2. TOC and HI values used in the model of K-1 are estimated from averages of measured data of the source rocks intervals in SK-2 at the respective depths of the source rocks in K-1. Therefore, the model of K-1 has a TOC of 1.65% and an HI of 360.5mgHC/gTOC.

Based on Kiomourtzi (2016), the kerogen is defined as type II.

## Petroleum kinetics

A quite important part of basin modelling is the prediction of petroleum generation within the possible source rocks using kinetic models. Kinetic modelling is the process that defines the chemical rates of oil and gas generation from kerogen, and varies with time and temperature.

In PetroMod, there is a wide variety of petroleum kinetics to choose from in order to determine the generation of oil and gas. Petroleum kinetics in PetroMod are separated into the following: bulk, kerogen oil and gas, compositional, compositional for phase separation, miscellaneous, biogenic and secondary reactions. The criteria for the separation of the kinetics of the petroleum are: the type of kerogen, the cracking type (primary or secondary), and the number and type of the generated petroleum components (bulk, oil/gas, compositional). The kerogen oil and gas was selected for this study.

Pepper and Corvi (1995) Type III H(DE) was used to simulate thermal cracking of kerogen in the Pre-Prinos 1 formation in the model of well PN-2. The kinetics for the Pre-Prinos 1 and Pre-Prinos 3 formations in the models of wells E-1 and K-1 were assigned to Pepper and Corvi (1995) Type II (B).

The reason for selecting the specific kinetic model is that gives the possibility to gas to be generated, not only from oil cracking, but from kerogen as well (Pepper and Corvi, 1995). Moreover, this kinetic model distributes kinetic parameters based on depositional environments and stratigraphic ages. It uses five different organofacies. The term organofacies is referred to kerogen derived from the same source deposited under similar environmental conditions (Pepper and Corvi, 1995). The kinetic model selected for E-1 and K-1 is described as aquatic, marine environment, siliciclastic lithofacies of any ages, whereas, the kinetic model for PN-2 is described as terrigenous, non-marine, ever-wet coastal environment of Mesozoic or younger age (Pepper and Corvi, 1995).

The following three figures present the main input tables for the three modelled well locations, including all information mentioned in chapter 4.1.

| Age [Ma] | Name top/well pick | Depth [m] | Thickness [m] | Event type | Name layer/event | Paleodeposition/ erosion [m] | Lithology | PSE | Kinetic | TOC [%] | HI [mgHC/gTOC] |
|---|---|---|---|---|---|---|---|---|---|---|---|
| 0.00 | Post-Evap L1 | 38 | 647 | ↓ Deposition | Post-Evap L1 | | PostEvapL1_PN2 | Overburden Rock | | | |
| 3.00 | Post-Evap L2 | 685 | 730 | ↓ Deposition | Post-Evap L2 | | PostEvapL2_PN2 | Overburden Rock | | | |
| 4.00 | Post-Evap L3 | 1415 | 561 | ↓ Deposition | Post-Evap L3 | | PostEvapL3_PN2 | Overburden Rock | | | |
| 5.33 | Erosion 1 | 1976 | 0 | ↑ Erosion | Erosion 1 | -30 | | | | | |
| 6.00 | Calcareous Claystone | 1976 | 47 | ↓ Deposition | Calcareous Claystone | 30 | CalcareousClaystone | Seal Rock | | | |
| 6.39 | Stray Evaporite | 2023 | 3 | ↓ Deposition | Stray Evaporite | | Stray Evaporite_K1 | Seal Rock | | | |
| 6.42 | SlstAnhLmstClstSst | 2026 | 85 | ↓ Deposition | SlstAnhLmstClstSst | | SlstAnhLmstClstSst | Seal Rock | | | |
| 7.12 | Lower Main Salt | 2111 | 5 | ↓ Deposition | Lower Main Salt | | LMS_PN2 | Seal Rock | | | |
| 7.16 | Cap Rock | 2116 | 10 | ↓ Deposition | Cap Rock | | CapRock_PN2 | Seal Rock | | | |
| 7.25 | Prinos Turbidites | 2126 | 44 | ↓ Deposition | Prinos Turbidites | | Sandstone (quartzite, typical) | Reservoir Rock | | | |
| 8.00 | Prinos Unit | 2170 | 200 | ↓ Deposition | Prinos Unit | | PrinosUnit_PN2 | Reservoir Rock | | | |
| 10.00 | Pre-Prinos 1 L1 | 2370 | 190 | ↓ Deposition | Pre-Prinos 1 L1 | | PrePrinos1L1_PN2 | Source Rock | Pepper&Corvi(1995)_TIIIH(DE) | 1.34 | 244.00 |
| 11.00 | Pre-Prinos 1 L2 | 2560 | 162 | ↓ Deposition | Pre-Prinos 1 L2 | | PrePrinos1L2_PN2 | Source Rock | Pepper&Corvi(1995)_TIIIH(DE) | 1.34 | 244.00 |
| 12.00 | Pre-Prinos 3 | 2722 | 280 | ↓ Deposition | Pre-Prinos 3 | | Pre-Prinos3_PN2 | Source Rock | Pepper&Corvi(1995)_TIIIH(DE) | 1.34 | 244.00 |
| 15.00 | Erosion 2 | 3002 | | | | | | | | | |

*Figure 15: Main input data for burial and thermal histories reconstruction in PetroMod for the PN-2 well.*

| Age [Ma] | Name top/well pick | Depth [m] | Thickness [m] | Event type | Name layer/event | Paleodeposition/ erosion [m] | Lithology | PSE | Kinetic | TOC [%] | HI [mgHC/gTOC] |
|---|---|---|---|---|---|---|---|---|---|---|---|
| 0.00 | Post-Evap L1 | 40 | 1323 | ↓ Deposition | Post-Evap L1 | | PostEvapL1 | Overburden Rock | | | |
| 3.60 | Post-Evap L2 | 1363 | 500 | ↓ Deposition | Post-Evap L2 | | PostEvapL2 | Overburden Rock | | | |
| 5.33 | Erosion 1 | 1863 | 0 | ↑ Erosion | Erosion 1 | -30 | | | | | |
| 6.00 | CalcClaystone | 1863 | 30 | ↓ Deposition | CalcClaystone | 30 | CalcareousClaystone | Seal Rock | | | |
| 6.04 | Stray Evaporite | 1893 | 40 | ↓ Deposition | Stray Evaporite | | StrayEvap | Seal Rock | | | |
| 6.09 | CalcSlstSstLmst1 | 1933 | 48 | ↓ Deposition | CalcSlstSstLmst1 | | CalcSlstSstLmst | Seal Rock | | | |
| 6.16 | Sub-stray Evaporite | 1981 | 4 | ↓ Deposition | Sub-stray Evaporite | | Halite | Seal Rock | | | |
| 6.16 | CalcSlstSstLmst2 | 1985 | 109 | ↓ Deposition | CalcSlstSstLmst2 | | CalcSlstSstLmst | Seal Rock | | | |
| 6.30 | Evaporite 1 | 2094 | 34 | ↓ Deposition | Evaporite 1 | | Evap1 | Seal Rock | | | |
| 6.35 | SstClstCalcSlstLmst1 | 2128 | 65 | ↓ Deposition | SstClstCalcSlstLmst1 | | SstClstCalcSlstLmst | Seal Rock | | | |
| 6.43 | Evaporite 2 | 2193 | 50 | ↓ Deposition | Evaporite 2 | | Evap1 | Seal Rock | | | |
| 6.50 | SstClstCalcSlstLmst2 | 2243 | 77 | ↓ Deposition | SstClstCalcSlstLmst2 | | SstClstCalcSlstLmst | Seal Rock | | | |
| 6.60 | Evaporite 3 | 2320 | 35 | ↓ Deposition | Evaporite 3 | | Evap3 | Seal Rock | | | |
| 6.65 | SstClstCalcSlstLmst3 | 2355 | 127 | ↓ Deposition | SstClstCalcSlstLmst3 | | SstClstCalcSlstLmst | Seal Rock | | | |
| 6.81 | Evaporite 4 | 2482 | 48 | ↓ Deposition | Evaporite 4 | | Evap1 | Seal Rock | | | |
| 6.88 | SstClstCalcSlstLmst4 | 2530 | 101 | ↓ Deposition | SstClstCalcSlstLmst4 | | SstClstCalcSlstLmst | Seal Rock | | | |
| 7.01 | Upper Main Salt | 2631 | 50 | ↓ Deposition | Upper Main Salt | | UMS_E1 | Seal Rock | | | |
| 7.08 | SstClstCalcSlstLmst5 | 2681 | 86 | ↓ Deposition | SstClstCalcSlstLmst5 | | SstClstCalcSlstLmst | Seal Rock | | | |
| 7.19 | Lower Main Salt | 2767 | 30 | ↓ Deposition | Lower Main Salt | | LMS_E1 | Seal Rock | | | |
| 7.23 | Cap Rock | 2797 | 14 | ↓ Deposition | Cap Rock | | CapRock_E1 | Seal Rock | | | |
| 7.25 | Prinos Turbidites | 2811 | 92 | ↓ Deposition | Prinos Turbidites | | PrinosTurb | Reservoir Rock | | | |
| 8.00 | Prinos Unit L1 | 2903 | 51 | ↓ Deposition | Prinos Unit L1 | | PrinosUnit_E1 | Reservoir Rock | | | |
| 8.50 | Prinos Unit L2 | 2954 | 142 | ↓ Deposition | Prinos Unit L2 | | PrinosUnit_E1 | Reservoir Rock | | | |
| 10.00 | Pre-Prinos 1 | 3096 | 158 | ↓ Deposition | Pre-Prinos 1 | | Pre-Prinos1_E1 | Source Rock | Pepper&Corvi(1995)_TII(B) | 1.51 | 119.00 |
| 12.00 | Erosion 2 | 3254 | | | | | | | | | |

*Figure 16: Main input data for burial and thermal histories reconstruction in PetroMod for the E-1 well.*

| Age [Ma] | Name top/well pick | Depth [m] | Thickness [m] | Event type | Name layer/event | Paleodeposition/ erosion [m] | Lithology | PSE | Kinetic | TOC [%] | HI [mgHC/gTOC] |
|---|---|---|---|---|---|---|---|---|---|---|---|
| 0.00 | Post-Evap L1 | 50 | | | | | | | | | |
| | | | 1075 | ↓ Deposition | Post-Evap L1 | | PostEvapL1_K1 | Overburden Rock | | | |
| 3.00 | Post-Evap L2 | 1125 | | | | | | | | | |
| | | | 310 | ↓ Deposition | Post-Evap L2 | | PostEvapL2_K1 | Overburden Rock | | | |
| 4.00 | Post-Evap L3 | 1435 | | | | | | | | | |
| | | | 58 | ↓ Deposition | Post-Evap L3 | | PostEvapL3_K1 | Overburden Rock | | | |
| 5.33 | Erosion 1 | 1493 | | | | | | | | | |
| | | | 0 | ↑ Erosion | Erosion 1 | -30 | | | | | |
| 6.00 | CalcClaystone | 1493 | | | | | | | | | |
| | | | 55 | ↓ Deposition | CalcClaystone | 30 | CalcareousClaystone | Seal Rock | | | |
| 6.09 | Stray Evaporite | 1548 | | | | | | | | | |
| | | | 13 | ↓ Deposition | Stray Evaporite | | Stray Evaporite_K1 | Seal Rock | | | |
| 6.11 | CalcClstLmst | 1561 | | | | | | | | | |
| | | | 17 | ↓ Deposition | CalcClstLmst | | CalcClstLmst | Seal Rock | | | |
| 6.14 | Sub-Stray Evaporite | 1578 | | | | | | | | | |
| | | | 4 | ↓ Deposition | Sub-Stray Evaporite | | SubStray Evap | Seal Rock | | | |
| 6.15 | SlstSstLmst | 1582 | | | | | | | | | |
| | | | 42 | ↓ Deposition | SlstSstLmst | | SlstSstLmst | Seal Rock | | | |
| 6.22 | Evaporite 1 | 1624 | | | | | | | | | |
| | | | 14 | ↓ Deposition | Evaporite 1 | | Halite | Seal Rock | | | |
| 6.24 | CalcClstSstLmst1 | 1638 | | | | | | | | | |
| | | | 75 | ↓ Deposition | CalcClstSstLmst1 | | CalcClstSstLmst | Seal Rock | | | |
| 6.37 | Evaporite 2 | 1713 | | | | | | | | | |
| | | | 35 | ↓ Deposition | Evaporite 2 | | Evaporite2 | Seal Rock | | | |
| 6.42 | CalcClstSstLmst2 | 1748 | | | | | | | | | |
| | | | 49 | ↓ Deposition | CalcClstSstLmst2 | | CalcClstSstLmst | Seal Rock | | | |
| 6.51 | Evaporite 3 | 1797 | | | | | | | | | |
| | | | 33 | ↓ Deposition | Evaporite 3 | | Halite | Seal Rock | | | |
| 6.56 | CalcClstSstLmst3 | 1830 | | | | | | | | | |
| | | | 87 | ↓ Deposition | CalcClstSstLmst3 | | CalcClstSstLmst | Seal Rock | | | |
| 6.70 | Evaporite 4 | 1917 | | | | | | | | | |
| | | | 23 | ↓ Deposition | Evaporite 4 | | Evap4_K1 | Seal Rock | | | |
| 6.74 | CalcSlstSstAnh | 1940 | | | | | | | | | |
| | | | 74 | ↓ Deposition | CalcSlstSstAnh | | CalcSlstSstAnh | Seal Rock | | | |
| 6.87 | Upper Main Salt | 2014 | | | | | | | | | |
| | | | 71 | ↓ Deposition | Upper Main Salt | | UMS_K1 | Seal Rock | | | |
| 6.98 | CalcClstSstAnh | 2085 | | | | | | | | | |
| | | | 43 | ↓ Deposition | CalcClstSstAnh | | CalcClstSstAnh | Seal Rock | | | |
| 7.05 | Lower Main Salt | 2128 | | | | | | | | | |
| | | | 100 | ↓ Deposition | Lower Main Salt | | Halite | Seal Rock | | | |
| 7.22 | Cap Rock | 2228 | | | | | | | | | |
| | | | 15 | ↓ Deposition | Cap Rock | | CalcareousClaystone | Seal Rock | | | |
| 7.25 | Prinos Unit | 2243 | | | | | | | | | |
| | | | 197 | ↓ Deposition | Prinos Unit | | PrinosUnit_K1 | Reservoir Rock | | | |
| 10.00 | Pre-Prinos 1 L1 | 2440 | | | | | | | | | |
| | | | 90 | ↓ Deposition | Pre-Prinos 1 L1 | | PrePrinos1L1_K1 | Source Rock | Pepper&Corvi(1995)_TII(B) | 1.65 | 360.50 |
| 11.00 | Pre-Prinos 1 L2 | 2530 | | | | | | | | | |
| | | | 42 | ↓ Deposition | Pre-Prinos 1 L2 | | Pre-Prinos1L2_K1 | Source Rock | Pepper&Corvi(1995)_TII(B) | 1.65 | 360.50 |
| 12.00 | Erosion 2 | 2572 | | | | | | | | | |

*Figure 17: Main input data for burial and thermal histories reconstruction in PetroMod for the K-1 well.*

## 4.2 BOUNDARY CONDITIONS

The next step of basin modelling is to define the boundary conditions for the burial and thermal histories reconstruction. These are past conditions that need to be determined along with the model properties, and consist of: paleo water depth, which is related to the location and type of deposition, sediment water interface temperature and paleo heat flow estimates through geological time, which both of them are required to calculate the burial and temperature histories (Al-Hajeri et al., 2009).

### 4.2.1 Paleo water depth

Paleo water depth (PWD) shows the depth of the water column during deposition of each chrostratigraphic unit. Present water depth value for the PN-2 well location was obtained from the website of Energean Oil & Gas (https://www.energean.com) and is equal to 38m. Regarding the modelled well location of K-1, Mertzanides et al. (2010) refer that the South Kavala gas field has been discovered in 52m of water depth, therefore, the present water depth of K-1 was estimated at 50m, due to its vicinity of the South Kavala field (Figure 18). Well E-1 is located between PN-2 and K-1, taking into account the water depths of these two wells and the bathymetric map of Kavala bay (Figure 19) created by Kiomourtzi (2016), it was assumed that the water depth in E-1 is 40m.

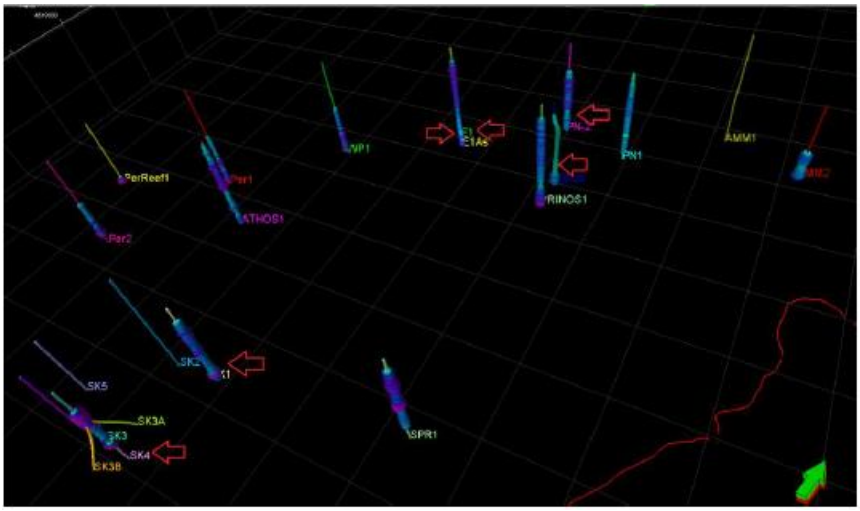


*Figure 18: 3D map of wells within the Prinos-Kavala basin created by Kiomourtzi (2016) in Petrel software.*

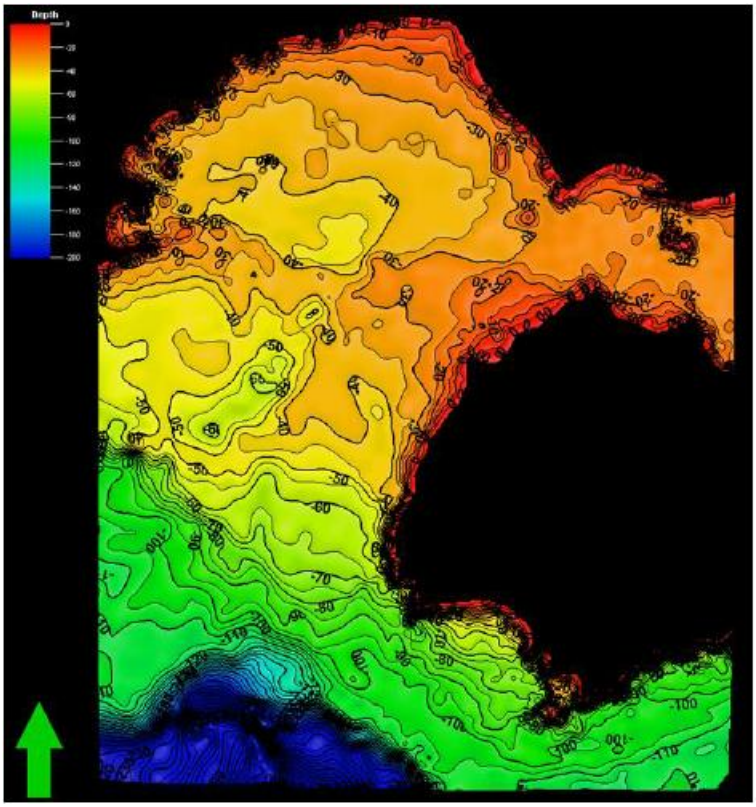


*Figure 19: Bathymetric map of Kavala bay constructed by Kiomourtzi (2016) in Surfer software.*

Literature searching gave no information about paleo water depths in Prinos-Kavala basin. For this reason, the assigned PWD values in all three modelled well locations are estimated. Based on the geotectonic evolution of the basin and the depositional environment at each phase of the development of the basin, it was attempted to create a general trend of the water depth in each modelled location, providing thus, a depth constrain to the reconstruction of the burial histories of the three models. Characteristic depositional or erosional events were chosen to be assigned with PWD values, for instance, the deposition of turbidites and evaporites, as well as periods of strong

erosions. Taking into account the depositional environments, Figure 20 was used as a guide for the determination of PWD.

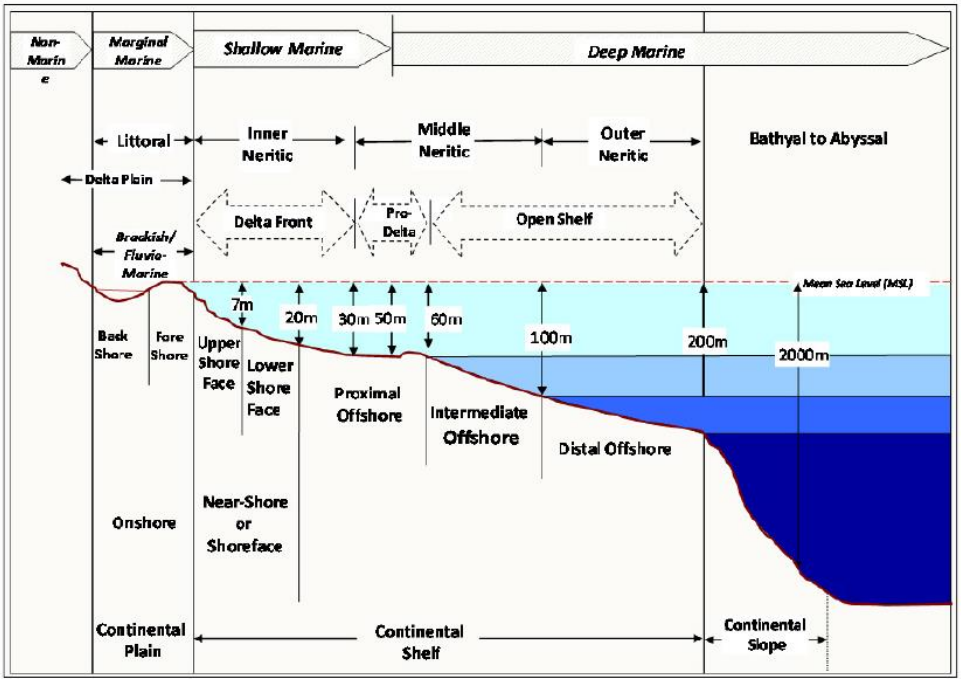


*Figure 20: Diagram showing depositional environments and bathymetric changes used in paleoenvironmental interpretations (modified after Allen, 1965, 1970). Figure form Okosun and Osterloff (2014).*

The estimated paleo water depth profiles through time for wells PN-2, E-1 and K-1 are shown in the following figures.

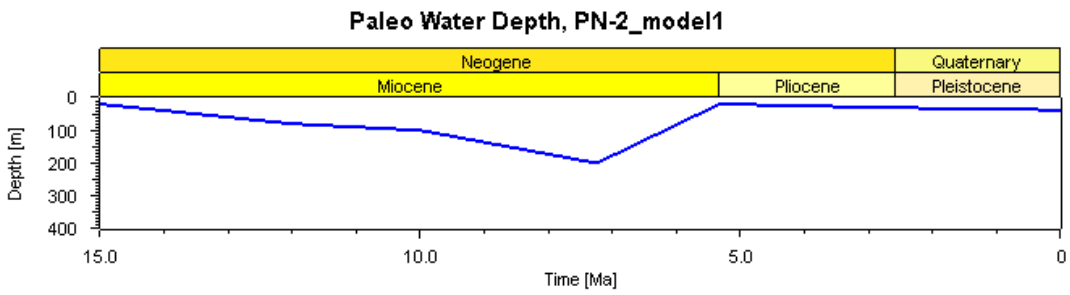


*Figure 21: Paleo water depth profile through time for well PN-2.*

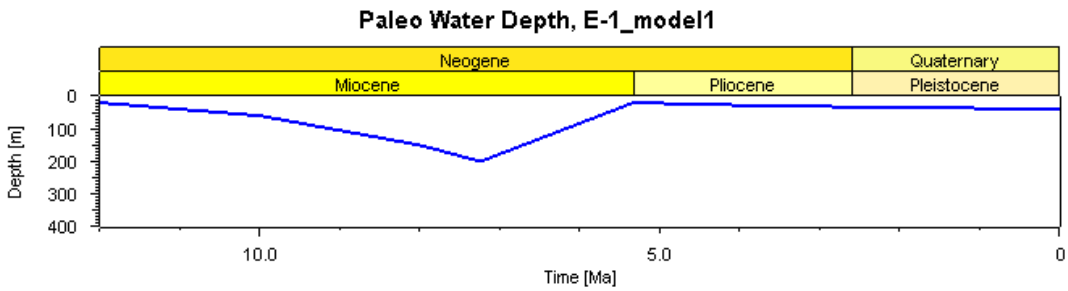


*Figure 22: Paleo water depth profile through time for well E-1.*

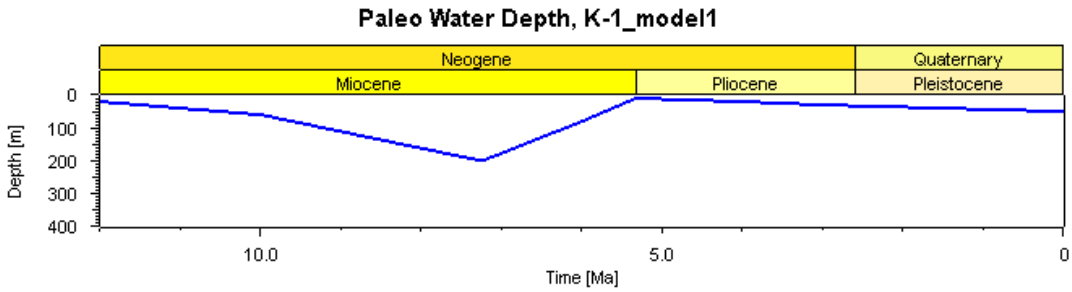


*Figure 23: Paleo water depth profile through time for well K-1.*

### 4.2.2 Sediment water interface temperature

Sediment water interface temperatures through geological time are another boundary condition, which, along with paleo heat flow estimates, are a prerequisite for the calculation of the temperature history.

The boundary condition of SWIT was entered in the models via the 'Calc. Settings' function of PetroMod 1D from the option of 'From global mean temperature at sea level' using the 'Auto SWIT' tool (Wygrala, 1989). This is an integrated tool of PetroMod that uses the paleo water depth and the evolution of ocean surface temperatures through time depending on the paleo latitude of the area. The only input that PetroMod needs for the calculation of SWIT trends is the location of the model. Prinos-Kavala basin is in the Northern hemisphere in the Mediterranean Sea at a latitude of 41° (40.5°). The 'Auto SWIT' tool using the location and the geographical latitude of the area, extracts a standard temperature at sea level over geological time (PetroMod 1D User Guide). Then, the 'auto transformation' choice was selected to correct the surface temperature against the paleo water depth and calculate the SWIT from the sea level temperature (PetroMod 1D User Guide).

The estimated sediment water interface temperature trends through time for wells PN-2, E-1 and K-1 are presented in Figure 25, Figure 26, and Figure 27, respectively.

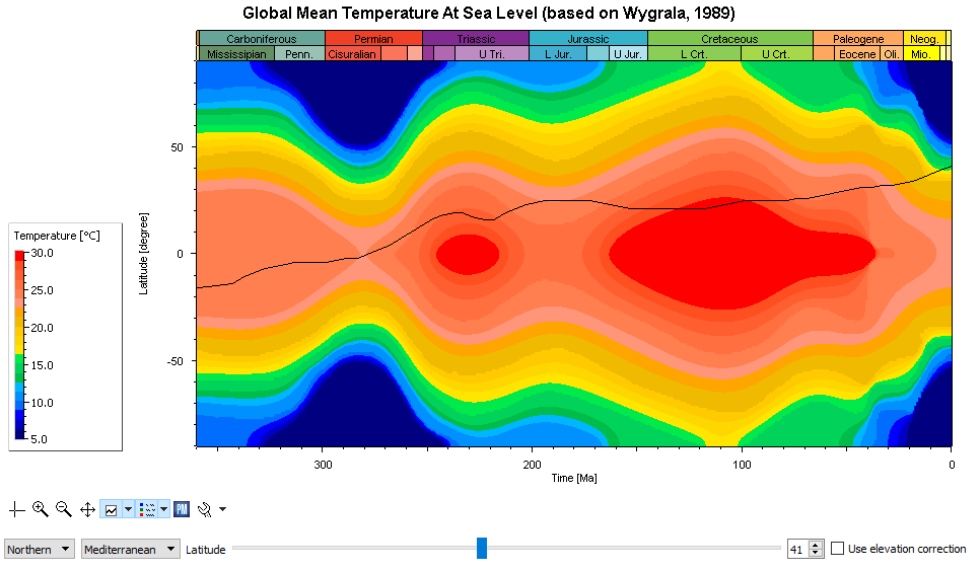


*Figure 24: Global mean surface temperature through geological time. The black line shows changes in latitude with time for Prinos-Kavala basin.*

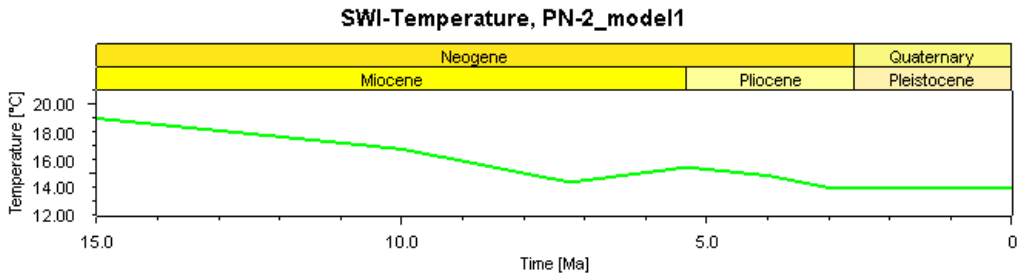


*Figure 25: Estimated sediment water interface temperature (SWIT) trend defined for the PN-2 well location.*

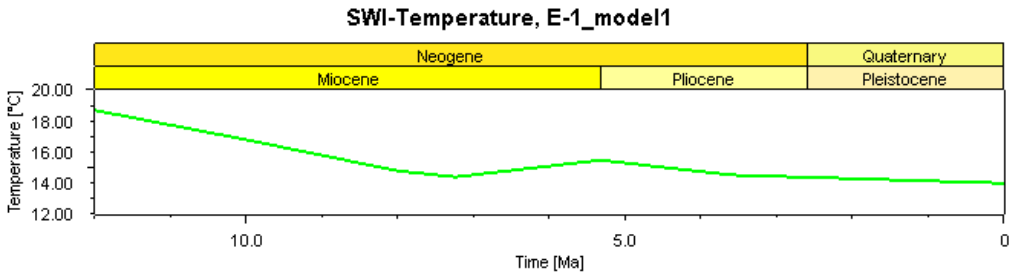


*Figure 26: Estimated sediment water interface temperature (SWIT) trend defined for the E-1 well location.*

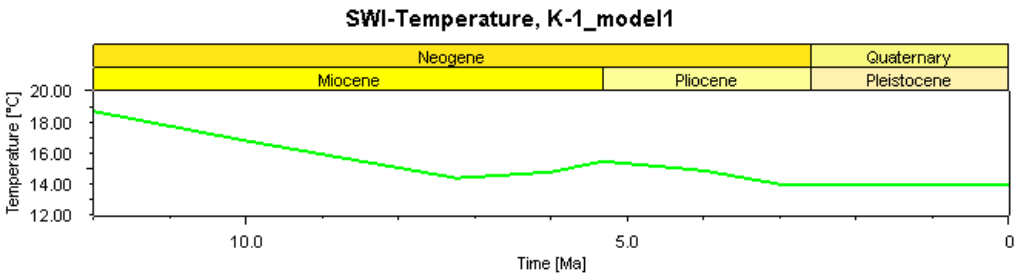


*Figure 27: Estimated sediment water interface temperature (SWIT) trend defined for the K-1 well location.*

### 4.2.3 Heat flow

Basal heat flow together with the sediment water interface temperatures are the main boundary conditions for heat flow analysis. The main goal of heat flow analysis is the calculation of temperature, which is used for determining geochemical reaction rates (Hantschel and Kauerauf, 2009). All three sources of heat generation must be taken into account. These are heat convection, heat conduction and heat generation by radioactive decay (Hantschel and Kauerauf, 2009).

The values of basal heat flow are usually predicted using crustal models. PetroMod's McKenzie crustal model is based on the crustal stretching model by Jarvis & Mckenzie (1980) (PetroMod 1D User Guide) and calculates the heat flow history by using subsidence, timing and crust parameters, and generates stretching and heat flow maps. In this study, the basal heat flow wasn't determined from PetroMod's McKenzie crustal model due to lack of the required data, but it was estimated by systematically adjusting the imported surface heat flow, and then, it was calibrated with thermal calibration parameters (Hantschel and Kauerauf, 2009).

In all three locations, the present heat flow values were estimated based on heat measurements in the broader area of the Aegean Sea obtained by Jongsma (1974). In the context of the work that was conducted by Jongsma (1974), two of the stations, which were used for data collection, are south of Thassos island and opposite the south part of the eastern finger of Chalkidiki peninsula. The heat flow measurements in stations 311 and 312 are 67.78mW/m$^2$ and 65.27mW/m$^2$, respectively.

As far as paleo heat flow values in Prinos-Kavala basin are concerned, no information was available in literature. Therefore, it was attempted to estimate these values by considering various type of data relating to paleo heat flow. The factors that contributed to the estimation of the paleo heat flow values are presented in the following paragraphs.

First or all, heat flow measurements from the above-mentioned stations from the study of Jongsma (1974) were used as a basis for the recent heat flow estimations. Secondly, the type of the sedimentary basin played a quite important role, as according to Allen and Allen (2005), different types of sedimentary basins exhibit different heat flow ranges (Figure 28). Prinos-Kavala basin can be placed in the group of extensional, active (synrift) back-arc basins, which are characterized by a heat flow range of 67-120mW/m$^2$.

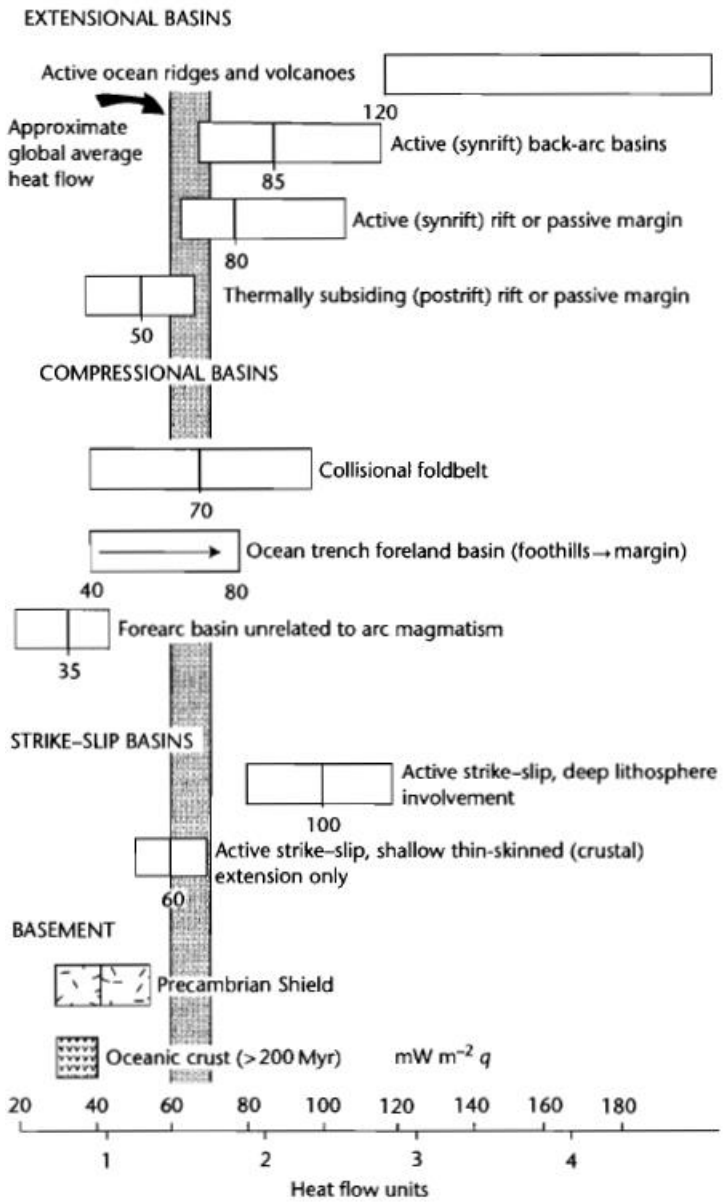


*Figure 28: Summary of the typical heat flows associated with sedimentary basins of various types (Allen and Allen, 2005).*

Moreover, taking into account that during deposition, heat flow decreases towards the surface (as the new volume of sediments deposited absorb part of the heat flow coming from the basement), and during erosion, heat flow increases towards the surface (as the sediments exposed to the surface contain excess of heat flow which dissipates to the surrounding rocks) (Hantschel and Kauerauf, 2009; Dembicki, 2017), paleo heat flow values were estimated for the three modelled well locations.

Finally, the magmatic intrusions (Tertiary plutonic and volcanic rocks) in the broader area of Prinos-Kavala basin play a quite important role in the increased regional heat flow and were taken considered for the estimation of paleo heat flow values in the models. Tertiary granitic rocks intruded the Rhodope metamorphic rocks at various times from Eocene to Miocene, 50-14Ma (Mountrakis, 2010).

Based on recent studies, the exhumation of the Rhodope massif due to extensional tectonics took place during Lower Miocene and Upper Pliocene, (Dinter and Royden, 1993; Sokoutis et al., 1993; Wawrzenitz and Korohe, 1998). However, quite important is also the volcanic activity in the area, which has an age of Oligocene (35-25Ma) (Mountrakis, 2010).

Several authors have studied the thermal events of the specific area. For instance, Chiotis (1985) shows that three significant thermal events took place in Northern Greece close to the examined area. During the Serravalian (13.8-11.6Ma), granitic intrusions east of the Nestos wells in the sedimentary basin of the Nestos River delta heated the region to a maximum temperature of 270°C, which was depicted from vitrinite reflectance measurements in drilling cores. In addition, a granitic vein of 15.5 ± 0.5Ma age 15km west of Nestos wells, and a re-heating age of 17.8 ± 0.8Ma is mentioned for magmatic rocks from the Symvolon Mountains west of Kavala.

Taking into account all this information, it was tried to define paleo heat flow values for the three modelled well locations trying to estimate as best as possible a more representative paleo heat flow trend for each model. After several trials of adjusting the imported surface heat flow, and calibrating with thermal calibration parameters, the best paleo heat flow estimates were determined and are presented in Figure 29, Figure 30, and Figure 31 for wells PN-2, E-1, and K-1, respectively.

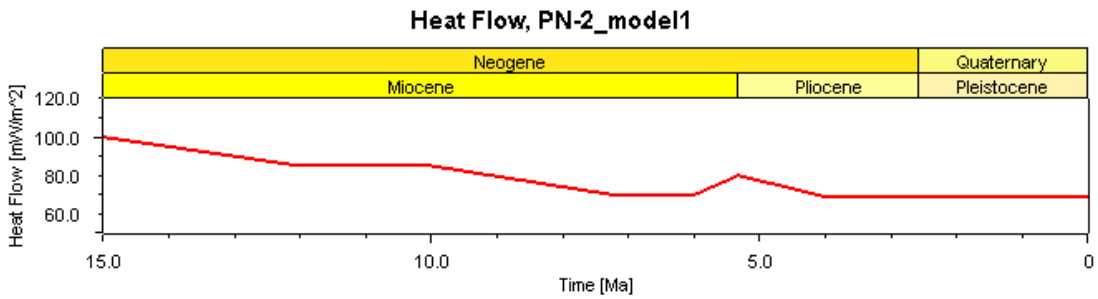


*Figure 29: Modelled heat flow curve over time for PN-2.*

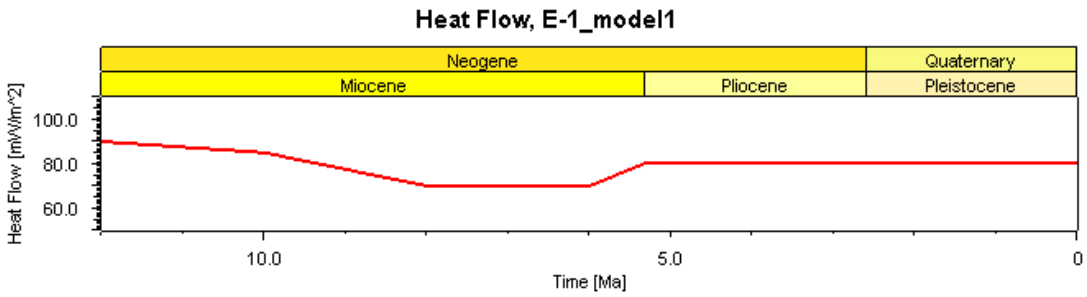


*Figure 30: Modelled heat flow curve over time for E-1.*

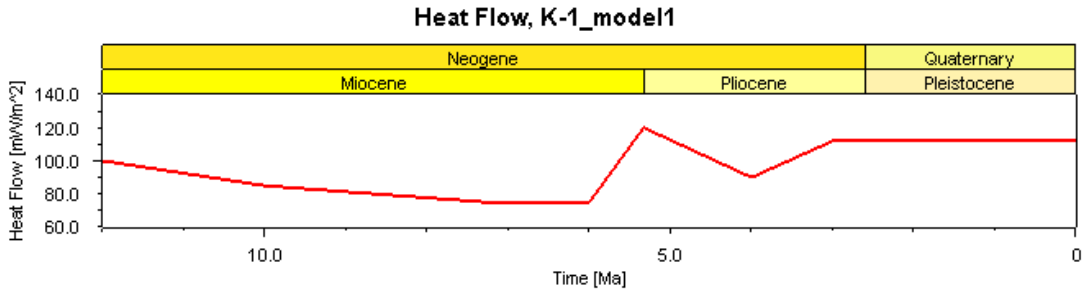


*Figure 31: Modelled heat flow curve over time for K-1.*

The heat flow values have been calibrated using vitrinite reflectance data. The above figures show the heat flow distributions used in the models. In order to fit the vitrinite reflectance, the heat flow values in each well were modified differently. The present-day heat flow for PN-2 is 69mW/m$^2$, for E-1 is 80mW/m$^2$, and for K-1 is 112mW/m$^2$. The highest values in each well have been assigned to the period of the strong erosional event (5.33Ma) and the deeper formations lying on top of the eroded metamorphic basement. However, it is observed that the sediments of the K-1 well are today anomalously hot relative to the formations of the other two wells (PN-2 and E-1). Even though a geological evidence for this is missing, it could be explained by the fact that well K-1 is located closer to the South Kavala Ridge, which has a high geothermal gradient, and as the study of Kiomourtzi (2016) showed, the samples of the South Kavala field are within the oil window and present a much higher thermal maturity level compared to the samples of the other wells. Moreover, the observed gradual increase in the heat flow values from well PN-2, to E-1, and eventually, to K-1 can confirm that the high heat flows in K-1 are expected. On the other hand, the lowest values of 69mW/m$^2$ is recorded for the present-day heat flow in PN-2, which is quite close to the heat flow measurements from Jongsma (1974).

| Age [Ma] | HF [mW/m^2] |
|---|---|
| 0.00 | 69.00 |
| 3.00 | 69.00 |
| 4.00 | 69.00 |
| 5.33 | 80.00 |
| 6.00 | 70.00 |
| 7.25 | 70.00 |
| 10.00 | 85.00 |
| 12.00 | 85.00 |
| 15.00 | 100.00 |

| Age [Ma] | HF [mW/m^2] |
|---|---|
| 0.00 | 80.00 |
| 3.60 | 80.00 |
| 5.33 | 80.00 |
| 6.00 | 70.00 |
| 7.25 | 70.00 |
| 8.00 | 70.00 |
| 10.00 | 85.00 |
| 12.00 | 90.00 |

| Age [Ma] | HF [mW/m^2] |
|---|---|
| 0.00 | 112.00 |
| 3.00 | 112.00 |
| 4.00 | 90.00 |
| 5.33 | 120.00 |
| 6.00 | 75.00 |
| 7.25 | 75.00 |
| 10.00 | 85.00 |
| 12.00 | 100.00 |

*Table 6: Heat flow input data for wells PN-2, E-1, and K-1 from left to right, respectively.*

## 4.3 SIMULATION

Petromod's 1D simulator was used to construct the thermal maturation and burial histories of wells PN-2, E-1, and K-1 within the Prinos-Kavala basin from the deeper sediments overlying the basement until the sediments today. The chapters above describe the input data and boundary conditions needed for the simulation and here follows a description of the simulation process. The simulation process will be constrained to outputs relating to the burial and thermal histories, timing of hydrocarbon generation and timing of hydrocarbon expulsion. No migration outputs will be included.

First of all, during the simulation process PetroMod will restore the original thickness of each imported layer in the model, applying the porosity-controlled backstripping method by Watts and Ryan (1976), which starts by using with present-day thickness. Essentially, this method removes the sediment/water load component from the total subsidence of a horizon and leaves only the effect of the tectonic driving force component (Allen and Allen, 2005) determining thus, the shape of the geological structures at paleo times. Then, the subsidence of the basin is simulated by PetroMod by using pressure and compaction.

Heat flow analysis is performed for calculating temperature, which is required for geochemical reaction rates. Primary and secondary cracking can be described by decomposition kinetics of sets of parallel reactions. PetroMod has a database of reaction kinetics for predicting hydrocarbons phases and properties from sources rocks of various types and also, adsorption models show the release of generated hydrocarbons into the free pore space of the source rock (Al-Hajeri et al., 2009). Further steps that are conducted by PetroMod are fluid analysis, fluid-flow calculations and reservoir volumetrics. However, these are not relevant to the aim of this thesis and for this reason, they won't be developed more.

### Simulator settings

The number of runs was set equal to 3 for PN-2 and E-1, and 2 for K-1. This was done based on the criterion that the "optimization" value in PetroMod 1D software should be smaller than 0.1%, as it is defined in PetroMod 1D user guide. This "optimization" value is the relative difference between the input layer thicknesses and the calculated values after the forward modelling (PetroMod 1D user guide).

The maximum cell thickness and time step duration were set to 40m and 0.50Ma for all three models. These values were selected based on the thickness and geological age of the formations of interest, that is, the source rocks of Pre-Prinos 1 and Pre-Prinos 3, in order to attain the required level of resolution in all models.

As it has been mentioned before, this study focuses only on generation modelling and not migration. Consequently, only petroleum generation were selected to be calculated, which includes secondary cracking and adsorption. Moreover, the features of organic secondary porosity, secondary cracking, and radiogenic heat were enabled.

The evolution of the vitrinite reflectance in time is modelled by the same equations of the EASY %Ro by Burnham and Sweeney (1990) regardless the choice of petroleum kinetics that has been made earlier. So, it produces the same results for all models.

## 4.4 CALIBRATION

After having defined the input data and boundary conditions, and have run the simulation, the simulation output need to be calibrated with well data. This is achieved by comparing calculated and measured data from the well. In this case, temperature and vitrinite reflectance data are used to calibrate the 1D models. This must be done until the calculated data match the measured ones within an acceptable range of accuracy. Once the two data sets match, a possible solution for the well has been achieved.

From the calibration procedure, it was noticed that simulated vitrinite reflectance and temperature are only affected by recent heat flow and surface temperature. They are not affected by the heat flow history except for the most recent part.

All calibration data has been provided by Dr Paschalia Kiomourtzi.

### 4.4.1 Temperature

Bottom-hole temperature data from well E-1 has been used for the 1D models of PN-2 and E-1, whereas bottom-hole temperature data from well K-2 was used for the model of K-1. There wasn't available temperature measurements from wells PN-2 and K-1, this is why the corresponding models were calibrated with data from nearby wells.

Regarding the temperature measurements from both E-1 and K-2, it should be noted that they haven't been corrected by the Horner method due to no availability of the required information, such as, the time (usually in hours) since the circulation of the drilling mud was stopped for each logging run and the length of time of the drilling mud circulation prior to this. Consequently, the uncorrected temperature data from E-1 and K-2 used for calibration are not fully representative because they underestimate the real temperatures of the formations.

The original bottom-hole temperature data from E-1 presents two displacements around the depths of 1900m and 2700m, as it is shown in the left graph of Figure 32. It was attempted to remove these

features from the temperature log of E-1 by shifting all temperature measurements according to the slope of the trendline of the deeper and hotter section. The result is displayed in the right graph of Figure 32.

From the available recorded bottom-hole temperature data of K-2, the maximum values from each depth point that measurements had been taken from were selected to be used for calibrating the model of K-1. Between the depths of 2666m and 2737m, the temperature measurements present an unusual behaviour, which wasn't taken into account during calibration.

Having modified the bottom-hole temperatures from wells E-1 and K-2, the geothermal gradient is estimated to be 3.76°C/100m and 5.97°C/100m, respectively, which is in accordance with estimates of the geothermal gradient in the surrounding area, as shown from other sources. Based on Kolios et al. (2007), the geothermal gradient from wells in the adjacent area of the Nestos Delta Basin is estimated to be normal (3.0°C/100m) within the younger formations up to Upper Miocene, and reaches as high as 5.6°C/100m within the Lower Miocene formations. Moreover, from personal communication with Dr Paschalia Kiomourtzi, it is suggested the broader area has a geothermal gradient that ranges between 3.85°C/100m and 4.5°C/100m. However, the geothermal gradient from K-2 is even higher, this could possibly be explained similarly to the cause that the deeper formations in the Nestos Delta Basin give higher geothermal gradient than the shallower ones, specifically, the Lower-Middle Miocene sediments have low thermal conductivity decreasing the heat flow from the metamorphic basement (Kolios et al., 2007). The K-2 well is near the uplifted basement of the South Kavala Ridge. As a consequence, the temperature difference with the overlying cooler sediments is much greater implying a higher geothermal gradient.

The calibration of the 1D models for all three well locations using temperature are displayed in Figure 33, Figure 34, and Figure 36.

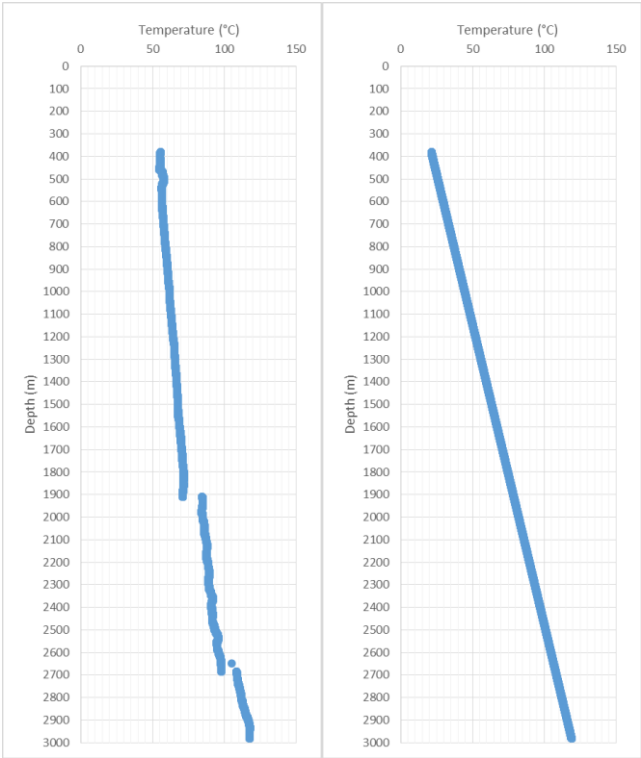


*Figure 32: Original (left graph) and modified (right graph) temperature measurements from well E-1.*

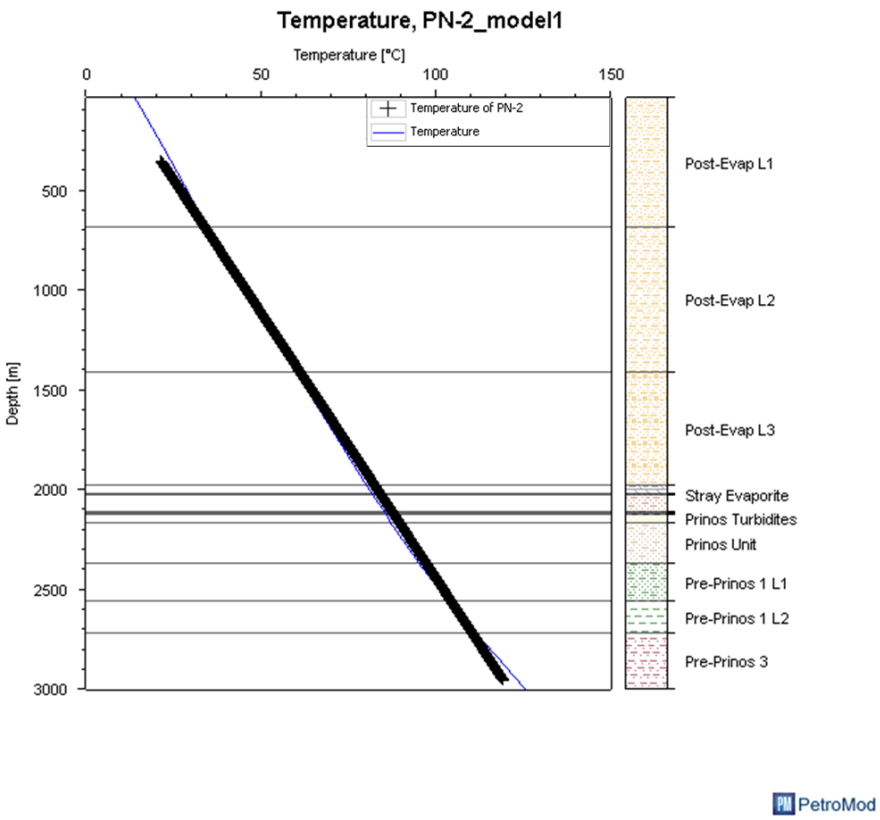


*Figure 33: Bottom-hole temperature calibration plot for modelled well location PN-2.*

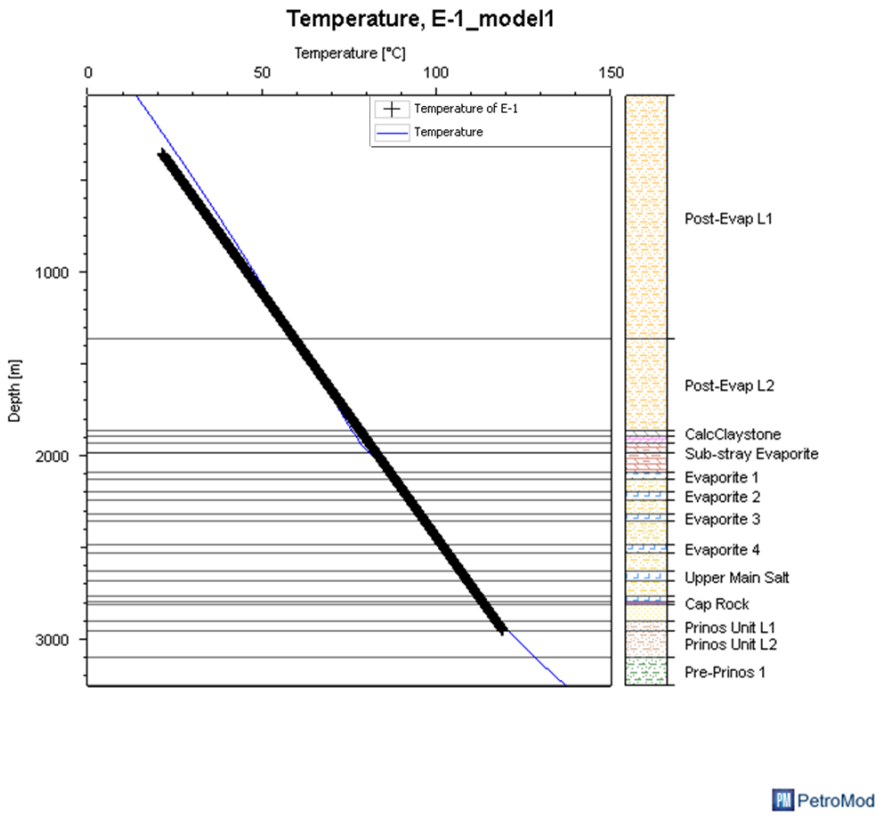


*Figure 34: Bottom-hole temperature calibration plot for modelled well location E-1.*

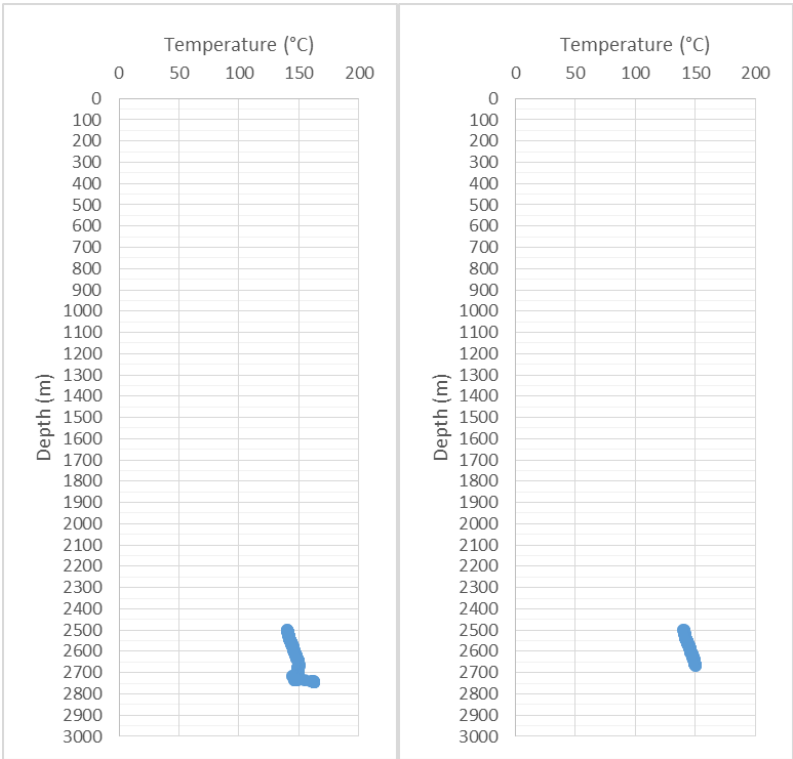


*Figure 35: Original (left graph) and modified (right graph) temperature measurements from well K-2.*

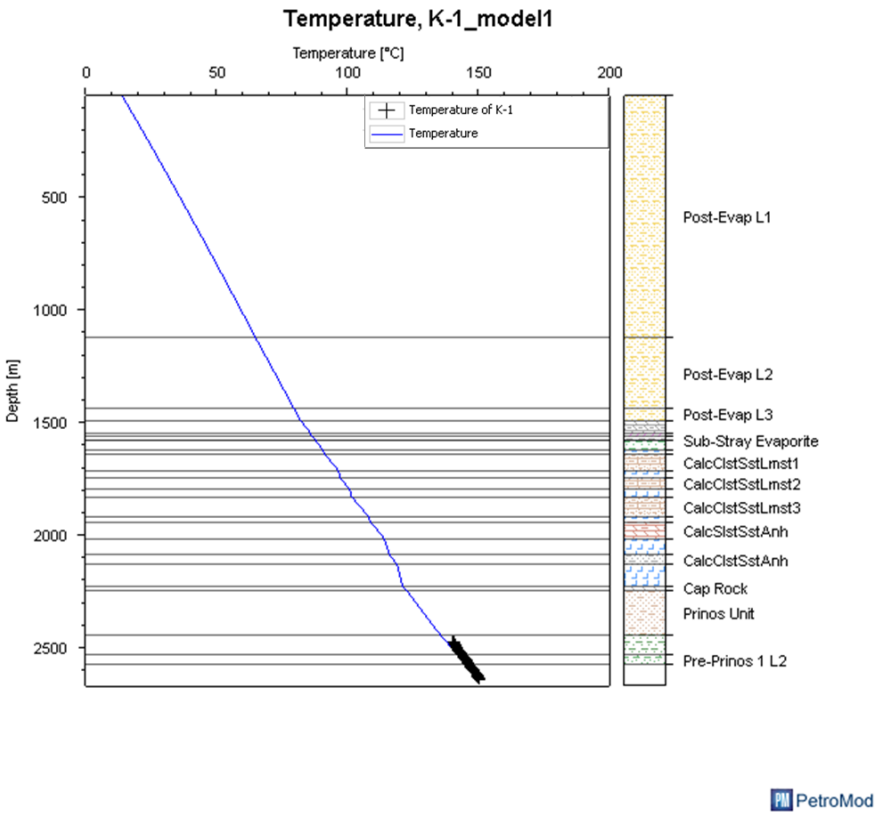


*Figure 36: Bottom-hole temperature calibration plot for modelled well location K-1.*

### 4.4.2 Vitrinite reflectance

The second type of data that was used for calibrating the models is vitrinite reflectance. The predictions of temperature and vitrinite reflectance were compared with measured data to calibrate uncertain thermal input data, as for example, paleo heat flow values.

There weren't available vitrinite reflectance measurements from the examined wells, and for this reason, vitrinite reflectance data was taken from bibliography from nearby wells in the broader area. This data was available in Kiomourtzi (2016). In particular, vitrinite reflectance data from well P-1 has been used for the 1D models of PN-2 and E-1, whereas vitrinite reflectance data from wells SK-1 and SK-2 was used for the model of K-1.

The calibration of the 1D models for all three well locations using vitrinite reflectance are displayed in Figure 37, Figure 38, and Figure 39.

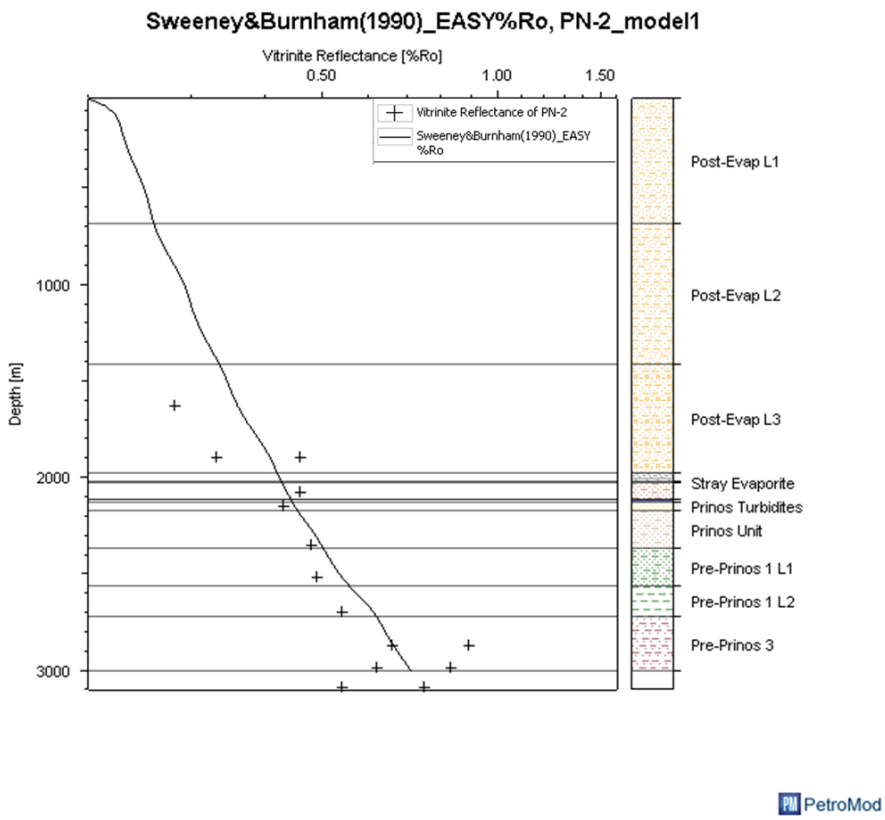


*Figure 37: Vitrinite reflectance calibration plot for well PN-2.*

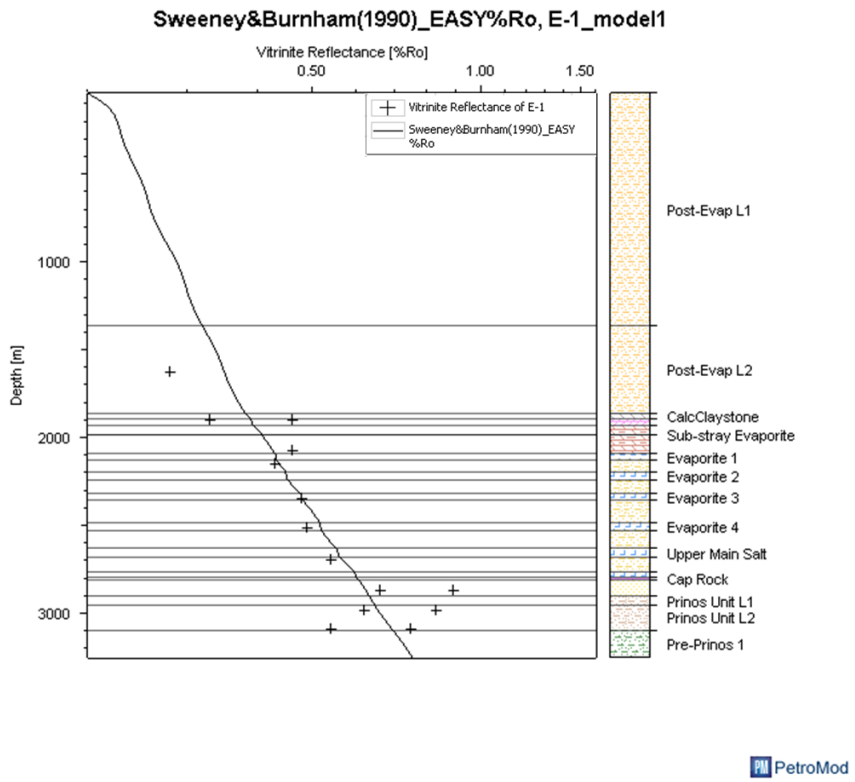


*Figure 38: Vitrinite reflectance calibration plot for well E-1.*

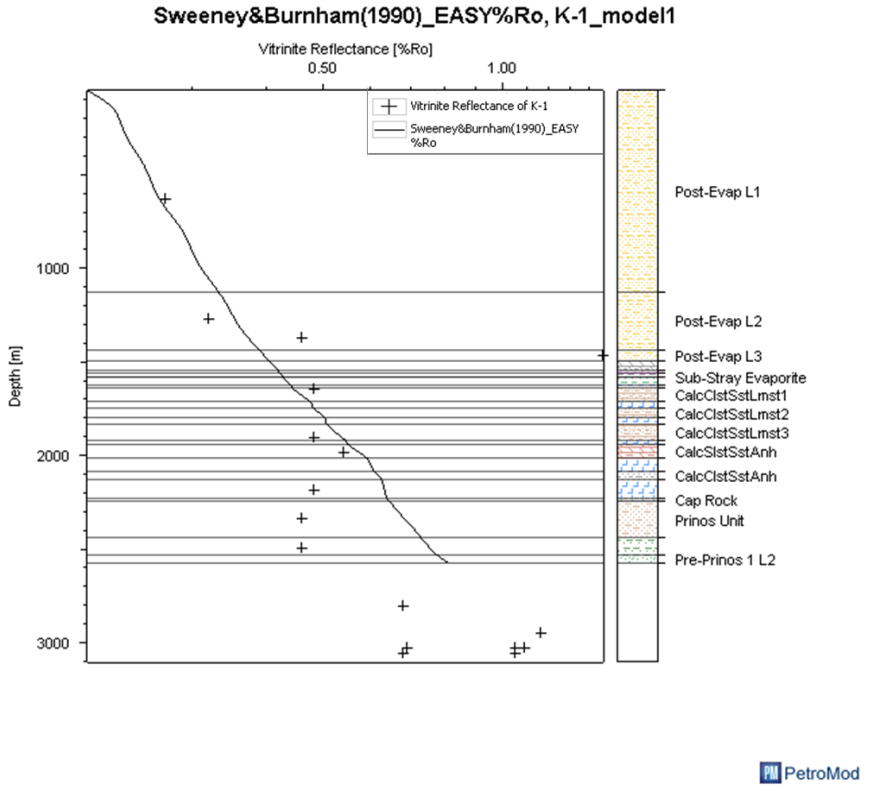


*Figure 39: Vitrinite reflectance calibration plot for well K-1.*

## 4.5 ASSUMPTIONS IN THE INPUT DATA

This chapter discusses briefly all assumptions and uncertainties that the input data encompasses. The geological model itself contains a lot of uncertainties. One method that brings the model closest to the reality and tries to increase the accuracy level of its prediction is calibration.

Stratigraphic data is the primary parameter that has been used for the construction of the models. This data in all three models of the present study came from the published work of Kiomourtzi (2016). The broader area of the Prinos-Kavala basin is well-studied due to its interest for hydrocarbon exploration and therefore, there is greater confidence about its stratigraphy. However, the hyper-saline and reducing conditions that prevailed during sedimentation hindered the development of life in the basin and thus, the procedure of age assignment is quite difficult due to lack of fossils. However, Kiomourtzi (2016) correlated the results from her work with old palynology and nannofossils studies from bibliography (Kavala Oil records), and ages were assigned to the main stratigraphic sequences. Regarding the ages of the unassigned layers in the models, they were calculated proportional to the thicknesses of the layers within the Evaporitic series, whereas in the other two series, they were estimated using the available information. This method premises that the sedimentation rate is the same, which may not be true.

Other assumptions in the models are these of the boundary conditions. Information about paleo water depth and heat flow data couldn't be found in the literature and for this reason, the imported values in the models do not show the actual circumstances, but instead, they are just indicative showing the changes in the corresponding parameters through the evolution of the basin.

Finally, many uncertainties and assumptions are included in the data used for calibration, that is, temperature measurements and vitrinite reflectance data. Much of the calibration data were derived from wells near the modelled ones. Bottom-hole temperature data was used without applying Horner plot correction method, as the required information wasn't available. Finally, all vitrinite reflectance data is derived from bibliography and belongs to nearby drilled wells.

Nevertheless, this preliminary study, which acts as a starting point, uses all these approximations and assumptions trying to model the burial and thermal history of the selected locations, and understand the maturity level of the potential source rocks.

# 5 RESULTS

Several models have been tested by changing the boundary conditions and parameters in the input table, for example, thickness of eroded sediments or erosion duration, in order to observe the effects in the simulation outputs. The results from this process will be described in chapter 5.5. Chapters 5.1-5.4 will present the results of 1D modelling in wells PN-2, E-1, and K-1 from the best matching between measured and calculated data. This case corresponds to model 1 in all three wells.

## 5.1 BURIAL HISTORY

Figure 40, Figure 41, and Figure 42 present the burial history reconstructions for each of the three modelled well locations. The deeper formations in each location overlies the eroded metamorphic basement, which wasn't included in these models. The basin experienced relatively slow and fairly constant subsidence during the Middle Miocene. The burial histories show one phase of strong uplift that occurred in the Upper Miocene, during which the sediments were eroded. The area remained uplifted up to the end of the Upper Miocene and started deepening from the Lower Pliocene until today. Moreover, it can be seen that the basin hadn't been subjected to periods of rapid subsidence and sedimentation. Finally, the burial histories of the three modelled well locations show that the basin has reached maximum burial depth at present-day. The E-1 well has the deepest burial among the three wells.

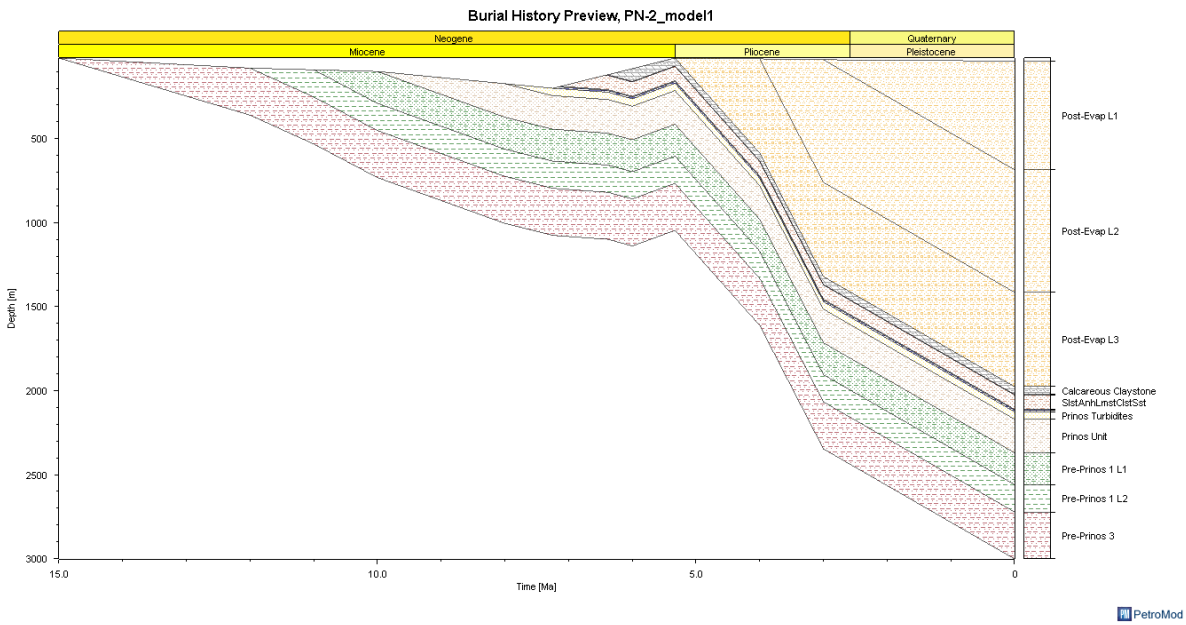


*Figure 40: Reconstructed burial history for the PN-2 well.*

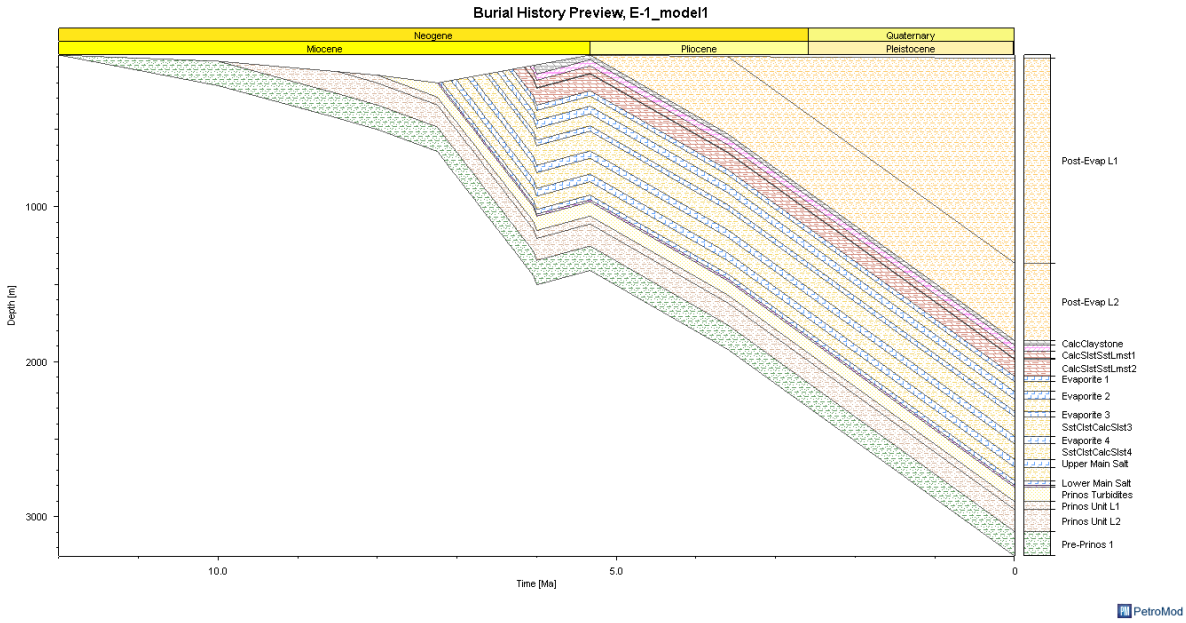


*Figure 41: Reconstructed burial history for the E-1 well.*

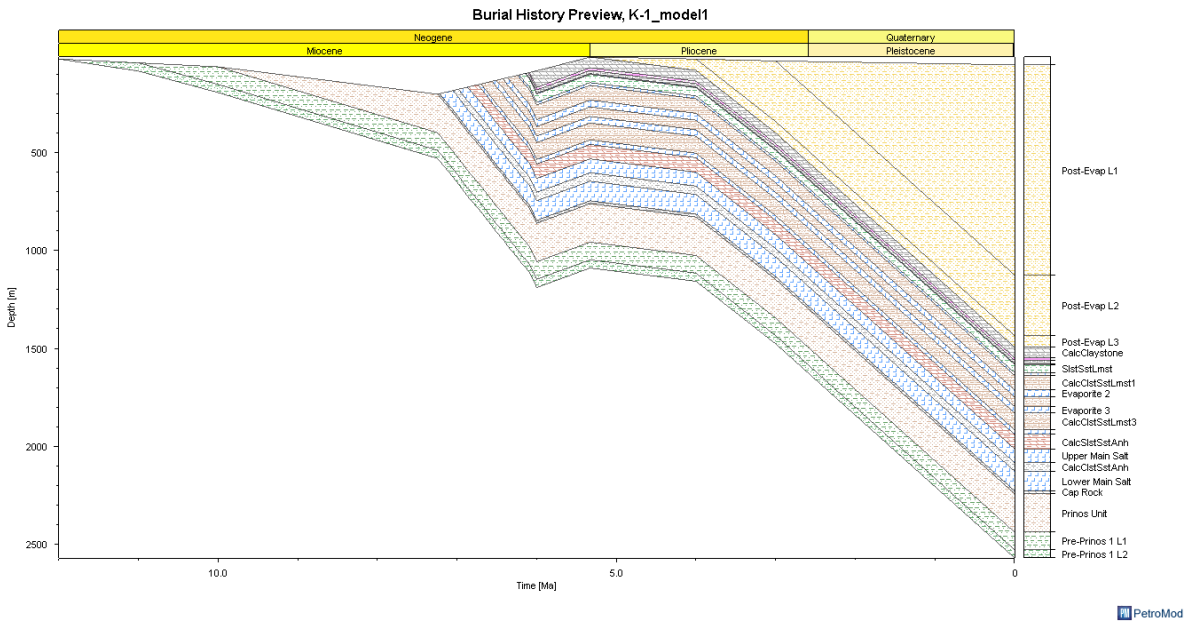


*Figure 42: Reconstructed burial history for the K-1 well.*

## 5.2 TEMPERATURE HISTORY

Modelled present-day temperatures in wells PN-2, E-1, and K-1 show a good fit with measured temperatures (Figure 33, Figure 34, and Figure 36). Figure 43, Figure 44, and Figure 45 present the temperature evolution of the three modelled well locations within the Prinos-Kavala basin.

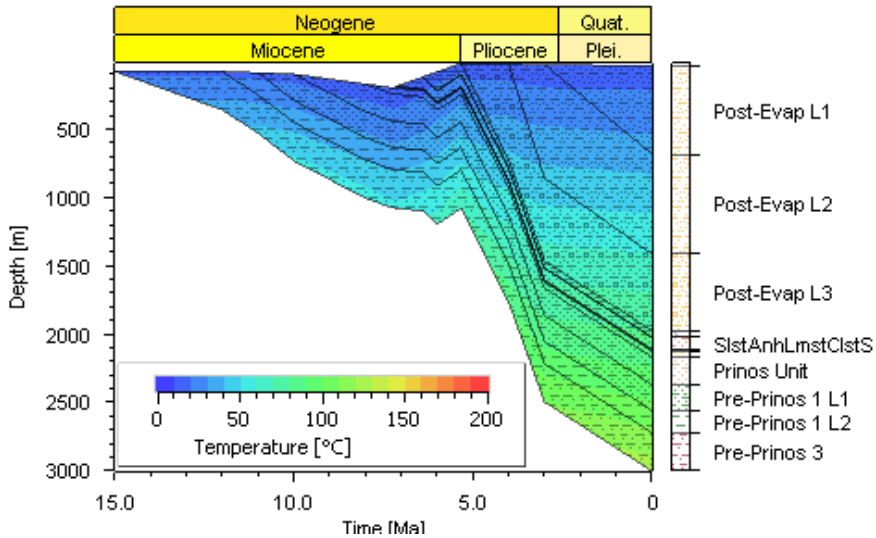


*Figure 43: Burial history of the PN-2 well with temperature overlay.*

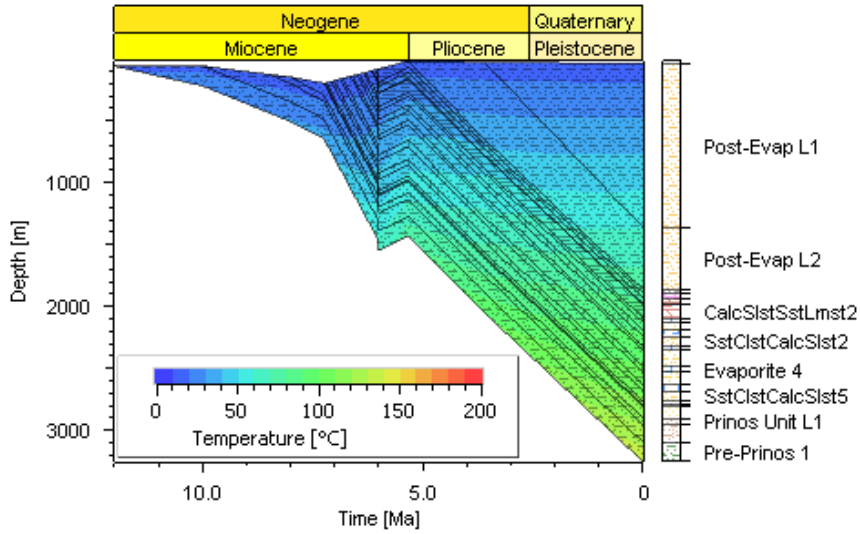


*Figure 44: Burial history of the E-1 well with temperature overlay.*

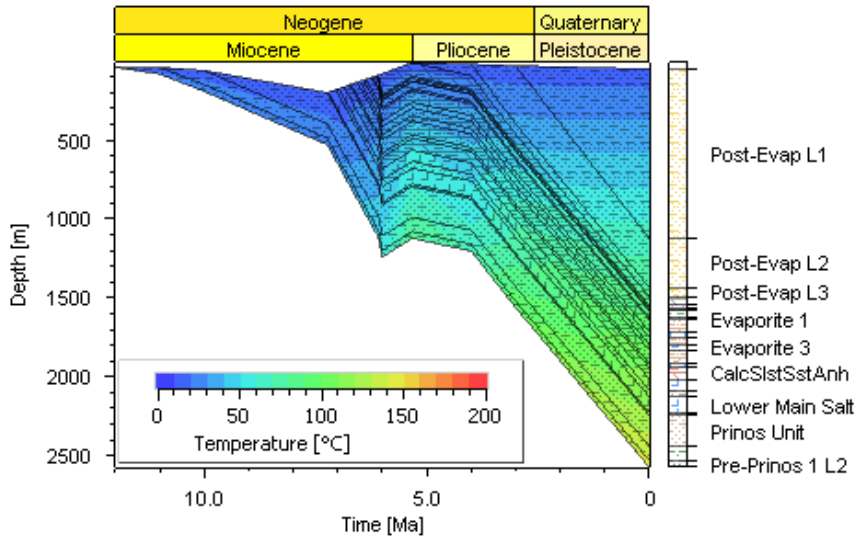


*Figure 45: Burial history of the K-1 well with temperature overlay.*

The results from the simulation indicate that all three locations have experienced pretty much the same temperature levels with higher temperatures in the southern part of the basin (well K-1). A steady temperature increase with time is observed in all three locations. The higher temperatures in all wells were reached at present-day. In particular, the Pre-Prinos 3 formation in well PN-2 reached a temperature up to 125.56°C in the deeper parts of the interval and the temperature of the overlying Pre-Prinos 1 goes up to 111.5°C. In well E-1, the present-day temperatures of the Pre-Prinos 1 layer vary between 127.8°C and 137.17°C, and in well K-1, they range from 135°C up to 145.77°C.

## 5.3 PRESENT-DAY VITRINITE REFLECTANCE VALUES

Vitrinite reflectance is one of the most common indicators for thermal maturity. The default model of PetroMod for calculating vitrinite reflectance is the EASY %Ro by Sweeney and Burnham (1990). The ranges of the maturity levels for primary oil and gas generation from kerogen of type II and type III used in this model are the following: immature (Ro ≤ 0.55%), early oil (Ro ≤ 0.70%), main oil (Ro ≤ 1.0%), late oil (Ro ≤ 1.30%), wet gas (Ro ≤ 2.0%), dry gas (Ro ≤ 4.0%), and overmature (Ro ≥ 4.0%) (Hantschel and Kauerauf, 2009).

Vitrinite reflectance measurements match quite well with the predicted vitrinite reflectance values. Modelled maturity (vitrinite reflectance) in wells PN-2, E-1, and K-1 is presented in Figure 37, Figure 38, and Figure 39, respectively. Figure 46, Figure 47, and Figure 48 present the maturity history of the three modelled well locations within the Prinos-Kavala basin.

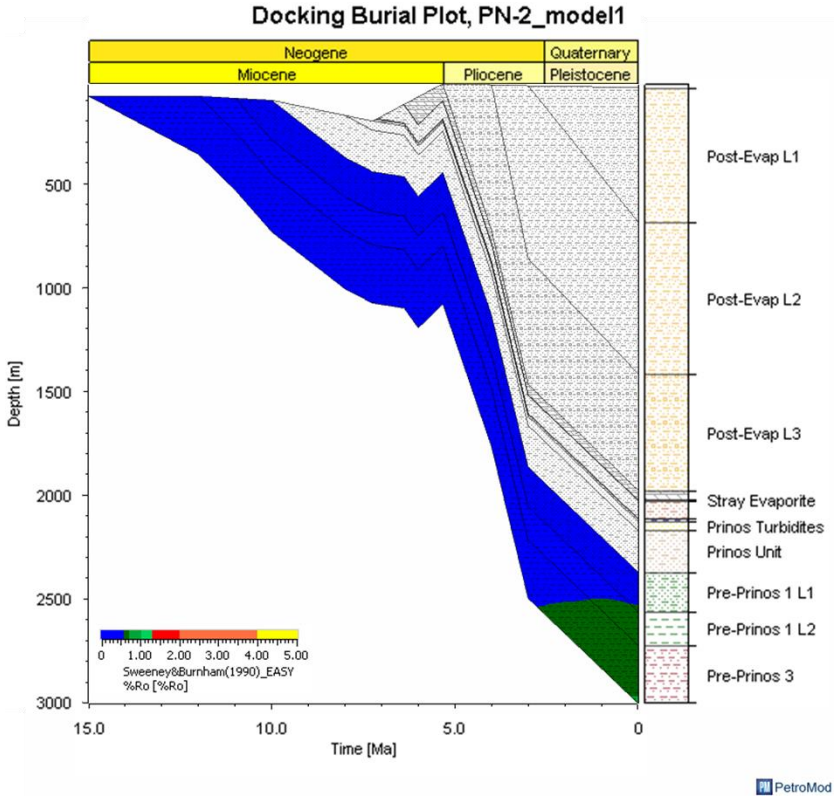


*Figure 46: Modelled present-day maturity (vitrinite reflectance) of the assigned source rock layers in the PN-2 well.*

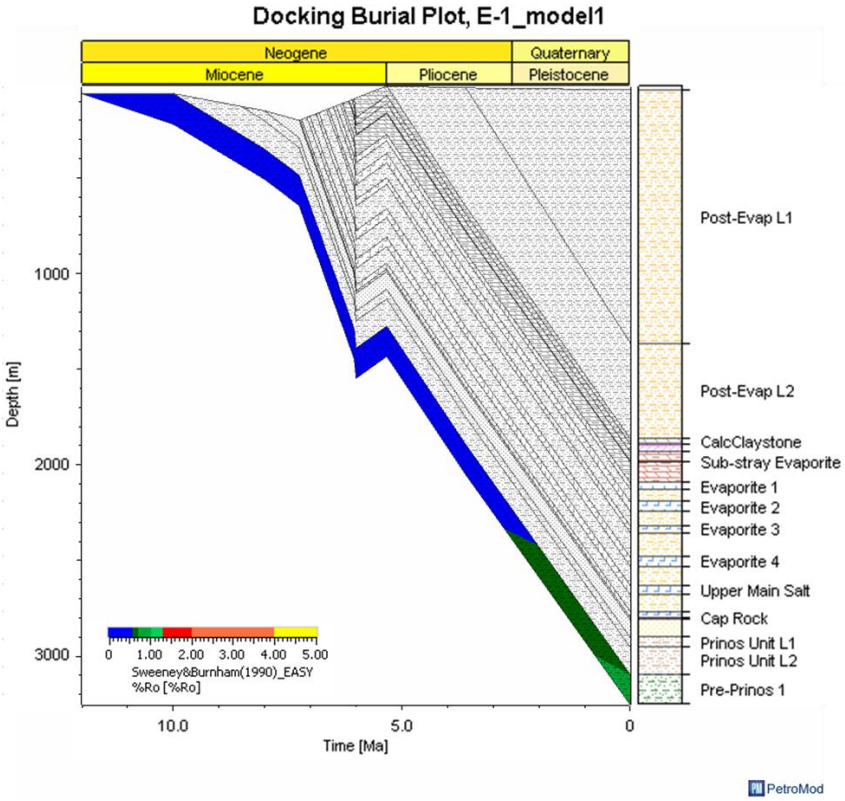


*Figure 47: Modelled present-day maturity (vitrinite reflectance) of the assigned source rock layer in the E-1 well.*

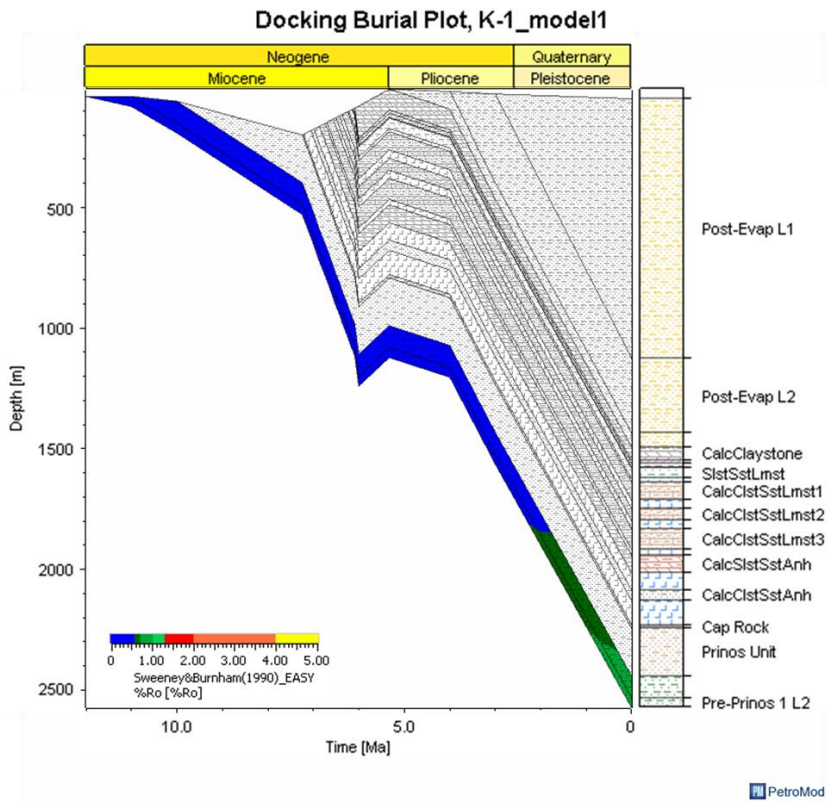


*Figure 48: Modelled present-day maturity (vitrinite reflectance) of the assigned source rock layers in the K-1 well.*

The maturity history plots indicate that the deepest parts of the assigned source rocks (Pre-Prinos 3 and Pre-Prinos 1) entered the hydrocarbon generation ranges around the Pliocene-Pleistocene boundary in all three well locations. Since then, the maturity keeps increasing up to today as the basin sinks at greater depths. The most mature source rocks seem to be those in the K-1 well. The onset of the hydrocarbon generation in the PN-2 well occurred at 2.67Ma at 2547m depth and the zone of the main oil was reached at 0.17Ma at 2973m depth. Whereas, Pre-Prinos 1 started generating hydrocarbons at 1.26Ma at a depth of 2508m. In the E-1 well, initial oil generation occurred at 2.65Ma at 2362m depth, whereas the main oil maturity zone was reached at 0.74Ma at 3005m depth. The shallowest transition to the early oil zone (that is, onset of hydrocarbon generation) is observed in the K-1 well at 2.15Ma when the basin had been buried to 1841m depth, and the main oil maturity zone in this well started at 0.87Ma at 2275m.

## 5.4 Transformation Ratio

One of the simulation outputs of PetroMod is the transformation ratio (TR), which indicates the percentage of kerogen transformed into petroleum for each source rock (Al-Hajeri et al., 2009) and depends on the temperature history and sedimentation rate (Hantschel and Kauerauf, 2009). As it has been mentioned earlier in Chapter 2.2.3, the critical moment, which is a point in time that best depicts

the most generation-migration-accumulation of hydrocarbons in a petroleum system (Magoon and Dow, 1994), is usually the onset of expulsion/migration (Dembicki, 2017). And it lies in a TR range from 50% to 90% (Al-Hajeri et al., 2009). Figure 49, Figure 50, and Figure 51 display the transformation ratios in the base of the assigned source rocks in the three modelled wells (PN-2, E-1, and K-1), as overlays on the burial histories. The overlay of TR (all) in PetroMod indicates the quantitative transformation ratio related to total organic carbon and production index for source rocks referring to the expulsion of oil and gas (https://www.software.slb.com/products/petromod/petromod-composition).

Transformation in Pre-Prinos 3 began at 3.76Ma at a depth of 1827m and the formation has a present-day TR of 9.04% at its base. E-1 is slightly more mature than PN-2. Specifically, the organic matter transformation in the formation of Pre-Prinos 1 in well E-1 started at 5.23Ma at 1433m. The present-day transformation ratio is at 42.87% at the base of the assigned source rock. The K-1 well has higher transformation ratio compared to the other two wells. The transformation in this well began at 4.73Ma at 1138m, whereas the present-day TR value at the base of Pre-Prinos 1 is 55.60%. Figure 52 is a comparison among time plots of the transformation ratio among the three wells showing the difference in the onset of the transformation of the organic matter in each well. Consequently, taking into account the present-day transformation ratios in all three wells, only in the K-1 well, the threshold for hydrocarbon expulsion has been reached allowing the possibility for hydrocarbon generation and expulsion.

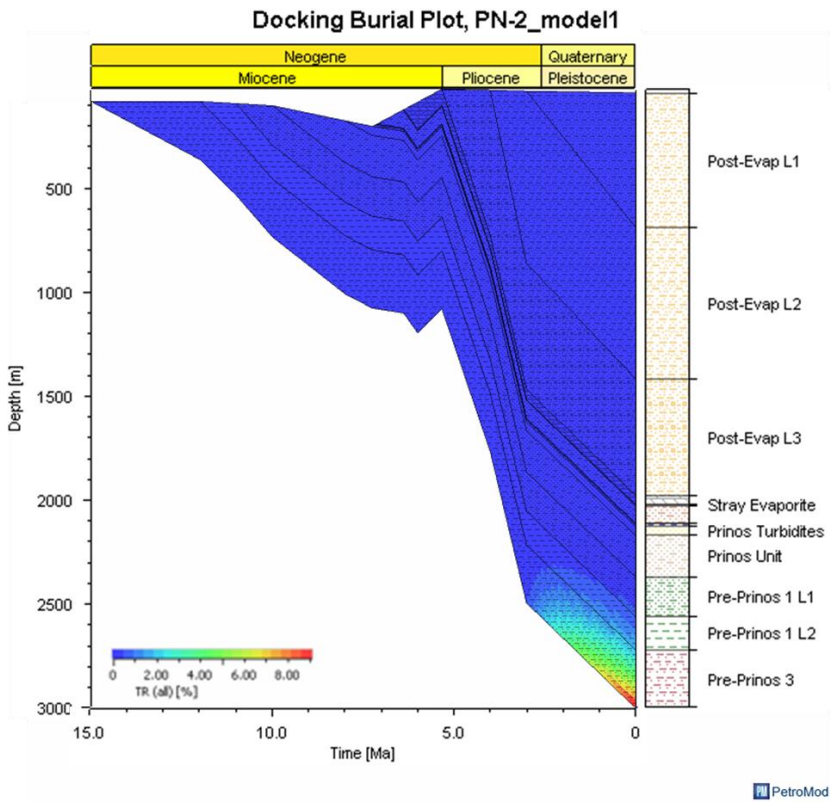


*Figure 49: Burial history plot of the PN-2 well with a transformation ratio overlay.*

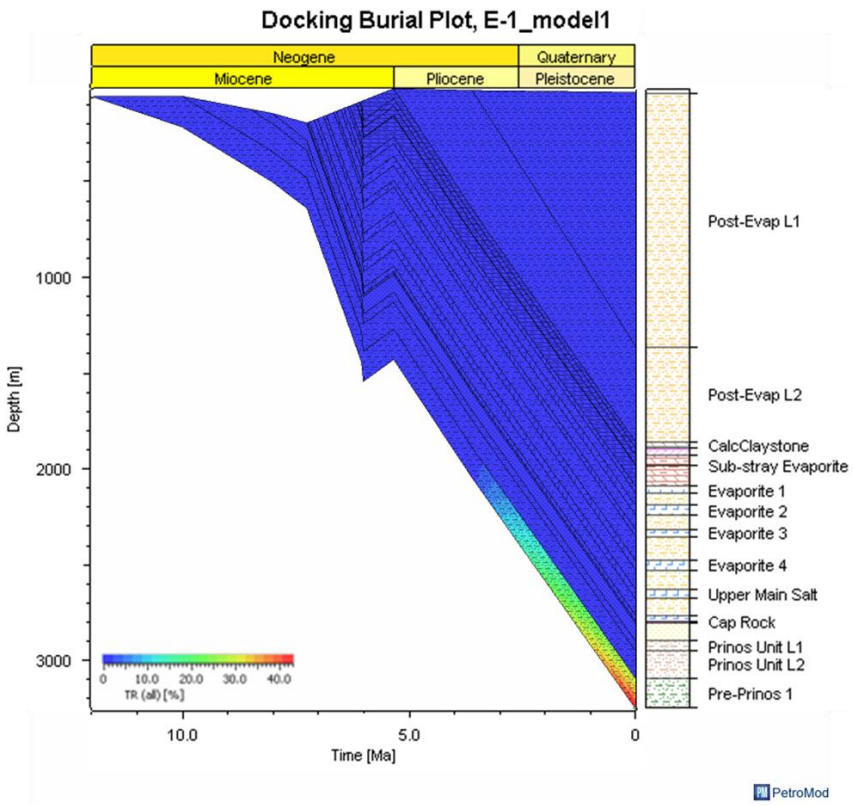


*Figure 50: Burial history plot of the E-1 well with a transformation ratio overlay.*

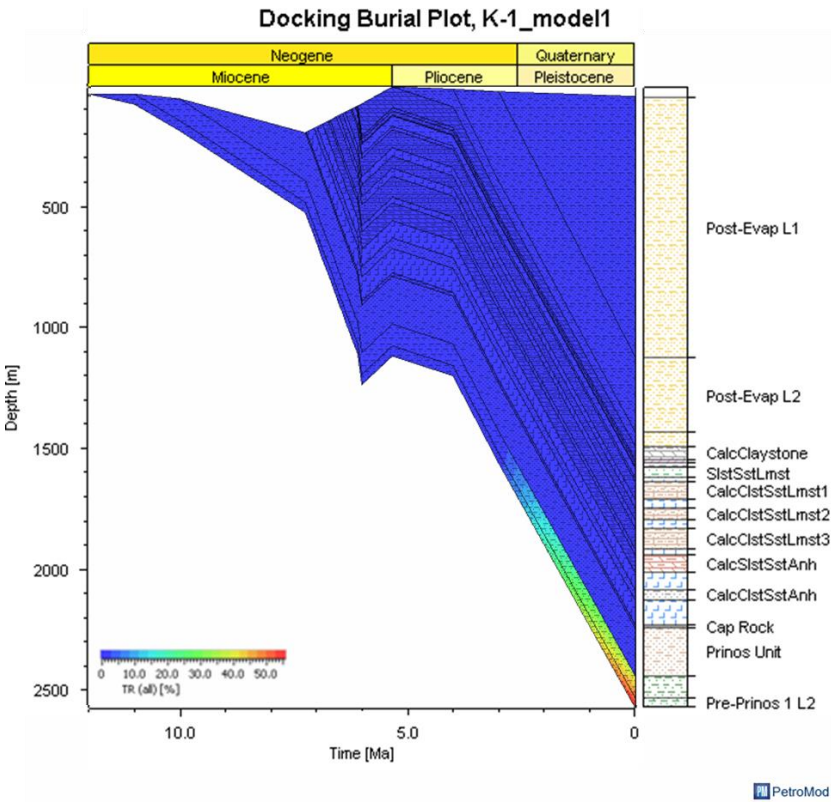


*Figure 51: Burial history plot of the K-1 well with a transformation ratio overlay.*

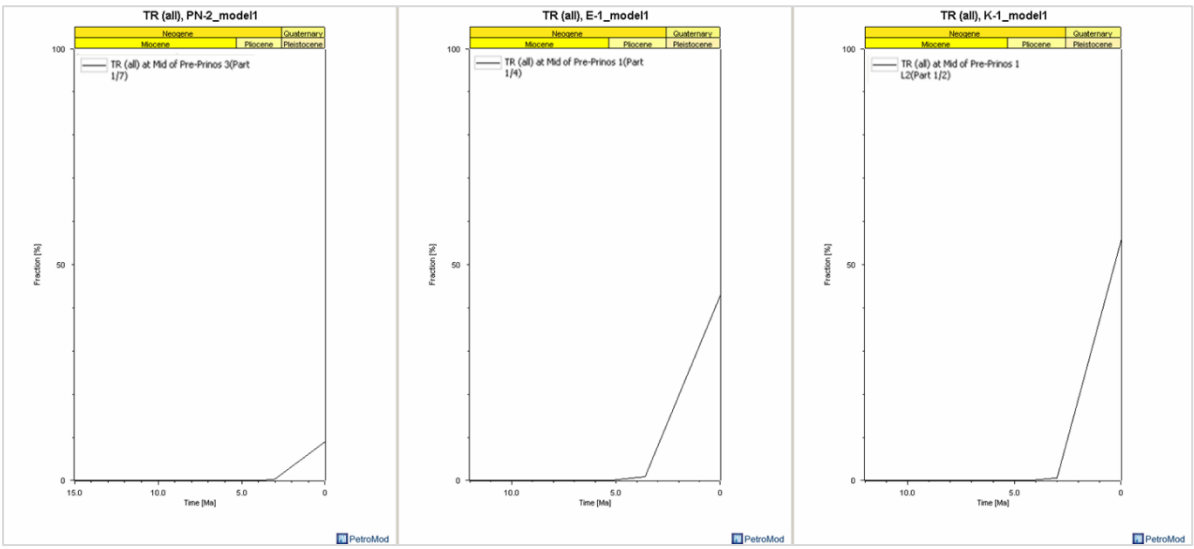


*Figure 52: Transformation ratio time plots in the three modelled wells (PN-2, E-1 and K-1).*

## 5.5 PETROLEUM GENERATION AND EXPULSION HISTORY

The aim of 1D modelling is to reconstruct the geological history at one or more points in an area. As no volume is defined in 1-D modelling, generated petroleum mass can't be predicted. Instead, the potential generation oil and gas masses in mgHC/gTOC were estimated in this study by the selected

petroleum kinetics model, Pepper & Corvi (1995). This was done in order to acquire a better understanding for what it can be expected from each assigned source rock formation. Burial plots with potential oil and gas generation mass overlays for each well are displayed in Figure 53, Figure 54, and Figure 55.

**PN-2**

Hydrocarbon generation started in all source rocks from Pliocene-Pleistocene boundary and continues up to now, as is seen in the maturity plots (chapter 5.3). Among the wells used for this study, the Pre-Prinos 3 formation appears only in well PN-2 and is less thermally mature than the assigned source rock formation, Pre-Prinos 1, in the other two wells. Little hydrocarbon generation from the Pre-Prinos 3 formation is predicted to date. In particular, 31.37mgHC/gTOC of potential oil mass and 1.26mgHC/gTOC of gas mass. The second assigned source rock in this well is Pre-Prinos 1 and for this formation, the model predicts 6.27mgHC/gTOC of potential oil generation mass and no gas. The onset of the hydrocarbon generation in the PN-2 well occurred at 2.67Ma at a depth of 2547m from the Pre-Prinos 3 formation with a present-day vitrinite reflectance value of 0.71% and a present-day transformation ratio equal to 9.04%, showing that the formation hasn't yet reached peak oil expulsion in the specific area.

**E-1**

In well E-1, the assigned source rock is the Pre-Prinos 1 formation, which is thinner than the corresponding formation in PN-2, and lies at greater depths. The model for E-1 predicts the petroleum system to have attained the stage of main oil generation at 0.74Ma, earlier than PN-2, and the source rock interval to be more thermally mature than in PN-2. Therefore, more potential masses for oil and gas are expected to have been generated in this well by the Pre-Prinos 1 formation. The potential oil generation mass is predicted at 259.61mgHC/gTOC and for gas at 7.38mgHC/gTOC. The base of the formation is predicted to have a present-day vitrinite reflectance value of 0.75% and a present-day transformation ratio equal to 42.87%, from which it is inferred that the source rock formation hasn't yet reached peak oil expulsion in the specific area.

**K-1**

K-1 well is located in the Kallirachi field in the south part of the Prinos-Kavala basin. This is the most productive well in the study area resulting potential generation masses relatively high compared to the other two places. Potential oil generation mass is predicted to be 362.15mgHC/gTOC and for gas is predicted at 12.23mgHC/gTOC. The model has predicted that the stage of main oil generation was reached at 0.87Ma and the base of the source rock (Pre-Prinos 1) has a present-day vitrinite

reflectance value of 0.81% and a present-day transformation ratio equal to 55.60%. Hence, it is concluded that the formation of Pre-Prinos 1 has reached peak oil expulsion. Figure 56 shows that hydrocarbon expulsion started at 0.44Ma.

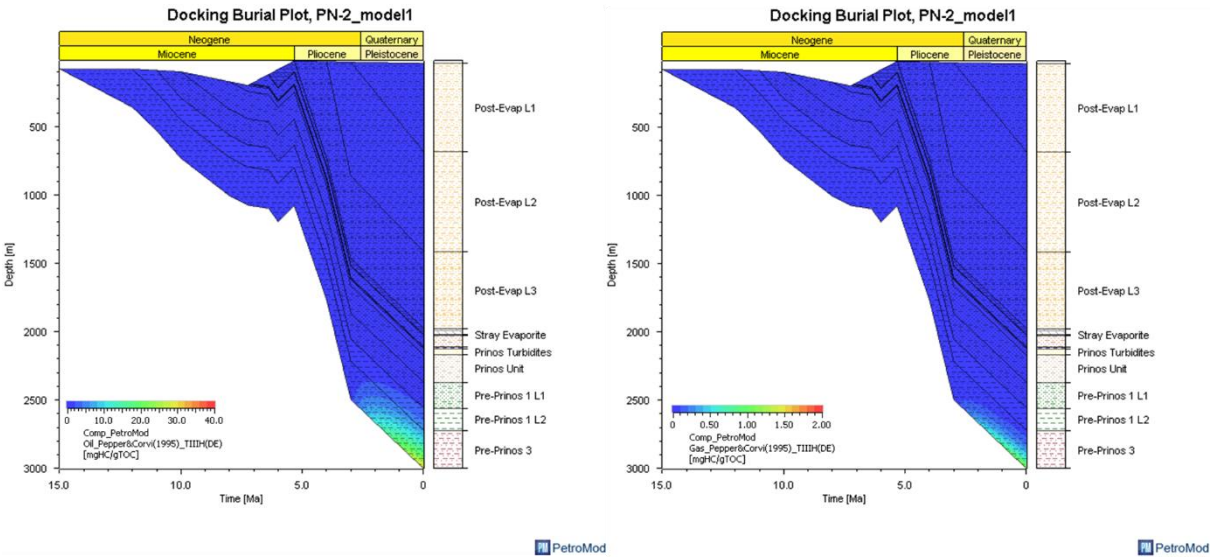


*Figure 53: Potential generation oil and gas masses by Pepper & Corvi (1995) for the assigned source rocks in the PN-2 well.*

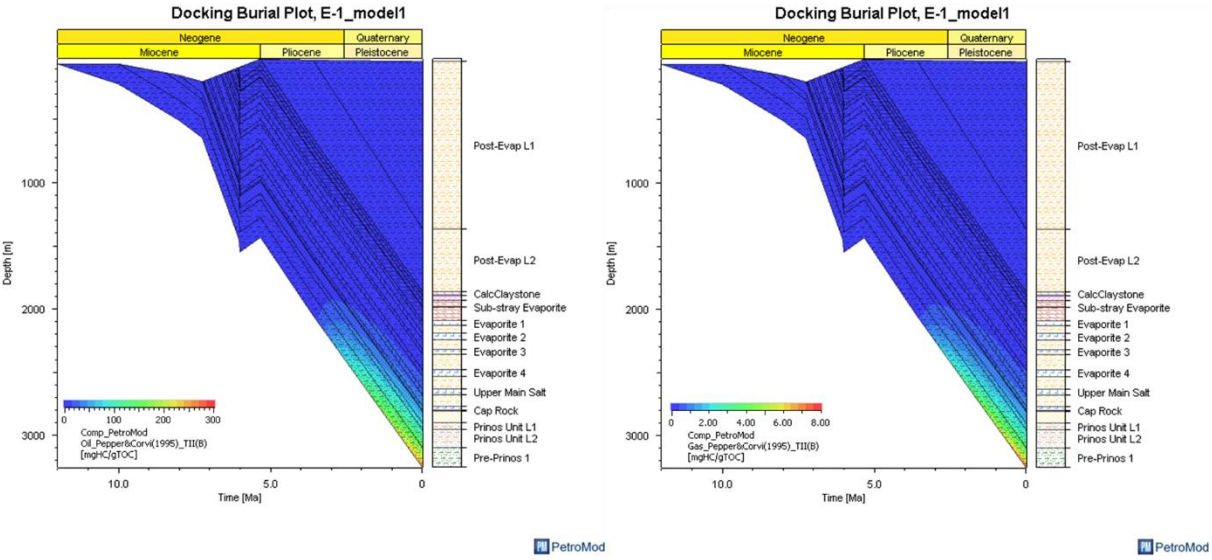


*Figure 54: Potential generation oil and gas masses by Pepper & Corvi (1995) for the assigned source rock in the E-1 well.*

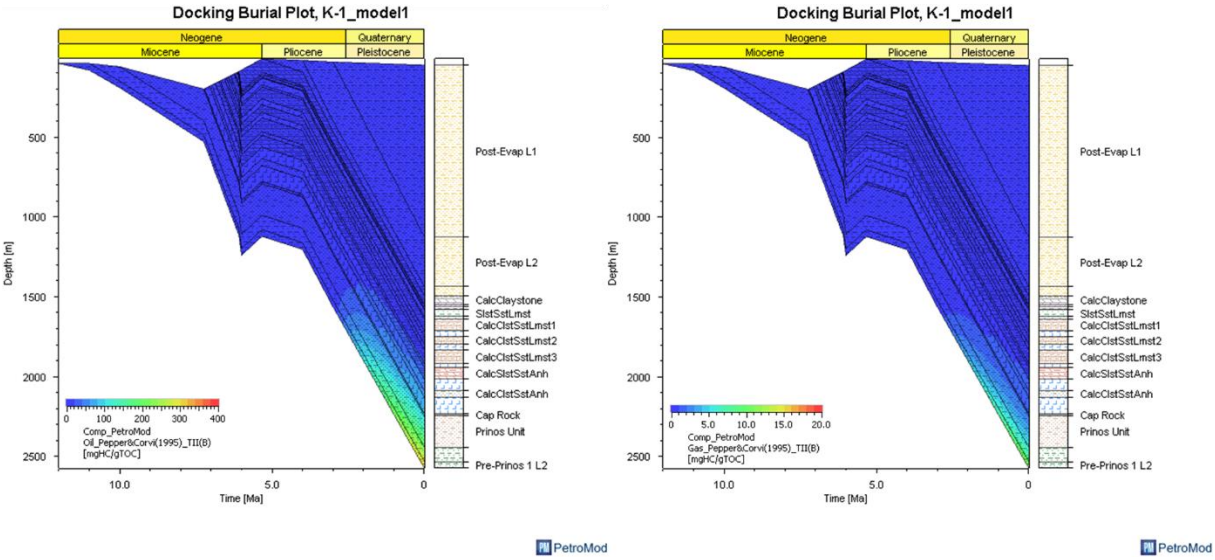


*Figure 55: Potential generation oil and gas masses by Pepper & Corvi (1995) for the assigned source rock in the K-1 well.*

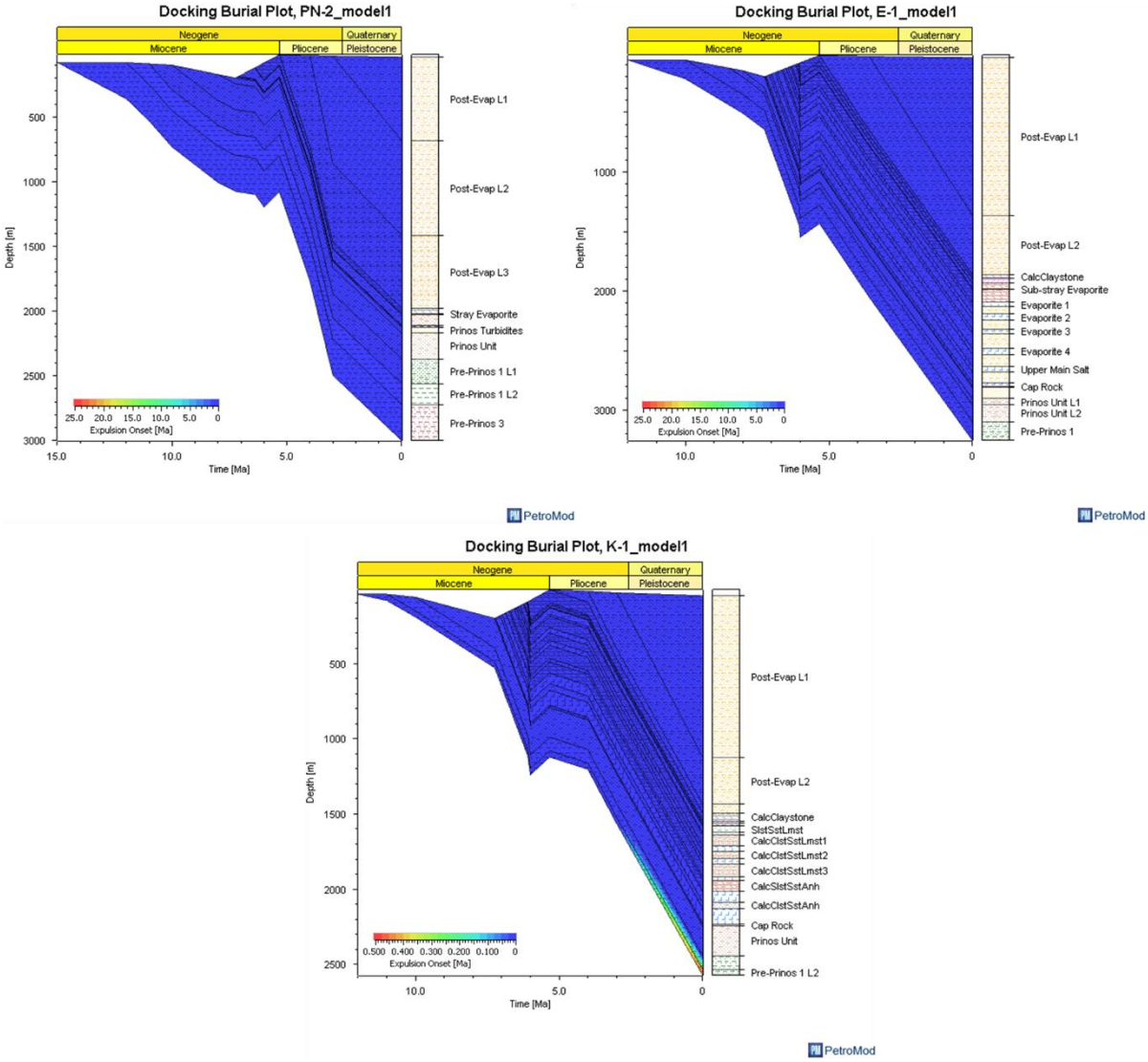


*Figure 56: Burial plots of the modelled wells with an expulsion onset overlay.*

## 5.6 SENSITIVITY ANALYSIS

In the context of this study, it was also attempted to test the influence of some input parameters and to assess the resultant effect of varying some input parameters in the models. This was accomplished by performing sensitivity analysis, a method which is used to measure susceptibility to changes in the model's input and to determine how sensitive the results are to these variations (Dembicki, 2017). Sensitivity analysis involves making finite changes in the input parameters of the previously optimized model and recalculation of the results (Welte et al., 1997). The input parameters that were varied to test their effects on the simulation results for the temperature and maturity history are the following: heat flow, paleo water depth, thickness of eroded sediments, timing and duration of erosional events and source rock characteristics. The original input of lithologies wasn't included in sensitivity analysis because this type of input data is based on real observations and measurements, and therefore, cannot be significantly changed. Additionally, the boundary condition of sediment water interface temperature wasn't included because it was calculated using the integrated tool (Wygrala, 1989) of PetroMod. The sections below present the results from further analyses with multiple scenarios.

**Timing and duration of the erosion between the Evaporitic and Post-Evaporitic series**

Varying the timing and duration of the erosional event between the Evaporitic and Post-Evaporitic series in the Pliocene-Pleistocene boundary, showed that no changes were caused to the results of the simulation, temperature and vitrinte reflectance (Figure 57). Specifically, the erosional event was changed to have less duration, from 5.54Ma to 5.33Ma, as well as to last longer, from 6.19Ma to 5.00Ma. Moreover, the timing of the erosion was changed to 5.33-4.66Ma. However, all these changes didn't have any effects to the simulated temperature and maturity. Figure 57 presents the predicted temperature and vitrinite reflectance profiles in well PN-2 for the optimized model (1) and the above three changes (2-4).

**Original thickness of eroded sediments**

Another parameter that was checked was the original thickness of eroded sediments. In all three modelled wells, it has been set to 30m in the optimized models (after personal communication with Dr. Kiomourtzi Paschalia). In the case of well PN-2, it was changed to 100m and 10m and the results can be seen in temperature and vitrinite reflectance graphs (5) and (6) of Figure 57, respectively. Again, there is no difference with those of the optimized model. Consequently, it is concluded that the original thickness of eroded sediments doesn't affect the temperature and maturity history of the models.

**Paleo Water depth**

The effect of paleo water depth was tested by changing its values in two periods of the evolution of the basin in which there is more confidence about the range of the specific boundary condition, that is, the upper boundaries of the Evaporitic sequence and the Prinos Turbidites formation. Paleo water depth was changed in these two events so as to be within geologically acceptable ranges. In the first scenario, paleo water depth at 5.33Ma (upper boundary of the Evaporitic series) was changed from 20m to 7m, and at 7.25Ma (upper boundary of the Prinos Turbidites formation) was changed from 200m to 500m. At the second scenario, paleo water depth was set at 0m in the younger event of 5.33Ma and kept constant at 200m at the older event of 7.25Ma. As it is observed in Figure 58, there is no change in the modelled temperature and vitrinite reflectance.

**Heat flow**

The effect of heat flow on the models was tested by increasing and decreasing the heat flow compared to what was used in the optimized model (model 1) for each well. In all three wells, model 2 corresponds to a lower heat flow scenario and model 3 to a higher heat flow scenario. The heat flow values for each model in wells PN-2, E-1 and K-1 are presented in Table 7, Table 8, and Table 9, respectively.

The source rocks formations are more mature in the high heat flow scenarios than in the optimized models (Figure 59). In PN-2, hydrocarbon generation in the Pre-Prinos 3 formation began at the depth of 2547m in the optimized model, 2449m in the high heat flow scenario and 2630m in the low heat flow scenario. Regarding the Pre-Prinos 1 formation, generation began at 2508m in the optimized model, 1415m in the high heat flow scenario and 2625m in the low heat flow scenario. This shows that hydrocarbon generation begins at shallower depths in higher heat flows. The same is observed in the other two wells. In particular, in E-1, oil generation begins at 2362m in the optimized model, 2139m in the high heat flow scenario and 2707m in the low heat flow scenario. Finally, in K-1, oil generation begins at 1841m in the optimized model, 1660m in the high heat flow scenario and the source rock is still immature in the low heat flow scenario.

It was also observed that transformation of the kerogen occurs slightly earlier in higher heat flow scenarios (Figure 60). In PN-2, transformation in the Pre-Prinos 3 formation began at 3.76Ma in the optimized model, 3.88Ma in the high heat flow scenario and 3.57Ma in the low heat flow scenario. In the Pre-Prinos 1 formation, transformation began at 2.90Ma in the optimized model, 3.00Ma in the high heat flow scenario and 2.64Ma in the low heat flow scenario. In E-1, transformation began at 5.23Ma, 5.08Ma, and 5.28Ma for the optimized model, the low heat flow scenario and the high heat flow scenario, respectively. Finally, in K-1, transformation began at 4.73Ma, 4.69Ma, and 5.63Ma for the optimized model, the low heat flow scenario and the high heat flow scenario, respectively.

| PN-2 | | | |
|---|---|---|---|
| | Model 1 | Model 2 | Model 3 |
| Age (Ma) | HF (mW/m$^2$) | HF (mW/m$^2$) | HF (mW/m$^2$) |
| 0.00 | 69 | 65 | 75 |
| 3.00 | 69 | 65 | 75 |
| 4.00 | 69 | 69 | 69 |
| 5.33 | 80 | 80 | 80 |
| 6.00 | 70 | 70 | 70 |
| 7.25 | 70 | 70 | 70 |
| 10.00 | 85 | 85 | 85 |
| 12.00 | 85 | 85 | 85 |
| 15.00 | 100 | 100 | 100 |

*Table 7: Heat flows of the optimized model (1) and the low (2) and high (3) heat flow scenarios in well PN-2.*

| E-1 | | | |
|---|---|---|---|
| | Model 1 | Model 2 | Model 3 |
| Age (Ma) | HF (mW/m$^2$) | HF (mW/m$^2$) | HF (mW/m$^2$) |
| 0.00 | 80 | 65 | 90 |
| 3.60 | 80 | 75 | 90 |
| 5.33 | 80 | 80 | 80 |
| 6.00 | 70 | 70 | 70 |
| 7.25 | 70 | 70 | 70 |
| 8.00 | 70 | 70 | 70 |
| 10.00 | 85 | 85 | 85 |
| 12.00 | 90 | 90 | 90 |

*Table 8: Heat flows of the optimized model (1) and the low (2) and high (3) heat flow scenarios in well E-1.*

| K-1 | | | |
|---|---|---|---|
| | Model 1 | Model 2 | Model 3 |
| Age (Ma) | HF (mW/m$^2$) | HF (mW/m$^2$) | HF (mW/m$^2$) |
| 0.00 | 112 | 65 | 120 |
| 3.00 | 112 | 75 | 120 |
| 4.00 | 90 | 90 | 120 |
| 5.33 | 120 | 120 | 130 |
| 6.00 | 75 | 75 | 75 |
| 7.25 | 75 | 75 | 75 |
| 10.00 | 85 | 85 | 85 |
| 12.00 | 100 | 100 | 100 |

*Table 9: Heat flows of the optimized model (1) and the low (2) and high (3) heat flow scenarios in well K-1.*

## Source rock characteristics

In the end, the last input data that was tested was the source rock characteristics (TOC and HI). Here, all parameters were kept constant except for TOC and HI, which were modified. Specifically, the changes that were made are the following. In PN-2, TOC was changed from 1.34% to 2.01%, and HI from 244mgHC/gTOC to 289mgHC/gTOC. The new values are the maximum from the results of Rock-Eval analysis conducted for this study. In E-1, TOC was set to 1.90%, from 1.71% of the optimized model and HI was changed from 119mgHC/gTOC to 220mgHC/gTOC. 1.90% and 220mgHC/gTOC are the maximum values observed in the corresponding measurements of well P4. Finally, in K-1, TOC was

changed from 1.65% to 2.66%, and HI from 360.5mgHC/gTOC to 513mgHC/gTOC. 2.66% and 513mgHC/gTOC are the maximum values observed in the corresponding measurements of well P4

The results (Figure 61) showed that there is no effect on temperature and maturity histories. It is expected that there will be differences in the results associated with the volume of the generated oil and gas. However, these results are not part of the present study.

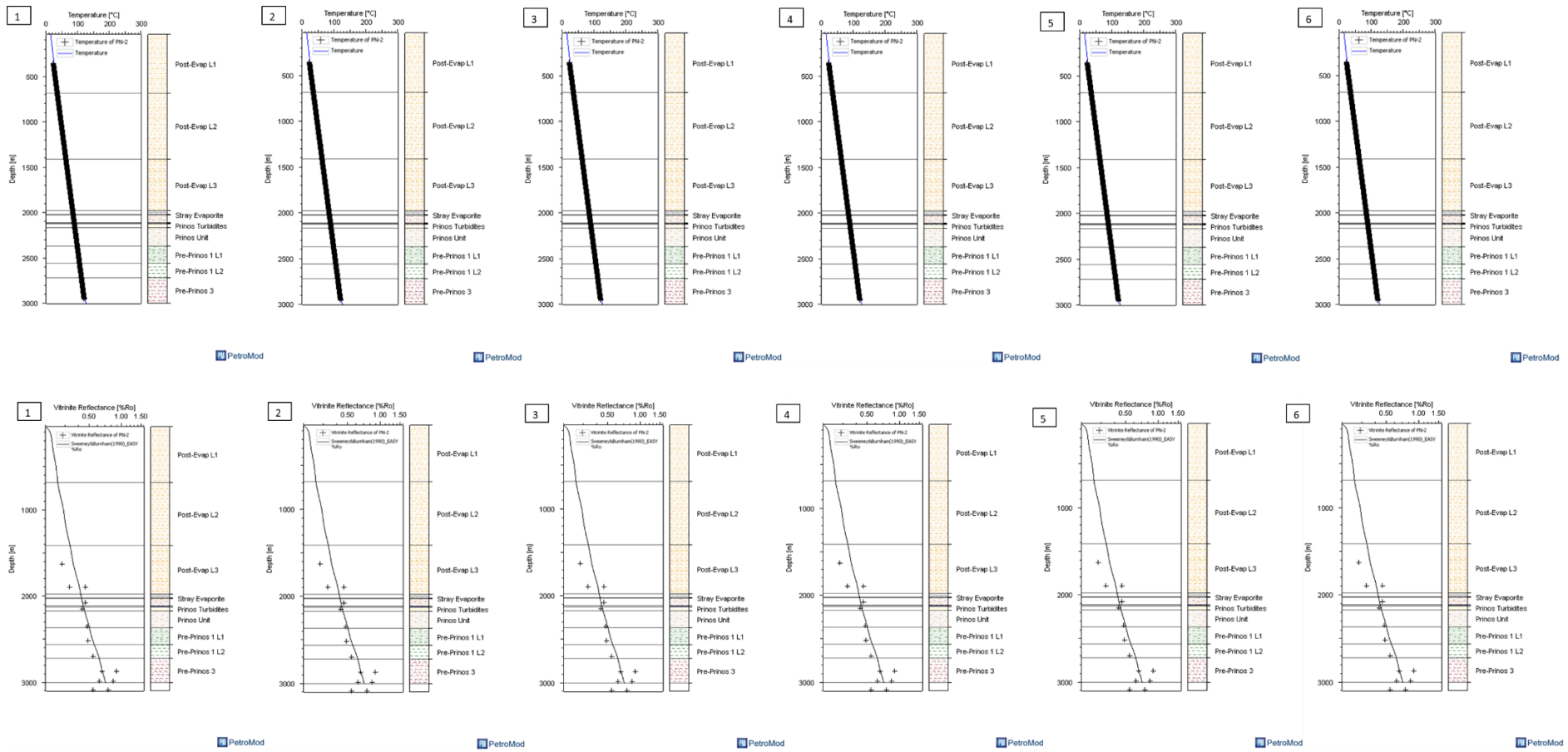


*Figure 57: Temperature and maturity (vitrinite reflectance) histories plots in PN-2 for: the optimized model (1) and multiple scenarios regarding the timing and duration of the erosional event in Pliocene-Pleistocene boundary and the original thickness of eroded sediments (2-6).*

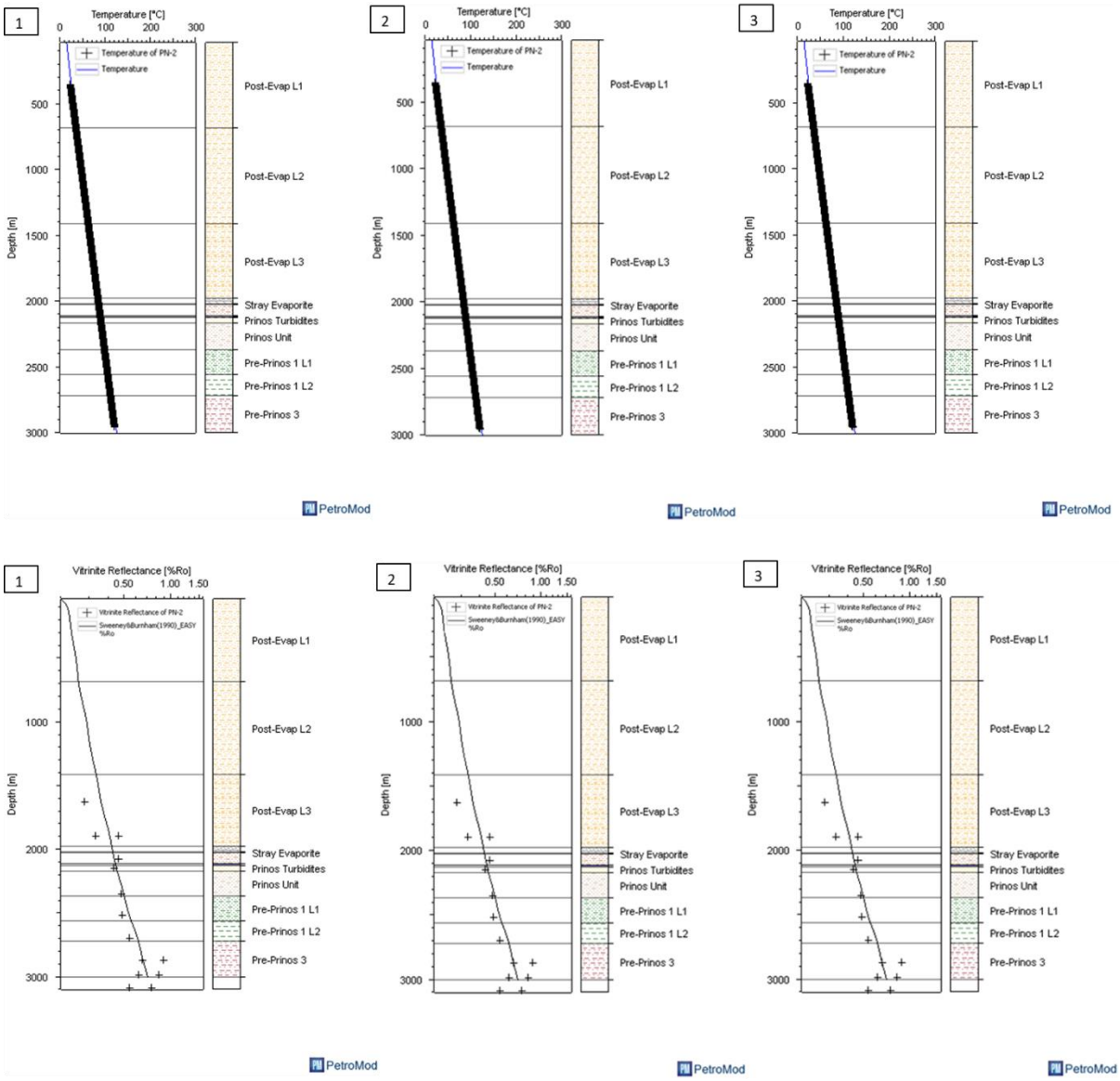


*Figure 58: Temperature and maturity (vitrinite reflectance) histories plots in PN-2 for: the optimized model (1) and multiple scenarios about PWD (2-3).*

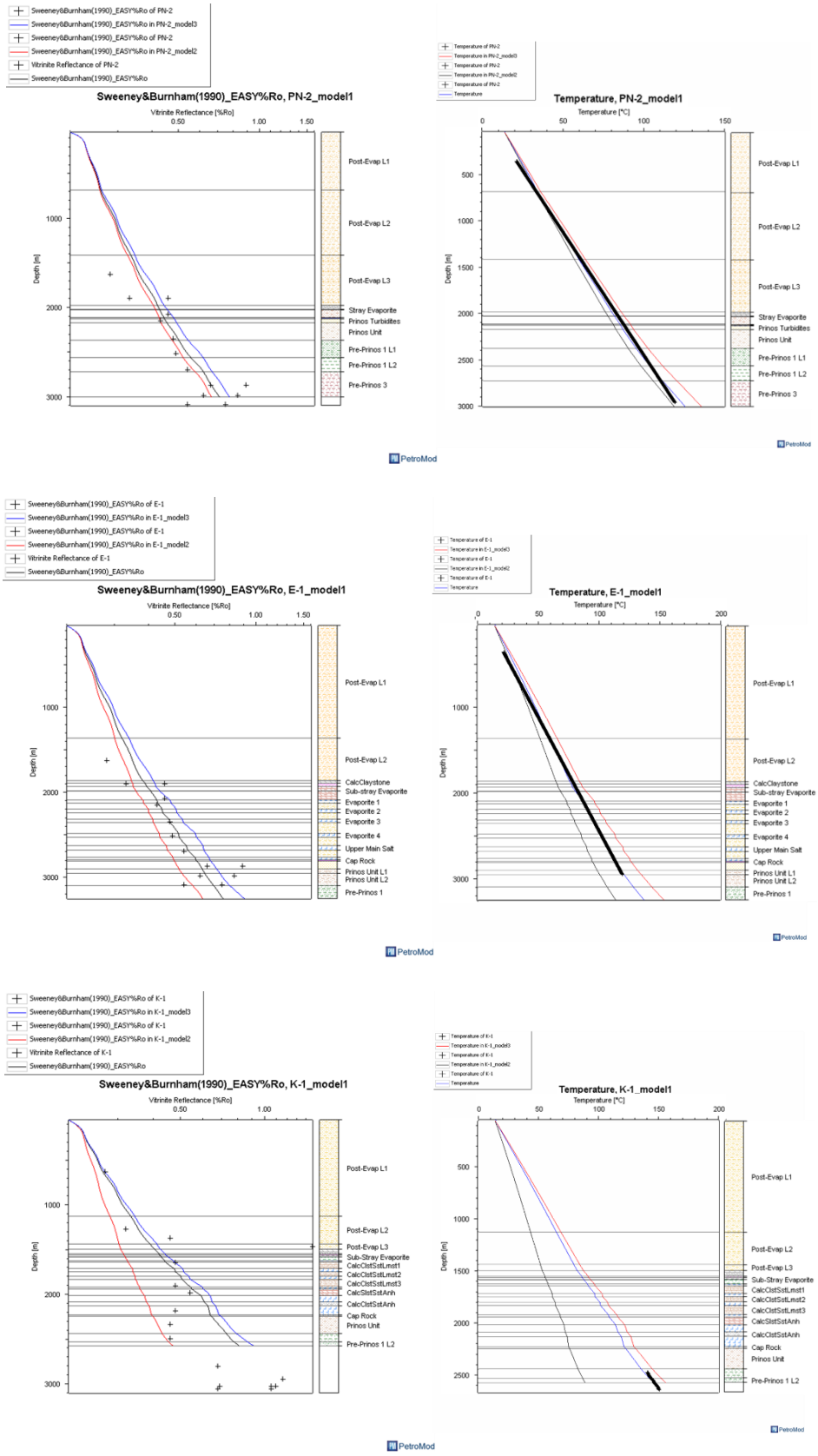


*Figure 59: Comparison graphs of temperature and vitrinite reflectance histories between the optimized model (model 1) and the low (model 2) and high (model 3) heat flow scenarios in the three modelled wells (PN-2: top, E-1: middle and K-1: bottom).*

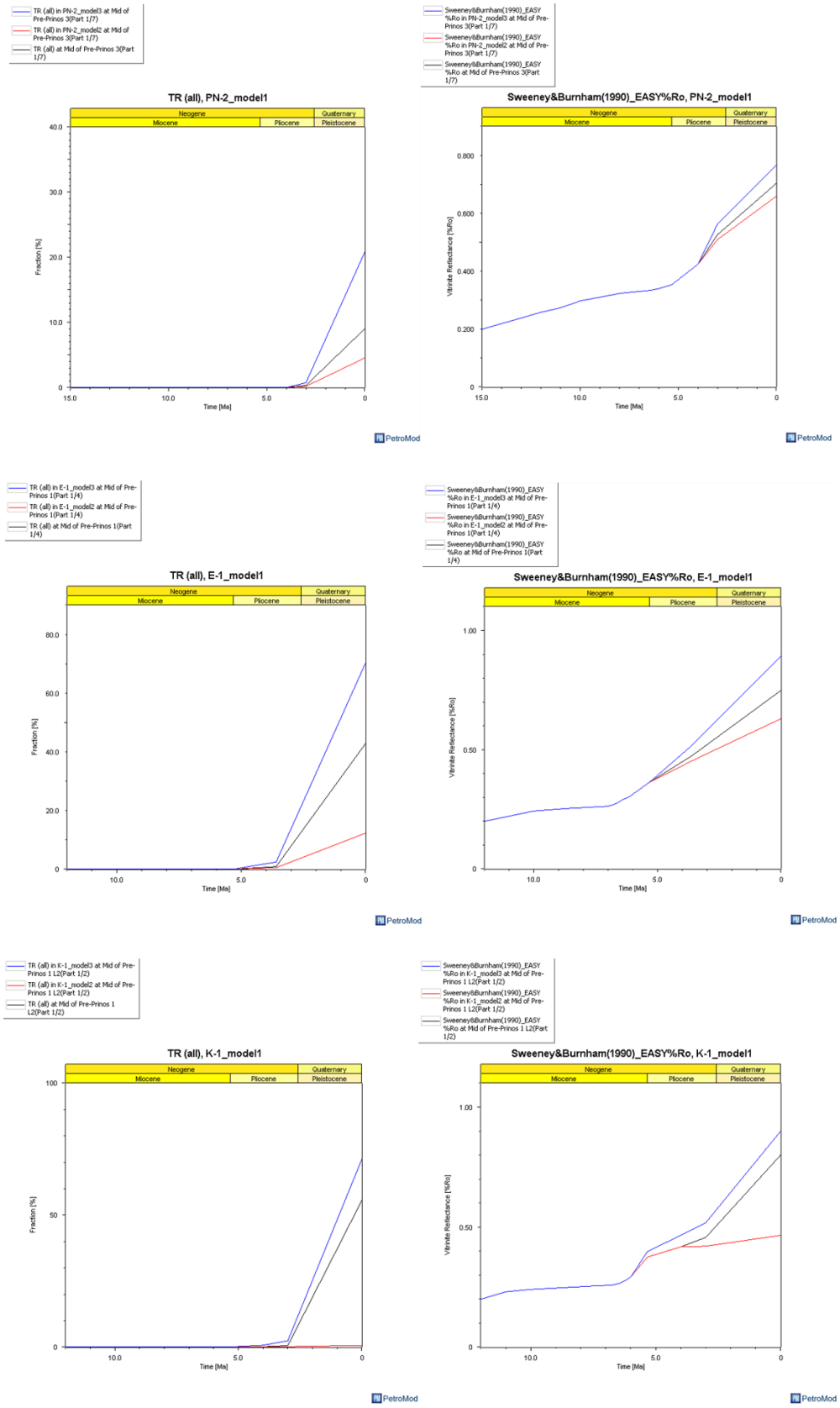


*Figure 60: Comparison graphs of simulated TR and vitrinite reflectance between the optimized model (model 1) and the low (model 2) and high (model 3) heat flow scenarios in the three modelled wells (PN-2: top, E-1: middle and K-1: bottom).*

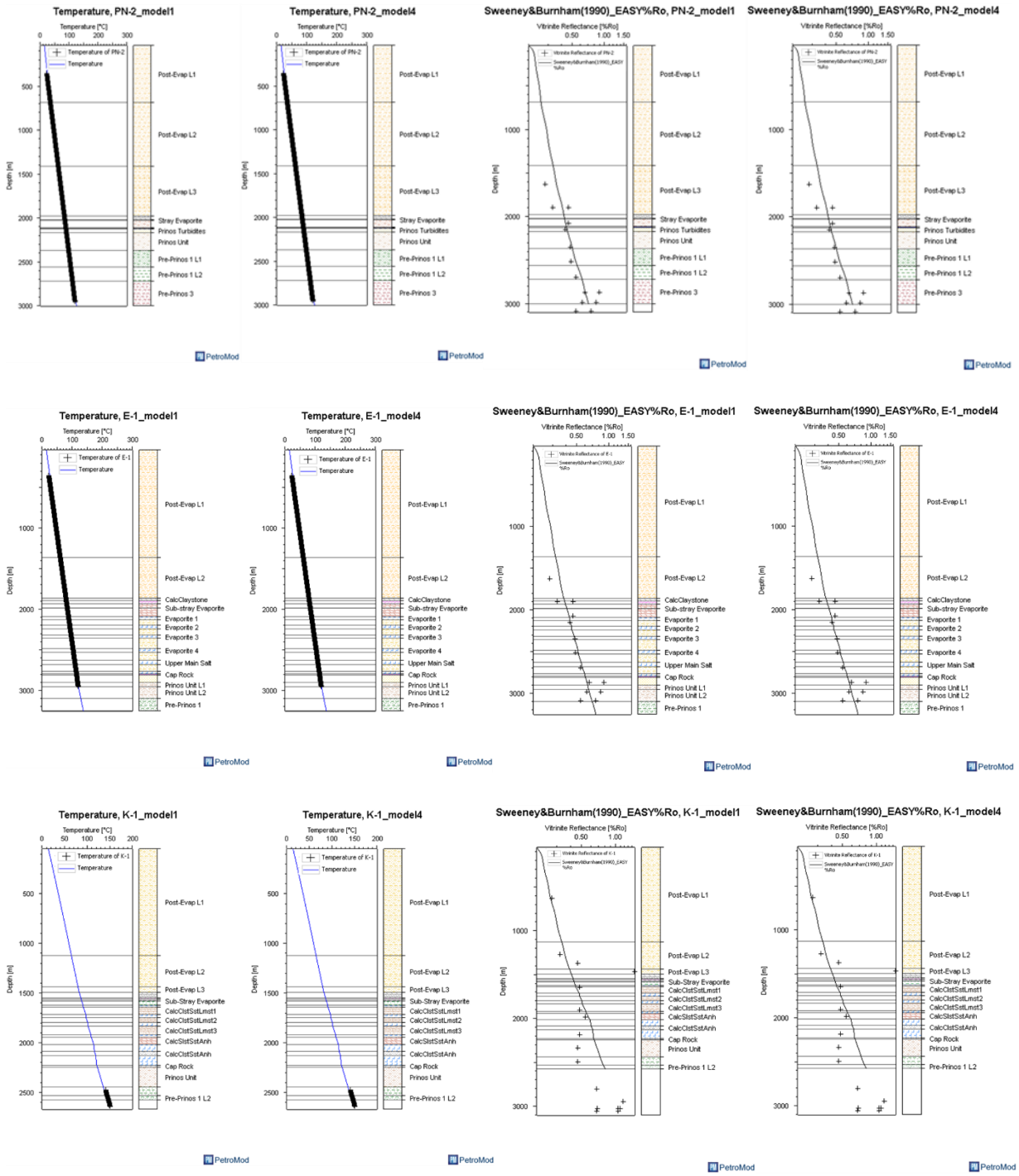


*Figure 61: Temperature and maturity (vitrinite reflectance) histories plots in all three wells (PN-2: top, E-1: middle and K-1: bottom) for the optimized model (model 1) and increased TOC and HI scenario (model 4).*

# 6 CONCLUSIONS

1D Basin and Petroleum system modelling was conducted on three exploration well locations within the Prinos-Kavala basin to find the temperature and maturity histories as well as the potential for generating oil and gas of the source rocks.

A lack of data imposed certain limitations on the produced 1D models. Age assignment, timing and duration of the erosion in the Upper Messinian, original thickness of eroded sediments, and the boundary conditions of PWD and heat flow have been inferred indirectly from available data in neighbouring places and similar conditions. Source rock characteristics and calibration temperature and vitrinite reflectance data, in modelled wells where there weren't the corresponding measurements, values were taken from nearby wells. All these assumptions and uncertainties led to a not fully representative modelling of the study area. However, a reasonable first estimation of past conditions and thermal and maturity histories was achieved.

The following findings were derived from the construction of the 1-D models:

- The basin experienced relatively slow and fairly constant subsidence during the Middle Miocene with one phase of strong uplift in the Upper Miocene. The area remained uplifted up to the end of the Upper Miocene and started deepening from the Lower Pliocene until today. Furthermore, the three modelled well locations have reached maximum burial depth at present-day with greater depth to be observed in E1.
- During the calibration of the heat flow values with vitrinite reflectance data, it was noted that the sediments of the K-1 well are today anomalously hot relative to the formations of the other two wells (PN-2 and E-1). This could probably be explained by the fact that well K-1 is located closer to the South Kavala Ridge, which is characterized by a high geothermal gradient.
- As the burial depth increases, more of the source rock enters the oil generation window, allowing more maturation of the organic matter. There is a discontinuity in source rock maturation and potential hydrocarbon generation due to the uplift of older units and the temperature decrease that were caused by the erosional event of the Upper Messinian.
- Temperature histories show that generally the temperature is steadily increasing in the area. The K-1 well presents slightly higher temperatures than the other two wells.
- From the figures of modelled maturity, it is observed that the assigned source rock formations of Pre-Prinos 3 and Pre-Prinos 1 have generated hydrocarbons. The source rock intervals was generally immature from the Middle Miocene until the Pliocene-Pleistocene boundary, after which maturity increases as the basin keeps sinking at greater depths. Well K-1 seems to have the

most mature source rocks, in which the early oil generation zone was reached at shallower depths and later compared to the other two wells.

- The highest present-day transformation ratio is observed in well K-1 with a value of 55.60%. Whereas, wells PN-2 and E-1 have present-day transformation ratios 9.04% and 42.87%, respectively.
- The formation of Pre-Prinos 3 in PN-2 is less thermally mature than the source rock of Pre-Prinos 1 in E-1 and K-1. The model of PN-2 predicts 31.37mgHC/gTOC of potential oil generation mass and 1.26mgHC/gTOC of gas. The potential oil generation mass in E-1 is predicted at 259.61mgHC/gTOC and for gas at 7.38mgHC/gTOC. In the end, K-1 has a potential for oil generation mass of 362.15mgHC/gTOC and for gas is predicted at 12.23mgHC/gTOC.
- Moreover, it was found that the only well in which the source rock has reached peak oil expulsion is K-1, which started at 0.44Ma.

Quite important results were also derived from sensitivity analysis that was carried out to test the influence of some input data and boundary conditions, and assess the resultant effect on temperature and maturity histories. The parameters that were selected are not based on real observations and measurements, but they are input parameters that there is not data for them, enabling us varying them within reasonable ranges. The results from this process indicated that timing and duration of the erosional event between the Evaporitic and Post-Evaporitic sequences, the original thickness of eroded sediments, the paleo water depth boundary condition and the source rock characteristics (TOC and HI) do not affect the temperature and maturity histories. On the contrary, the heat flow boundary conditions plays an important role to the temperature and maturity modelling. It was proven that high heat flow scenarios cause more mature source rock formations, shallower onset of hydrocarbon generation and earlier transformation of the kerogen.

# 7 BIBLIOGRAPHY


Al-Hajeri, M. M., Al Saeed, M., Derks, J., Fuchs, T., Hantschel, T., Kauerauf, A., Neumaier, M., Schenk, O., Swientek, O., and Tessen, N. (2009). Basin and petroleum system modeling. Oilfield Review, 21(2), p. 14–29.

Allen, J.R.L. (1965). A review of the origin and characteristics of recent alluvial sediments. Sedimentology, 5: p. 89-191.

Allen, J.R.L. (1970). Studies in fluvial sedimentation: composition of fining-upwards cyclothemes with special reference to coarse member composition and interpretation. J. Sediment. Petrol., 40: p. 298-323.

Allen, P. A. and Allen, J. R. (2005). Basin Analysis: Principles and Applications. Wiley-Blackwell, 2nd edition.

Bache, F., Olivet, J. L., Gorini, C., Rabineau, M., Baztan, J., Aslanian, D. and Suc, J. P. (2009). Messinian erosional and salinity crises: View from the Provence Basin (Gulf of Lions, Western Mediterranean). Earth and Planetary Science Letters, August 2009, Volume 286, Issues 1-2, p. 139-157.

Beardsmore, G.R. and Cull, J.P. (2001). Crustal Heat Flow: A Guide to Measurement and Modelling. Cambridge University Press, Cambridge.

Brun, J. P. and Faccenna, C. (2008). Exhumation of high-pressure rocks driven by slab rollback, Earth and Planetary Science Letters, 272, p. 1–7.

Brun, J. P. and Sokoutis, D. (2007). Kinematics of the Southern Rhodope Core Complex (North Greece), International Journal of Earth Sciences, 96-6, p. 1079-1099.

Burnham, A. K. and Sweeney, J. J. (1989). A chemical kinetic model of vitrinite maturation and reflectance. Geochim. Cosmochim. Acta, 53: p. 2649–2657.

Chiotis, E. D. (1985). A Middle Miocene thermal event in northern Greece confirmed by coalification measurements. In: Dixon J.E. and Robertson, A.H.F. (eds). The geological evolution of the Eastern Mediterranean, Spec. Publ. Geol. Soc., 17, Blackwell Sc Publ., Oxford, p. 815-818.

Cross, T. A., Harbaugh, J. W. (1990). Quantitative dynamic stratigraphy: a workshop, a philosophy, a methodology. In: Cross TA (ed) Quantitative dynamic stratigraphy. Prentice Hall, Englewood Cliffs, p. 3-20.

Dembicki, Jr. H. (2013). Shale Gas Geochemistry Mythbusting. Oral Presentation at the American Association of Petroleum Geologists 2013 Annual Convention and Exhibition, May 19–22, 2013. American Association of Petroleum Geologists Search and Discovery Article # 80294, Pittsburgh, PA.

Dembicki, Jr. H. (2017). Practical petroleum geochemistry for exploration and production. Elsevier.

Dewey, J. F., and Sengor, A. M. C. (1979). Aegean and surroundings regions: Complex multiplate and continuum tectonics in a convergent zone, Geolog. Soc. Of Amer. Bull., 90, p. 84–92.

Dinter, D. (1991). Neogene detachment faulting and the Rhodope metamorphic core complexes, northern Greece. EOS Trans. AGU, 72, p. 460.

Dinter, D. A. (1994). Tectonic evolution of the Rhodope metamorphic core complex, northeastern Greece. PhD thesis, Mass Inst. Of Technol. Cambridge, p. 320.

Dinter, D. A. and Royden, L. (1993), Late Cenozoic extension in northeastern Greece: Strymon valley detachment system and Rhodope metamorphic core complex. Geology, 21, p. 45-48.

Georgakopoulos, A. (1998). Lithology and stratigraphy of the Neogene Prinos-Kavala basin, Northern Greece, Proceedings Interim Colloquium RCMNS, p. 79-84.

Georgakopoulos, A. (1998). Organic geochemical study of Greek oil source rocks, Proc. Of the 2nd International Conference and Exhibition – Modern Exploration and Improved oil and gas recovery methods, p. 208-213.

Georgakopoulos, A. (1998). Study of source rocks of the petroliferous Prinos-Kavala oil bearing basin using organic geochemical methods. Bull. Geol. Soc. Greece, 32, Proc. 8th International Congress, p. 325-334.

Georgakopoulos, A. (2000). Lithology and stratigraphy of the Neogene Prinos-Kavala basin, Northern Greece. Proc. R.C.M.N.S. Interim Colloquium, (Ed.) G.D. Koufos & Ch.E. Ioakim, Mediterranean Neogene Cyclostratigraphy in marine-continental palaeoenvironments, Geol. Soc. Greece Sp. Publ., 9, p. 79-84.

Gretener, P. E. (1981). Geothermics: using temperature in hydrocarbon exploration: AAPG Education Course Notes Series v. 17, p. 1-156.

Hantschel, T. and Kauerauf, A. I. (2009). Fundamentals of Basin and Petroleum Systems Modeling. Springer, Berlin.

Haubold, G. (2007) Hattingen, GFDL-Rechte verliehen von Gerhard Haubold Wikipedia, http://commons.wikimedia.org/wiki/File:Thasos-Horst_und_umgebende Bruchbecken.jpg?uselang=de

https://wiki.aapg.org/Vitrinite_reflectance

https://www.energean.com

https://www.software.slb.com/products/petromod

https://www.software.slb.com/products/petromod/petromod-composition

Ioakim, C., Rondoyanni, T. and Mettos, A. (2005). The Miocene basins of Greece (Eastern Mediterranean) from a palaeoclimatic perspective, Revue de Paleobiologie, v. 24, 2, p. 735-748.

Jarvis, G. T. and McKenzie, D. P. (1980). Sedimentary basin information with finite extension rates. Earth and Planet. Sci. Lett., 48: p. 42–52.

Jolivet, L., Faccenna, C., Huet, B., Labrousse, L., Le Pourhiet, L., Lacombe, O., Lecomte, E., Burov, E., Denèle, Y., Brun, J. P., Philippon, M., Paul, A., Salaün, G., Karabulut, H., Piromallo, C., Monié, P., Gueydan, F., Okay, A. I., Oberhänsli, R., Pourteau, A., Augier, R., Gadenne, L., Driussi, O. (2013). Aegean tectonics: Strain localisation, slab tearing and trench retreat, Tectonophysics, vol.597-598, p. 1–33. doi:10.1016/j.tecto.2012.06.011

Jongsma, D. (1974). Heat flow in the Aegean Sea. Geophysical Journal of the Royal Astronomical Society, 37: p. 331-346.

Karakitsios, V., Cornée, J. J., Tsourou, T.,Moissette, P., Kontakiotis, G., Agiadi, K., Manoutsoglou, E., Triantaphyllou, M., Koskeridou, E., Drinia, H. and Roussos, D. (2017). Messinian salinity crisis record under string freshwater input in marginal, intermediate, and deep environments: The case of the North Aegean. In: Palaeogeography Palaeoclimatology Palaeoecology 485 (2017). p. 316-335.

Kilias, A. and Mountrakis, D. (1998). Tertiary extension of the Rhodope massif associated with granite emplacement (Northern Greece). Acta Vulcanologica, 10, p. 331-337.

Kiomourtzi, P., Papaconstantinou, C., Pasadakis, N., Zelilidis, A. (2007). Geochemical Characterization of Satellite Hydrocarbon Formations in Prinos – Kavala Basin (North Greece), Bulletin of the Geological Society of Greece vol. XXXX, 2, p. 839-850.

Kiomourtzi, P., Anagnostoudi, Th., Zelilidis, A. (2008). Depositional Environments in Prinos – Kavala Basin. A Palaeogeographic Evolutionary Model, 26th IAS meeting of Sedimentology, Bochum, Germany.

Kiomourtzi, P., Pasadakis, N., Zelilidis, A. (2008). Source Rock and Depositional Environment Study of Three Hydrocarbon Fields in Prinos – Kavala Basin (North Aegean), The Open Petroleum Engineering Journal, Volume 1, pp 16-29.

Kiomourtzi, P., Pasadakis, N., Zelilidis, A. (2008). Source Organic Matter and Depositional Environment in Prinos – Kavala Basin (Greece), International Geological Congress, Oslo, Norway.

Kiomourtzi, P., Zelilidis, A. (2009). Prinos-Kavala Basin: A Palaeogeographic Evolutionary Model (Kavala, Greece), 27th IAS meeting of Sedimentology, Alghero, Italy.

Kiomourtzi, P., Zelilidis, A., Pasadakis, N. (2009). Organic geochemical study of the Kalirahi formation (Prinos-Kavala basin), 3rd AMIREG International Conference, Athens, Greece.

Kiomourtzi, P. (2016). Depositional Environments and hydrocarbon potential basins in the North Aegean Sea. PhD thesis.

Kolios, N., Fytikas, M., Arvanitis, A., Andritsos, N., and Koutsinos, S. (2007). Prospective Medium Enthalpy Geothermal Resources in Sedimentary Basins of Northern Greece. Proceedings European Geothermal Congress 2007, Unterhaching, Germany, 30 May-1 June 2007.

Koukouvelas, I. and Aydin, A. (2002). Fault structure and related basins of the North Aegean Sea and its surroundings. Tectonics, 21, p. 1-27.

Lalechos, N., and E. Savoyat, (1977). La sedimentation Neogene dans le Fosse Nord Egeen, in paper presented at 6th Colloquium on the Geology of the Aegean Region, Athens, Inst. Geol. Miner. Explor.

Larter, S.R. (1989). Chemical models of vitrinite reflectance evolution. Geologische Rundschau 78, p. 349–359.

Lopatin, N.V. (1971). Temperature and geologic time as factors in coalification. Izvestiya Akademii Nauk. Seriya Khimicheskaya 3, p. 95–106.

Magoon, L. B. and Beaumont, E. A. (1999). Treatise of Petroleum Geology/Handbook of Petroleum Geology: Exploring for Oil and Gas Traps. Chapter 3: Petroleum Systems.

Magoon, L. B. and Dow, W. G. (1994). The petroleum system-from source to trap. AAPG Memoir 60.

Maltezou, F., and Brooks, M. (1989). A geophysical investigation of post-Alpine granites and Tertiary sedimentary basins in northern Greece. Journal of the Geologial Society, 146, p. 53-59.

Maravelis, A. and Zelilidis, A. (2013). Discussion: "Unraveling the provenance of Eocene–Oligocene sandstones of the Thrace Basin, North-east Greece" by Caracciolo et al. (2011), Sedimentology, 60, 3, p. 860-864.

McKenzie, D. (1978). Some remarks on the development of sedimentary basins, Earth and Planet Sci. lett., 40, p. 25-32.

Mertzanides, Y., Kargiotis, E., Mitropoulos, A. (2010). Geological and Geophysical data of Epsilon field in Prinos oil basin, Bull. Geol. Soc. Greece, Proc. 12th International Congress, 5, p. 2257-2264.

Mountrakis, D.M. (2010). Geology and Geotectonic Evolution of Greece. University Studio Press. (in greek)

Okosun, E. A., and Osterloff, P. (2014). Ostracod, Diatom and Radiolarian Biostratigraphy of the Niger Delta, Nigeria. Earth Science Research; Vol. 3, No. 1; 2014. Published by Canadian Center of Science and Education.

Papazachos, C. B. and Scordilis, E. M. (1998). Crustal structure of the Rhodope and surrounding area obtained by non-linear inversion of P and S travel times and its tectonic implication, Acta Vulcanologica, 10, p. 339-345.

Pe-Piper, G. and Piper, D. J. W. (2001). Late Cenozoic post-collisional Aegean igneous rocks: Nd and Sr isotopic constraints on petrogenetic and tectonic models, Geological magazine, 138, p. 653-668.

Pepper, A.S. and Corvi, P.J. (1995). Simple kinetic models of petroleum formation. Part I: oil and gas generation from kerogen. Mar. Pet. Geol., 12, p. 291–319.

PetroMod 1D User Guide (2017). Schlumberger.

Pickard, G.L. (1963). Descriptive Physical Oceanography. Pergamon Press, New York. p. 200.

Pollak, W. H. (1979). Structural and lithological development of the Prinos-Kavala basin, sea of Thrace, Greece. Annex Geologique pays Hellenic tome hors serie, fash 2, 7th International Congress on Mediterranean Neogene, p. 1003-1011.

Proedrou, P. (1979). The Evaporite formation in the Nestos-Prinos graben in the northern Aegean sea. Ann. Geol. Pays Hellen., Tome hors serie 1979, fasc. 2, 7th International Congress on Mediterranean Neogene, p. 1013-1020.

Proedrou, P. (1988). New age determination of the Prinos basin. Bull. Geol. Soc., 20, n.2, p. 141-147.

Proedrou, P. (2001). South Kavala gas field-Taphrogenetic Prinos basin. Bull. Geol. Soc. 34, p. 1221-1228.

Proedrou, P. and Papaconstantinou, C. (2004). Prinos basin – a model for oil exploration, Proc. 10th International Congress, p. 327-333.

Proedrou, P. and Sidiropoulos, T. (1992). Prinos field – Greece, Aegean basin, structural traps. Treatise of petroleum Geology atlas of oil and gas fields, AAPG, p. 275-291. Reading, H. (). “Sedimentary Environments and Facies”, Elsevier, 615 p.

Reilinger, R., McClusky, S., Paradissis, D., Ergintav, S., Vernant, P. (2010). Geodetic constraints on the tectonic evolution of the Aegean region and strain accumulation along the Hellenic subduction zone, Tectonophysics, vol. 488, p. 22–30.

Rigakis, N., Roussos, N., Kamberis, E. and Proedrou, P. (2001). Hydrocarbon gas accumulations in Greece and their origin. Proc. 9th International Congress, p. 1265-1268.

Roussos, N., (1994). Stratigraphy and paleogeographic evolution of the Paleogene Molassic basins of the North Aegean area. Proc. 7th Congress, Bull. of the Geological Society of Greece,30, p. 275– 294.

Roveri, M., Gennari, R., Lugli, S., Manzi, V., Minelli, N., Reghizzi, M., Riva, A., Rossi, M. E. & Schreiber, C. (2016). The Messinian salinity crisis: open problems and possible implications for Mediterranean petroleum systems. In: Petroleum Geoscience June 2016.

Sclater, J.G. and Christie, P.A.F. (1980). Continental stretching; an explanation of the post-Mid Cretaceous subsidence of the central North Sea basin. Journal of Geophysical Research 85 (B7): p. 3711–3739.

Sokoutis, D., Brun, J.P., Van Den Driessche, J and Pavlides, S. (1993). A major Oligo-Mioeene detachment in southern Rhodopc controlling north Aegean extension. Journal of the Geological Society, 150, p. 243-246.

Suzuki, N., Matsubayashi, H., Waples, D.W. (1993). A simpler kinetic model of vitrinite reflectance. American Association of Petroleum Geologists Bulletin 77, p. 1502–1508.

Sweeney, J. J., and Burnham, A.K. (1990). Evaluation of a simple model of vitrinite reflectance based on chemical kinetics. American Association of Petroleum Geologists Bulletin, 74, p. 1559-1570.

Teichmuller, M. (1982a). Application of coal petrological methods in geology including oil and natural gas prospecting. In: Stach’s Textbook of Coal Petrology. Gebrubder Borntraeger, Berlin, p. 381–413.

Teichmuller, M. (1989). The genesis of coal from the viewpoint of coal petrology. International Journal of Coal Geology 12, p. 1–87.

Tissot, B. P. (1969). Premieres donnees sur les mecanismes et la cinetique de la formation du petrole dans les sediments: simulation d un schema rectionnel sur ordinateur: Revue de I Institut Francais du petrole, v. 24, p. 470-501.

Tissot, B. R., Pelet and P. Ungerer (1987). Thermal history of sedimentary basins, maturation indices and kinetics of oil and gas generation. Am. Assoc. Petr. Geol. B., 71: p. 1445-1466.

Ungerer, P., Espitalie, J., Behar, F., Eggen, S. (1988b). Modelisation mathemetique des interactions entre craquage thermique et migration lors de la formation du petrole et du gaz. Comptes Rendus de l’Académie des Sciences, Series II, p. 927–934.

Ungerer, P. (1990). State of the art of research in kinetic modelling of oil formation and expulsion. Org Geochem 16: p. 1-26.

Ungerer, P., Burrus, J., Doligez, B., Chenet, P. Y., & Bessis, F. (1990). Basin evaluation by integrated two dimensional modelling of heat transfer, fluid flow, hydrocarbon generation and migration: AAPG Bulletin, v. 74, p. 309-335.

Waples, D.W. (1980). Time and temperature in petroleum formation: application of Lopatin's method to petroleum exploration. American Association of Petroleum Geologists Bulletin 64 (6), p. 916–926.

Waples, D. W. (1984). Thermal models for oil generation: p. 7-67 in "Advances in Petroleum Geochemistry, Vol. 1" (Edited by J. Brooks and D. Welte), Academic Press, London.

Waples, D. W. (1994). Maturity Modelling: Thermal Indicator, Hydrocarbon generation and Oil Cracking. In: J. B. Magoon, W. G. Dow (eds.), The petroleum system - from source to trap. APPG Memoir 60, p. 285-306.

Wawrzenitz, N. and Krohe, A. (1998). Exhumation and doming of the Thasos metamorphic core complex (S. Rhodope, Greece): Structural and geochronological constraints. Tectonophysics, 285, p. 301-332.

Welte, D. H. and Yalcin, M. N. (1987). Formation and occurrence of petroleum in sedimentary basins as deduced from computer-aided basin modelling. In: Kumar SP, Dwivedi P, Banerjie V, Gupta V (eds) Petroleum geochemistry and exploration in the Afro-Asian region. Balkema, Rotterdam, p. 17-23.

Welte, D. H., Yalcin, M. N. (1988). Basin modelling - a new comprehensive methodology in petroleum geology. In: Matavelli L, Novelli L (eds) Advances in organic geochemistry l3. Pergamon, Oxford, p. 141-151.

Welte, D. H., Horsfield, B., & Baker, D. R. (1997). Petroleum and basin evolution: Springer-Verlag, p. 1-536.

White, D. (1915). Geology: Some relations in origin between coal and petroleum. J Wash Acad Sci 5: p. 189-212.

Wygrala, B. P. (1988). Integrated computer-aided basin modeling applied to analysis of hydrocarbon generation history in northern Italian oil field. In: Mattavelli L, Novelli L (eds) Advances in organic geochemistry l3. Pergamon, Oxford, p. 187-197.

Wygrala, B. P. (1989). Integrated study of an oil field in the southern Po basin, northern Italy. Diss, Univ Kaln, Berichte Kernforschungsanlage Jtilich, no 23l3, p. 1-217.

# 8 APPENDIX

## Mixed lithologies created for well PN-2

| | Lithology | Percent |
|---|---|---|
| 1 | Sandstone (quartzite, typical) | 70.00 |
| 2 | Clay-rich silic. mudstone | 10.00 |
| 3 | CalcareousSiltstone | 10.00 |
| 4 | Conglomerate (typical) | 10.00 |
| 5 | | |

Layer 1 of the Post-Evaporitic series

| | Lithology | Percent |
|---|---|---|
| 1 | Sandstone (quartzite, typical) | 40.00 |
| 2 | Carb.-rich silic. mudstone | 25.00 |
| 3 | CalcareousSiltstone | 15.00 |
| 4 | Conglomerate (typical) | 10.00 |
| 5 | Limestone (organic rich - typical) | 10.00 |

Layer 2 of the Post-Evaporitic series

| | Lithology | Percent |
|---|---|---|
| 1 | Sandstone (quartzite, typical) | 20.00 |
| 2 | Conglomerate (typical) | 30.00 |
| 3 | Clay-rich silic. mudstone | 10.00 |
| 4 | CalcareousSiltstone | 30.00 |
| 5 | Limestone (organic rich - typical) | 10.00 |

Layer 3 of the Post-Evaporitic series

| | Lithology | Percent |
|---|---|---|
| 1 | Siltstone (organic rich, typical) | 20.00 |
| 2 | Anhydrite | 20.00 |
| 3 | Limestone (organic rich - typical) | 20.00 |
| 4 | Clay-rich silic. mudstone | 20.00 |
| 5 | Sandstone (quartzite, typical) | 20.00 |

Formation consisting of siltstone, anhydrite, limestone, claystone and sandstone

| | Lithology | Percent |
|---|---|---|
| 1 | Halite | 60.00 |
| 2 | Anhydrite | 40.00 |

Lower Main Salt

| | Lithology | Percent |
|---|---|---|
| 1 | Siltstone (organic rich, typical) | 80.00 |
| 2 | Anhydrite | 20.00 |

Cap rock formation

| | Lithology | Percent |
|---|---|---|
| 1 | Sandstone (quartzite, typical) | 50.00 |
| 2 | Limestone (organic rich - typical) | 20.00 |
| 3 | CalcareousSiltstone | 30.00 |

Prinos Unit

| | Lithology | Percent |
|---|---|---|
| 1 | CalcareousSiltstone | 30.00 |
| 2 | Halite | 10.00 |
| 3 | CalcareousClaystone | 20.00 |
| 4 | Sandstone (typical) | 30.00 |
| 5 | Limestone (organic rich - typical) | 10.00 |

Layer 1 of the Pre-Prinos 1 formation

| | Lithology | Percent |
|---|---|---|
| 1 | CalcareousSiltstone | 40.00 |
| 2 | Clay-rich silic. mudstone | 40.00 |
| 3 | Sandstone (typical) | 10.00 |
| 4 | Anhydrite | 10.00 |

Layer 2 of the Pre-Prinos 1 formation

| | Lithology | Percent |
|---|---|---|
| 1 | Sandstone (typical) | 40.00 |
| 2 | Clay-rich silic. mudstone | 20.00 |
| 3 | Marl | 10.00 |
| 4 | Siltstone (organic rich, typical) | 15.00 |
| 5 | Limestone (organic rich - typical) | 10.00 |
| 6 | Coal (silty) | 5.00 |

Pre-Prinos 3

## Mixed lithologies created for well E-1

| | Lithology | Percent |
|---|---|---|
| 1 | Clay-rich silic. mudstone | 90.00 |
| 2 | Calcite | 10.00 |

Calcareous claystone

| | Lithology | Percent |
|---|---|---|
| 1 | Siltstone (organic rich, typical) | 90.00 |
| 2 | Calcite | 10.00 |

Calcareous siltstone

| | Lithology | Percent |
|---|---|---|
| 1 | Sandstone (quartzite, typical) | 60.00 |
| 2 | Conglomerate (quartzitic) | 10.00 |
| 3 | CalcareousClaystone | 10.00 |
| 4 | CalcareousSiltstone | 15.00 |
| 5 | Limestone (organic rich - typical) | 5.00 |

Layer 1 of the Post-Evaporitic series

| | Lithology | Percent |
|---|---|---|
| 1 | Sandstone (quartzite, typical) | 57.00 |
| 2 | Conglomerate (quartzitic) | 10.00 |
| 3 | CalcareousClaystone | 10.00 |
| 4 | CalcareousSiltstone | 15.00 |
| 5 | Limestone (organic rich - typical) | 8.00 |

Layer 2 of the Post-Evaporitic series

| | Lithology | Percent |
|---|---|---|
| 1 | Anhydrite | 35.00 |
| 2 | Salt | 35.00 |
| 3 | Clay-rich silic. mudstone | 10.00 |
| 4 | Limestone (organic rich - typical) | 10.00 |
| 5 | Sandstone (typical) | 10.00 |

Stray Evaporite

| | Lithology | Percent |
|---|---|---|
| 1 | CalcareousSiltstone | 65.00 |
| 2 | Sandstone (typical) | 20.00 |
| 3 | Limestone (organic rich - typical) | 15.00 |

Formation consisting of calcareous siltstone, sandstone, and limestone

| | Lithology | Percent |
|---|---|---|
| 1 | Halite | 100.00 |

Sub stray evaporite

| | Lithology | Percent |
|---|---|---|
| 1 | Halite | 90.00 |
| 2 | Anhydrite | 10.00 |

Evaporite 1

| | Lithology | Percent |
|---|---|---|
| 1 | Sandstone (quartzite, typical) | 57.00 |
| 2 | Clay-rich silic. mudstone | 25.00 |
| 3 | CalcareousSiltstone | 15.00 |
| 4 | Limestone (organic rich - typical) | 3.00 |

Formation consisting of sandstone, claystone, calcareous siltstone, and limestone

| | Lithology | Percent |
|---|---|---|
| 1 | Halite | 87.00 |
| 2 | Anhydrite | 10.00 |
| 3 | Gypsum | 3.00 |

Evaporite 3

| | Lithology | Percent |
|---|---|---|
| 1 | Halite | 90.00 |
| 2 | Anhydrite | 10.00 |

Upper Main Salt

| | Lithology | Percent |
|---|---|---|
| 1 | Halite | 100.00 |

Lower Main Salt

| | Lithology | Percent |
|---|---|---|
| 1 | CalcareousSiltstone | 80.00 |
| 2 | Clay-rich silic. mudstone | 20.00 |

Cap rock formation

| | Lithology | Percent |
|---|---|---|
| 1 | Sandstone (quartzite, typical) | 65.00 |
| 2 | CalcareousSiltstone | 20.00 |
| 3 | Clay-rich silic. mudstone | 15.00 |

Layer of turbidites of the Prinos Unit

| | Lithology | Percent |
|---|---|---|
| 1 | Siltstone (organic rich, typical) | 55.00 |
| 2 | CalcareousSiltstone | 15.00 |
| 3 | Sandstone (quartzite, typical) | 30.00 |

Prinos Unit

| | Lithology | Percent |
|---|---|---|
| 1 | Sandstone (typical) | 30.00 |
| 2 | Clay-rich silic. mudstone | 20.00 |
| 3 | Siltstone (organic rich, typical) | 20.00 |
| 4 | Anhydrite | 5.00 |
| 5 | Marl | 15.00 |
| 6 | Limestone (organic rich - typical) | 10.00 |

Pre-Prinos 1

## Mixed lithologies created for well K-1

| | Lithology | Percent |
|---|---|---|
| 1 | Sandstone (quartzite, typical) | 80.00 |
| 2 | Siltstone (organic rich, typical) | 10.00 |
| 3 | CalcareousSiltstone | 10.00 |

Layer 1 of the Post-Evaporitic series

| | Lithology | Percent |
|---|---|---|
| 1 | Sandstone (quartzite, typical) | 70.00 |
| 2 | Siltstone (organic rich, typical) | 10.00 |
| 3 | CalcareousSiltstone | 10.00 |
| 4 | Conglomerate (typical) | 10.00 |

Layer 2 of the Post-Evaporitic series

| | Lithology | Percent |
|---|---|---|
| 1 | Sandstone (quartzite, typical) | 60.00 |
| 2 | Siltstone (organic rich, typical) | 10.00 |
| 3 | CalcareousSiltstone | 10.00 |
| 4 | Conglomerate (typical) | 10.00 |
| 5 | Limestone (organic rich - typical) | 5.00 |

Layer 3 of the Post-Evaporitic series

| | Lithology | Percent |
|---|---|---|
| 1 | Anhydrite | 50.00 |
| 2 | Salt | 50.00 |

Stray Evaporite

| | Lithology | Percent |
|---|---|---|
| 1 | CalcareousClaystone | 60.00 |
| 2 | Limestone (organic rich - typical) | 40.00 |

Formation consisting of calcareous claystone and limestone

| | Lithology | Percent |
|---|---|---|
| 1 | Siltstone (organic rich, typical) | 40.00 |
| 2 | Sandstone (quartzite, typical) | 40.00 |
| 3 | Limestone (organic rich - typical) | 20.00 |

Formation consisting of siltstone, sandstone and limestone

| | Lithology | Percent |
|---|---|---|
| 1 | Sandstone (quartzite, typical) | 40.00 |
| 2 | CalcareousClaystone | 35.00 |
| 3 | Limestone (organic rich - typical) | 25.00 |

Formation consisting of sandstone, calcareous claystone and limestone

| | Lithology | Percent |
|---|---|---|
| 1 | Halite | 70.00 |
| 2 | Anhydrite | 10.00 |
| 3 | CalcareousClaystone | 20.00 |

Evaporite 4

| | Lithology | Percent |
|---|---|---|
| 1 | CalcareousSiltstone | 80.00 |
| 2 | Sandstone (quartzite, typical) | 10.00 |
| 3 | Anhydrite | 10.00 |

Formation consisting of calcareous siltstone, sandstone, and anhydrite

| | Lithology | Percent |
|---|---|---|
| 1 | Halite | 80.00 |
| 2 | Anhydrite | 10.00 |
| 3 | Siltstone (organic rich, typical) | 10.00 |

Upper Main Salt

| | Lithology | Percent |
|---|---|---|
| 1 | CalcareousClaystone | 45.00 |
| 2 | Sandstone (quartzite, typical) | 45.00 |
| 3 | Anhydrite | 10.00 |

Formation consisting of calcareous claystone, sandstone, and anhydrite

| | Lithology | Percent |
|---|---|---|
| 1 | Sandstone (quartzite, typical) | 60.00 |
| 2 | CalcareousClaystone | 25.00 |
| 3 | Limestone (organic rich - typical) | 10.00 |
| 4 | Anhydrite | 5.00 |

Prinos Unit

| | Lithology | Percent |
|---|---|---|
| 1 | Sandstone (typical) | 30.00 |
| 2 | Clay-rich silic. mudstone | 30.00 |
| 3 | Siltstone (organic rich, typical) | 25.00 |
| 4 | Anhydrite | 15.00 |

Layer 1 of the Pre-Prinos 1 formation

| | Lithology | Percent |
|---|---|---|
| 1 | Marl | 40.00 |
| 2 | Sandstone (typical) | 25.00 |
| 3 | Clay-rich silic. mudstone | 15.00 |
| 4 | Siltstone (organic rich, typical) | 10.00 |
| 5 | Limestone (organic rich - typical) | 10.00 |

Layer 2 of the Pre-Prinos 1 formation